UNIVERSIDADE DE LISBOA

FACULDADE DE CIÊNCIAS

Ciências
ULisboa

Simplified Modelling of Displacement Ventilation

Doutoramento em Energia e Ambiente
Especialidade em Energia e Desenvolvimento Sustentável

Nuno André Marques Mateus

Tese orientada por:
Professor Doutor Guilherme Carvalho Canhoto Carrilho da Graça

Documento especialmente elaborado para a obtenção do grau de doutor

2016

UNIVERSIDADE DE LISBOA

FACULDADE DE CIÊNCIAS

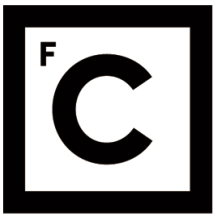

Ciências
ULisboa

Simplified Modelling of Displacement Ventilation

Doutoramento em Energia e Ambiente
Especialidade em Energia e Desenvolvimento Sustentável

Nuno André Marques Mateus

Tese orientada por:
Professor Doutor Guilherme Carvalho Canhoto Carrilho da Graça

Júri:
Presidente:
- Doutor João Catalão Fernandes (Faculdade de Ciências, Universidade de Lisboa)

Vogais:
- Doutor Paul Linden (Faculty of Mathematics, University of Cambridge)
- Doutor Eusébio Zeferino da Conceição (Faculdade de Ciências e Tecnologia, Universidade do Algarve)
- Doutor João Manuel de Almeida Serra (Faculdade de Ciências, Universidade de Lisboa)
- Doutor Guilherme Carvalho Canhoto Carrilho da Graça (Faculdade de Ciências, Universidade de Lisboa)
- Doutora Marta João Nunes Oliveira Panão (Faculdade de Ciências, Universidade de Lisboa)

Documento especialmente elaborado para a obtenção do grau de doutor

2016

Acknowledgements

This work would not have been possible without the financial support of Calouste Gulbenkian Foundation through Ph.D. Grant No. 126724.

I am grateful to my supervisor professor Guilherme Carrilho da Graça, for having accepted to guide me, for all the opportunities he provided me and the challenges he put me through which allowed me to learn more than I could ever expected.

To Filipa Silva, Daniel Albuquerque, António Soares and all the other students that contributed for an incredibly friendly and supportive working atmosphere in the “buildings team”.

To all my friends, for the friendship and support.

To my parents, my sister and my family for always encouraging me to keep improving.

To Luísa, who challenges me every days.

Finally, to Mariana, whom I admire deeply for being an example dedication and determination, and who always believed and encourage me.

.

Abstract

With the aim of creating adequate indoor conditions, modern buildings use energy for space heating, ventilation and air conditioning (HVAC). The environmental impact of this energy use creates an urgent need to develop strategies to reduce HVAC related energy consumption. This thesis contributes to this goal by testing and developing simplified models for highly efficient thermally stratified building displacement ventilation (DV) strategies. DV is characterized by thermal stratification that cannot be adequately modelled using the fully mixed room air approach that is common in overhead air conditioning system design. This thesis proposes a simplified approach for DV that models the room thermal stratification using three air temperature nodes: lower layer (floor level, 0.1m), occupied zone and upper mixed layer. The proposed approach is a development of one of the two models currently available in the open source thermal simulation tool EnergyPlus. A methodology for locating the neutral height in temperature profiles was developed. This methodology was used to verify the applicability of the Morton et al. (1956) plume flow equation to predict the neutral level in DV rooms. Detailed monitoring campaigns were carried out and the measurement results of several independent studies were analyzed in order to evaluate the performance of different DV systems configurations. The proposed model was successfully validated using thirty different full-scale experimental measurements in ten different room geometries, ranging from small laboratory test cells, classrooms, and a large concert hall. The model is able to simulate the air temperatures in the test cases with an average error of 5%, corresponding to a deviation of 0.4ºC. The experimental results show that the model provides significantly improved precision when compared to existing DV nodal models and demonstrate the ability of the three-node model to simulate DV systems in any of the configurations tested. The proposed model is simple and can be easily incorporated into a dynamic simulation program such as EnergyPlus.

Keywords

Displacement ventilation; thermal plume; neutral height; model validation; Energyplus.

Resumo

Com o intuito de criar condições ambientais adequadas, os edifícios modernos utilizam a energia para aquecimento, ventilação e ar condicionado (AVAC). O impacto ambiental da utilização desta energia cria a necessidade urgente de desenvolver estratégias para reduzir o consumo de energia associada aos sistemas de AVAC. Esta tese contribui para esse objetivo através do desenvolvimento de modelos simplificados para o eficiente sistema de ventilação por deslocamento do ar (DV). Os sistemas DV são caracterizados pelo desenvolvimento da estratificação térmica que não pode ser modelada adequadamente através da abordagem de ar completamente misturado, que é a mais comum no *design* de um sistema de AVAC. Nesta tese foi desenvolvida uma abordagem simplificada para modelar os sistemas DV que considera a estratificação térmica utilizando três nós de temperatura: a camada inferior (nível do chão, 0,1 m), zona ocupada e camada superior. A abordagem proposta consiste no desenvolvimento de um dos dois modelos atualmente disponíveis na ferramenta de simulação térmica EnergyPlus. Uma metodologia para localizar a altura neutra em perfis de temperatura foi também desenvolvida. Esta metodologia foi posteriormente utilizada para verificar a aplicabilidade da equação proposta por Morton *et al.* (1956) que permite prever a altura neutra em salas de DV.

Foram realizadas campanhas de monitorização detalhadas e os resultados de vários estudos independentes foram analisados com o intuito de avaliar o desempenho de diferentes configurações de sistemas DV. O modelo proposto foi validado com êxito, utilizando os resultados de trinta medições experimentais, considerando dez configurações diferentes, desde pequenas células de teste em laboratório, salas de aula, até uma grande sala de concertos. O modelo demonstrou ser capaz de simular os casos testados com um erro médio de 5%, o que corresponde a um desvio de 0.4ºC. Os resultados experimentais revelam que o modelo é significativamente mais preciso que os modelos nodais existentes e que tem a capacidade para simular qualquer uma das configurações de sistemas DV testadas. O modelo proposto demonstrou ainda ter a flexibilidade necessária para ser facilmente incorporado num programa de simulação dinâmica como EnergyPlus.

Palavras-Chave

Ventilação por deslocamento vertical; pluma térmica; altura neutra; validação de modelo; Energyplus.

Contents

List of nomenclature

DV	*Displacement ventilation*
CFD	*Computational fluid dynamics*
HVAC	*Heating, Ventilation and Air Conditioning*
NV	*Natural ventilation*
IAQ	*Indoor Air Quality*
CO_2	*Carbon dioxide*
SS	*Single-sided ventilation*
CV	*Cross-ventilation*
DSF	*Double skin façade*
Θ	*Adimensional temperature*
T	*Temperature (^0C)*
T_{in}	*Temperature of inflow air (^0C)*
T_{out}	*Room exhaust air temperature (^0C)*
z*	*Adimensional Height (m)*
z	*Height (m)*
z_{total}	*Total room height (m)*
F	*Inlet flow rate (m^3/s)*
α	*Plume entrainment constant*
g	*Acceleration of gravity (m/s^2)*
β	*Coefficient of thermal expansion (K^{-1})*
W	*Heat flux plume (W)*
h	*Neutral height (m)*

ρ	*Specific mass (Kg/m^3)*
C_p	*Thermal capacity of air at constant p (W m^3/ (kg K))*
n	*Number of thermal plumes*
NTG	*Average normalized temperature gradient along the total room height*
Z_0	*Virtual origin of thermal plume*
T_{OC}	*Temperature of room air in the occupied zone (^{0}C)*
T_f	*Temperature of floor surface (^{0}C)*
T_{Af}	*Temperature of room air in the horizontal layer adjacent to the room floor (^{0}C)*
T_{wl}	*Temperature of lateral surface that is below the mixed layer (^{0}C)*
T_{wu}	*Temperature of lateral surface that is above the mixed layer (^{0}C)*
T_{MX}	*Temperature of mixed layer node (^{0}C)*
T_c	*Temperature of ceiling surface (^{0}C)*
T_{in}	*Inflow air temperature (^{0}C)*
T_{CC}	*Chilled Ceiling surface temperature (^{0}C)*
T_{NCC}	*Non-chilled part of ceiling surface temperature (^{0}C)*
A_f	*Floor surface area (m^2)*
A_{wl}	*Lateral area exposed to the lower zone surface area (m^2)*
A_{wu}	*Lateral area exposed to the upper zone surface area (m^2)*
A_c	*Ceiling surface area (m^2)*
A_t	*Total area (m^2)*
h_f	*Heat transfer coefficient of floor surface (W/(m^2 K))*
h_{wl}	*Heat transfer coefficient of the lateral surface that is below the mixed layer (W/(m^2 K))*

h_{wu}	*Heat transfer coefficient of the lateral surface that is above the mixed layer (W/(m² K))*
h_c	*Heat transfer coefficient of ceiling surface (W/(m² K))*
h_{rc}	*Radiative heat transfer coefficient of ceiling surface (W/(m² K))*
h_{Rf}	*Radiative heat transfer coefficient of floor surface (W/(m² K))*
h_{rwl}	*Radiative heat transfer coefficient of the lateral surface that is below the mixed layer (W/(m² K))*
h_{rwu}	*Radiative heat transfer coefficient of the lateral surface that is above the mixed layer (W/(m² K))*
G	*Total internal heat gains (W)*
F_{MO}	*Fraction of the convective heat gains that is mixed into the occupied zone*
F_{GC}	*Fraction of total heat gains that are convective*
F_{GR}	*Fraction of total heat gains that are radiative*
I_M	*Inflow degree of mixing*
Sim	*Simulation result*
Meas	*Measurement result*
Avg. Error	*Average Error*
Avg. Dif.	*Average Difference*
Avg. Bias	*Averaged Bias*
h_{TMX}	*Room height where zero temperature gradient region begins*
CC/DV	*Displacement Ventilation system with Chilled Ceilings*
UFAD	*Under Floor Air Distribution*
R	*Cooling loads ratio*

Q_{DV}	*Portion of the total sensible gains that is removed by Displacement ventilation*
A^*	*Effective opening area*
a_t	*Top opening area*
a_b	*Bottom opening area*
H	*Total room height (m)*
UL	*University of Lisbon*
A_{in}	*Inlet opening area*
A_{out}	*Outlet opening area*
C_d	*Discharge coefficient*
ΔP	*Pressure difference*

List of figures

List of tables

1. Introduction

In the last decades the rising time that people spend in non-domestic buildings with heating, ventilation and air conditioning systems (HVAC) lead to a significant increase in HVAC related energy consumption in services buildings (up to 50% of the total energy consumed in these buildings [1]). In most non-domestic buildings the HVAC system is predominantly used to provide fresh air and cooling, ideally with the lowest energy consumption possible for a given location and internal load. In air based HVAC systems, the ventilation efficiency and inflow temperature can have a large impact in overall energy efficiency. In this context, the airflow distribution strategy is one of the most relevant decisions in HVAC system design [2,3]. The most commonly used airflow distribution method is mixing ventilation (MV). In MV systems the fresh air is supplied in the upper part of the room, at a temperature below 16ºC [4], mixing the high-level heat loads into the occupied zone promoting uniform air conditions (temperature and pollutants) throughout the whole space. However, the environmental impact of the HVAC systems energy consumption led to the continuous development of energy efficient solutions such as Displacement Ventilation (DV).

DV was initially developed in the 70's for applications in industrial halls in the Nordic countries. The ability of these systems to concentrate heat and pollutants in the upper portion of the space, where they can be exhausted without affecting the lower portion of the space, led to increased popularity and subsequent use in service buildings (starting in the early 80's [5]). In an effective DV system fresh air inserted near the floor, is drawn to the heat sources in a low velocity, self-regulating flow that was first studied by Sandberg and Sjoberg (1984) [6] and Skaret (1987) [7]. The inflow air should be supplied with low velocity and an inflow temperature that is 4-6ºC lower than the desired comfort temperature to avoid cold draft discomfort [6,7].The negatively buoyant inflow air spreads over the room floor until it reaches the heat sources where it expands and rises as a thermal plume. In DV, heat loads in higher levels of the room (above the occupied zone) are removed in an ideal way, with no impact in the occupied zone. In DV, whenever the room internal gains occur predominantly in the form of plumes, a noticeable interface occurs between the occupied zone of the room and a mixed hot layer near the ceiling of the room. This temperature and contaminant stratification removes heat and pollutants from the occupied zone with high ventilation efficiency [8,9].

The increased popularity of DV systems created difficulties for designers when sizing and predicting energy consumption of a stratified space that cannot be adequately

modeled with the fully mixed room air approach that is used for overhead air conditioning systems. The need to fine-tune the design of DV systems led to the development of several models with variable complexity. Sandberg and Lindstrom (1987) [10] proposed a mechanical DV design simplified model based on a two-region airflow structure, defining the lower boundary of the mixed upper layer, the neutral height, as the point where the total buoyancy induced plume flow equals the inflow rate [35]. Beyond the neutral height the continuously increasing plume flow is fed by room air, generating a mixed upper layer (this two layer structure is visible in figure 1a). In 1990, Linden et al. [11] developed a similar two-layer model for the more complex case of natural DV, using an experimental setup based on scaled salt-water models. In the salt-water experimental approach, buoyancy variations are generated by varying water salinity level in a container whose walls are impervious to salt, leading to a flow that only displays buoyancy effects from the plume sources (see figure 1a). DV airflows have internal heat sources that are part convective, part radiative and, even in the nearly adiabatic test chambers that are often used in DV system performance assessments, the room air exchanges heat with the room surfaces. The resulting air temperature profiles are smoother than the salinity, CO_2 or other non-buoyant pollutant profiles (see figure 1b): the effect of radiative heat transfer and resultant internal surface convective heat transfer is that part of the heat gains are mixed in the occupied zone and not convected upwards. Still, the DV vertical temperature variation profiles exhibit an upper mixed layer where the vertical temperature gradient is small. Controlling the neutral height is a DV system design objective: in most DV application cases there is a coincidence between heat and pollutant sources, resulting in a mixed layer region that contains the indoor pollutants and, therefore, should be kept above the occupants head height (above 1.3m for seated occupants or 1.8m for standing occupants). Increasing the room airflow-rate raises the neutral height by raising the point where the total thermal plume flow matches inflow. In addition to the neutral height, a successful DV system design must be able to control occupied zone and ankle level air temperatures.

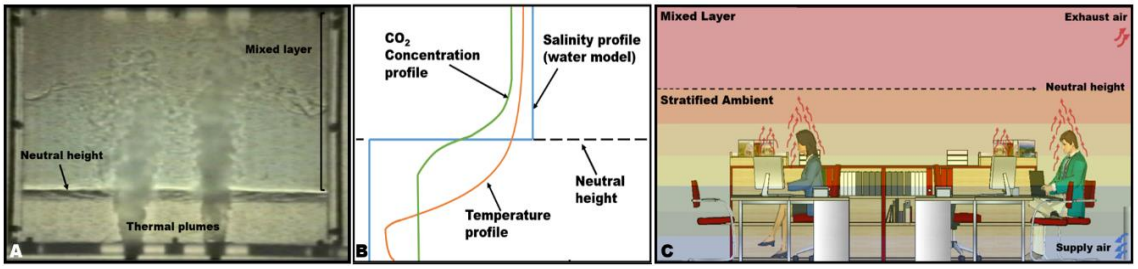

Figure 1. Image of DV flow in a scaled salt water mode (left [12]), typical temperature, concentration and salinity profiles (center), and a schematic depiction of a DV flow (right).

Currently, designers of DV systems have three methodologies for system sizing and prediction of energy consumption: simplified design methods [13], simplified models implemented in dynamic thermal simulation tools [14,15,16], and computational fluid dynamics (CFD) models [17,18,19]. With the widespread use of computer simulation, simplified sizing methods are becoming less popular due to their inability to predict whole year energy consumption. CFD is becoming more accessible, and should play an increasing role in HVAC design in the coming decades, but remains, for the moment, too time-consuming to be used in whole year simulation design scenarios. Simplified models implemented in dynamic thermal simulation tools are the most accessible option for design and building energy certification. Furthermore, a successful simplified model can provide insight and understanding of the design parameters that control the room flow field and air temperature.

1.1. Review of existing work

This review of existing work begins with a survey of experimental studies, followed by a brief discussion of the existing simplified models. In the last part, data from one of the experimental studies is used to assess the precision of the two models that are currently implemented in EnergyPlus.

1.1.1.Experimental studies

Existing experimental work on DV systems includes measurements in occupied buildings and test chambers. Model development and validation require complete data sets and controlled boundary conditions that, in the present case, can only be found in studies based on nearly adiabatic, mechanically conditioned test chambers. Table 1 shows the main characteristics of the DV test chamber studies that meet these criteria. Analysis of the table reveals a large range of mechanical ventilation flow rates, internal heat load and heat gain sources (thermal manikins, point sources, computers, etc.). The floor to ceiling height range is limited to typical office heights (2.2-2.8m), with the exception of one case with a large floor to ceiling height [20]. Most test chamber studies include experiments with two or more simultaneous heat sources with different magnitudes that generate asymmetric plumes.

In order to compare temperature profiles from different studies was introduced two commonly used non-dimensional variables (room temperature and height):

$$\theta = \frac{T - T_{in}}{T_{out} - T_{in}}, \quad z^* = \frac{z}{z_{total}} \qquad (1)$$

Figure 2 shows a typical test cell and the resulting average non-dimensional temperature profile obtained from the data of the first three studies in table 1.

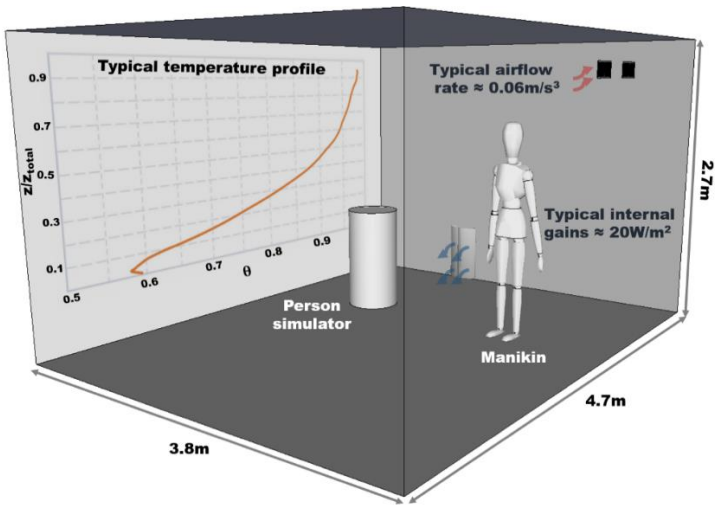

Figure 2. Typical geometry, heat gains, flow rate and temperature profiles for the test cell studies used to develop the present model.

Table 1 - Dimensions, internal gains and flow rates of DV test chamber experimental studies.

Reference	Test chamber dimensions		Plume type	Flow rate (m^3/h)	W/m^2
	Height (m)	Area (m^2)			
*H. Brohus, et al. [20]**	2.4 - 4	15 - 48	| vv | Vv|🧍|●|	8 - 27	145 – 395
*Yuan, X. [21]**	2.4	19	| Vv |🧍|💻|	23	183
*E. Mundt [22]**	2.6	17	| vv |🧍|	12	87 – 175
Ming Xu, et al. [23]	2.2	16	| v | vv |🧍|	6 - 26	162
G. He, et al.[24]	2.3	19	| Vv |🧍|💻|	5	202
I. Olmedo, et al. [25]	2.7	13	| Vv | ● |〰|	57	196
Simon J. Rees, et al. [26]	2.8	17	| v | vv |💻|	6 - 24	68 – 137
Xiufeng Yang, et al. [27]	2.6	11	| v | ● |	9	40
Josephine Lau, et al. [28]	2.7	25	| vv |🧍|	19	-
Lin Tian, et al.[29]	2.6	11	| Vv |🧍|💻|	23	-

v – single plume; vv - multiple symmetric plumes; Vv - multiple asymmetric plumes;

💻 – computer; 🧍 - person simulator; ● - point heat source; 〰 - radiator;

* - used to validate the model.

1.1.2. Existing simplified models

This bibliographic review identified three simplified nodal models with different approaches and number of nodes (table 2). There are two models that use a linear temperature variation along the room height. The simpler of these models, proposed by Mundt [30], uses two air nodes: a temperature near the floor surface (ankle level) and an upper node representing the exhaust air temperature. The second of the linear models (Li et al. [31]) is a development of the Mundt approach, using an additional node to characterize air temperature variations near the ceiling (leading to a total of three air nodes). The third model uses a three-node approach (near floor, occupied and mixed layer [32,33]) and predicts the neutral height using the inflow to total plume flow matching approach, discussed above. Temperature variation between the nodes is linear but with different slopes between the nodes (figure 3). This model requires a user-inputted coefficient to characterize the fraction of mixing of the heat gains into the occupied zone.

Table 2 - Displacement ventilation nodal models.

Reference	**Number of room air nodes**	**Temperature gradient**	**Neutral level calculation**
Mundt (1996) [30]	2	Linear	No
Li et al. (1992) [31]	3	Linear	No
Graça and Linden (2004) [33]	3	Linear, variable between nodes	Yes

1.1.3. Accuracy of existing models

Figure 3 shows two simulations of the test chamber study of Mundt [22] using the two models discussed above that are available in EnergyPlus: Mundt [30] and Graça & Linden [33]. Analysis of the results reveals qualities and limitations in both models, namely:

- As expected, both models have good accuracy when predicting the exhaust temperature: it is a direct application of energy conservation.
- Both models under predict the ankle level temperature; resulting in significant error in a design parameter that is used to define the inflow temperature and predict thermal comfort. Neither of the models considers mixing of inflow air with room air.

- In the Graça and Linden model the results are sensitive to a user-supplied coefficient: the fraction of heat gains mixing into the occupied zone. Further, there is no guidance for the value that the user should use in different gains scenarios.
- The linear temperature gradient used in the Mundt model does not display the two-layer behavior that is visible in the temperature profiles. This simplification prevents the designer from using the model to fine-tune the inflow rate for improved air quality in the occupied zone.

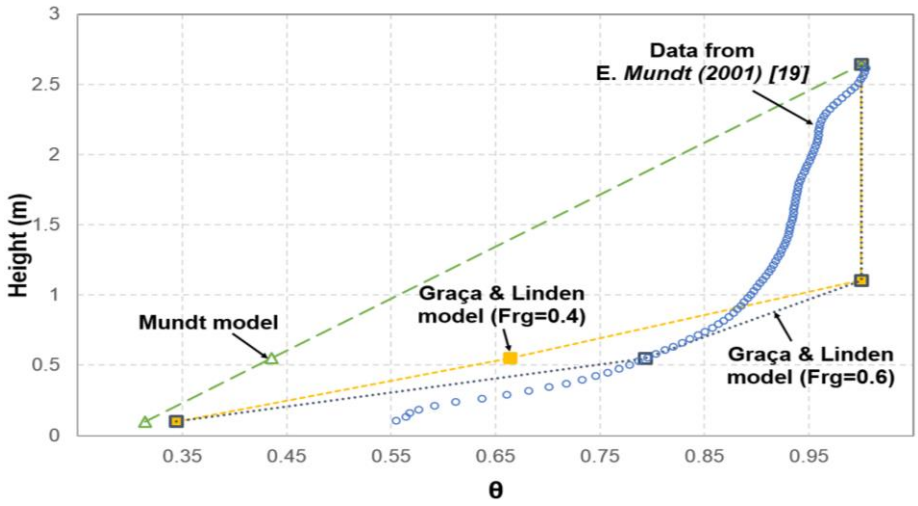

Figure 3. Comparison between Mundt [30], Graça and Linden [33] DV models and measured data.

The results indicate that the approach used by both models to calculate ankle level temperature, based on adjusting the inflow temperature to incorporate heat exchange with the room floor may be inadequate. This approach may have been more adequate for rooms with inflow through slots, with no diffusion since this simple inflow geometry generates a gravity current of cool inflow air that has limited mixing as it spreads across the room floor. More recent DV systems and experimental facilities use DV flow diffusers that promote mixing with warmer room air, thereby increasing ankle level air temperature and reducing cold draft induced discomfort.

1.1.4. Research questions

The analysis performed in the previous sections resulted in the following research questions that must be addressed in the development of simplified modelling approaches for DV systems:

1. Is the matching of plume flow to inflow approach valid for defining the neutral level in a room with mixed heat sources (convective and radiative)?

2. What is the fraction of heat gain mixing in the occupied zone that best fits the slowly varying temperature profiles found in the experimental data?
3. What is the level of mixing between inflow and room air that best fits the experimental data?
4. How the neutral height position is affected by chilled ceiling temperature in a CC/DV room? Could the proposed DV simplified model be applied to model CC/DV rooms?
5. Are the thermal stratification profiles in occupied buildings with active boundary conditions similar to the ones measured in (nearly adiabatic) test cell cases?
6. In large DV rooms, how do the radiative heat exchanges with the walls could affect the expected temperature and contaminants vertical profiles?
7. What is the impact of a thermal chimney in natural DV system performance?

1.2. Publications

The work developed in this thesis resulted in the publication of four papers in international peer-review journals and two refereed conference papers. Further, there are three more journal papers that are currently under review:

- *Paper I* – "Thermal and airflow simulation of the Gulbenkian Great hall" by Nuno M. Mateus and Guilherme Carrilho da Graça published in Proceedings of 13th international conference on building simulation, Chambery, France (2013).
- *Paper II* – "Validation of EnergyPlus thermal simulation of a double skin naturally and mechanically ventilated test cell", by Nuno M. Mateus, Armando Pinto and Guilherme Carrilho da Graça published in the journal Energy and Buildings, 2014.
- *Paper III* – "A validated three-node model for displacement ventilation", by Nuno M. Mateus and Guilherme Carrilho da Graça published in the journal Building and Environment, 2015.
- *Paper IV* – "Simplified modeling of displacement ventilation systems with chilled ceilings", by Nuno M. Mateus and Guilherme Carrilho da Graça published in the journal Energy and Buildings, 2015.
- *Paper V* – "Stack driven ventilative cooling for schools in mild climates: analysis of two case studies", by Nuno M. Mateus and Guilherme Carrilho da Graça, published in Proceedings of 36th AIVC Conference Conference, Madrid, Spain (2015).

- *Paper VI* – “Validation of a lumped RC model for thermal simulation of a double skin natural and mechanical ventilated test cell”, by Marta J.N. Oliveira Panão, Carolina A.P. Santos, Nuno M. Mateus and Guilherme Carrilho da Graça published in the journal Energy and Buildings, 2016.
- *Paper VII* - “The effect of typical buoyant flow elements and heat load combinations on room air temperature profile with displacement ventilation”, by Risto Kosonen, Natalia Lastovets, Panu Mustakallio, Nuno Mateus and Guilherme Carrilho da Graça, submitted to the journal Building and Environment, 2016.
- *Paper VIII* - "Comparison of measured and simulated performance of natural displacement ventilation systems for classrooms”, by Nuno M. Mateus and Guilherme Carrilho da Graça, submitted to the journal Energy and Buildings, 2016.
- *Paper IX* – “Measured performance of a displacement ventilation system in a large concert hall”, by Nuno M. Mateus and Guilherme Carrilho da Graça, submitted to the journal Building and Environment, 2016.

1.3. Outline of thesis

The thesis is organized in seven chapters. Chapter 1 presents a literature review about displacement ventilation concepts, the existing experimental work and the most used modelling approaches. Chapter 2 presents a validated simplified approach for DV that models the room thermal stratification using three air temperature nodes: lower layer (floor level), occupied zone and upper layer. An extension of the proposed model to CC/DV systems is showed and validated on Chapter 3. Chapter 4 presents a set of detailed measurements of buoyancy driven natural DV systems of three classrooms. The measurements were used to analyze the performance of natural DV systems and to validate the three-node DV model (presented on Chapter 2) implemented on the open-source thermal building simulation software EnergyPlus. In Chapter 5, the performance of two DV large rooms was analyzed using a set of detailed measurements. Chapter 6 presents the application of the modeling approaches developed along the thesis in three design projects: two naturally ventilated DV schools and the refurbishment of the Calouste Gulbenkian large concert hall HVAC system. Finally, Chapter 7 presents the conclusions of the work and a discussion of future developments.
Table 3 presents the relation between the papers that resulted from this thesis and the chapters.

Table 3 - Correspondence between papers and Chapters, referring its application and main topic

Chapter	Paper	Topic
1	III	Literature review
2	III	Proposed three-node DV model
3	IV	Extension of the proposed model to CC/DV systems
4	VIII	Analysis of Natural DV systems and model validation
5	IX	Analysis of DV systems in large rooms and model validation
6	I and V	Application of the developed DV model in real projects: 2 schools and a large concert hall

2. A validated three-node model for displacement ventilation

This chapter presents a simplified model for DV that approximates the room thermal stratification using three air temperature nodes: lower layer (floor level), occupied zone and upper layer. The proposed model is a development of a model that is currently available in the thermal simulation tool EnergyPlus. The proposed developments increase modeling accuracy and robustness by minimizing the need for user supplied coefficients. The following sections presents an analysis of the applicability of plume flow theory as a criterion to establish the neutral level, followed by a presentation of the model equations. Finally, in section 2.3, is presented the model validation using results from several independent experimental campaigns.

2.1. Prediction of neutral height

In concentration profiles, such as the ones shown in figure 5, the location of the neutral height can be defined by visual inspection. In contrast, in the temperature profiles found in DV rooms, this location is much more difficult to identify (Huijuan Xing et al. (2002) [34]). This section investigates whether the temperature gradient found in DV rooms with approximately adiabatic boundary conditions displays a neutral height that can be predicted using the plume flow to inflow matching principle. For this purpose, i begin by developing and validating a quantitative method to locate the neutral height in temperature gradients. Then, i proceed to use the method to obtain the neutral height for a set of experimental cases where only temperature profiles are available (the most common scenario). Finally, this dataset is used to check the applicability of the plume flow matching principle to rooms with mixed heat sources and heat transfer in the envelope.

To model the vertical variation of the total flow from a point plume the solution proposed by Morton et al. (1956) [35] was used:

$$F = \frac{6}{5}\,\alpha^{\frac{4}{3}}\,\sqrt[3]{\frac{9}{10}}\;\pi^{\frac{2}{3}}\,\sqrt[3]{\frac{g\,\beta\,W}{\rho\,Cp}\,h^5} \qquad (2)$$

This expression includes two coefficients, β and ρ, that are temperature dependent and were determined using the average values for the experimental cases that are used to test the model (resulting in, β= 0.0034 and ρ = 1.14kg/m^3). The other constant in this expression,α, accounts for ambient fluid entrainment (Morton et al. (1956) [35], α = 0.13).

Rearranging equation 2 to isolate the neutral height, h, for a given room inflow F, and point buoyancy source W, was obtained:

$$h = 23.95 \sqrt[5]{\frac{F^3}{W}} \quad (3)$$

When there are *n* non-coalescing plumes with equal strength the neutral height is given by:

$$h = 23.95 \sqrt[5]{\frac{F^3}{W\, n^3}} \quad (4)$$

Equation 2 was developed for plumes generated by point sources of convective heat. Yet, the heat gains found in real building are generated in the surface or a volume such as an occupant or a computer monitor (for both cases most experimental studies propose a 50% split between convective and radiative heat gains). To apply the point plume expression to these geometries a virtual origin must be defined for each heat source [36,37,38]. The virtual origin will be positioned at a height z_0 below the top of the heat source and can be calculated using two different approaches. In the minimum approach the spreading angle of the plume is 25º and the virtual origin is located approximately one third of the heat source characteristic diameter above the bottom of the heat source. In the maximum approach the point source is located in a point so that the border of plume above that point passes through the top edge of the real source [39]. In the present case, it was proposed to use the minimum approach to correct for the point plume height when using real sources (a conservative approach).

In cases where there are several buoyancy sources there is a need to check for two factors: thermal plume coalescence and relative strength of the buoyancy sources. Coalescence is a factor because the total plume flow rate of coalesced plumes increases less with height due to a smaller entrainment perimeter (compared to two isolated plumes). For this reason, the neutral height will rise if plumes coalesce before the mixed upper layer. Figure 4 shows the method used to check for plume coalescence (based on the minimum approach described above). In the example shown in the figure there is no coalescence effect since: $X_{plume1}+X_{plume2} > X_{12}$ is larger than h_{12} (the neutral height calculated using expression 4, with *n*=2). Expression 4 is valid for *n* plumes of equal strength. For *n* plumes of unequal strength was proposed an approximate application of this expression by considering *n* plumes of equal strength. Still, because the proposed method relies on an identifiable temperature transition, the experimental cases used below have, in each case, a maximum range of asymmetry in plume strength of two to one.

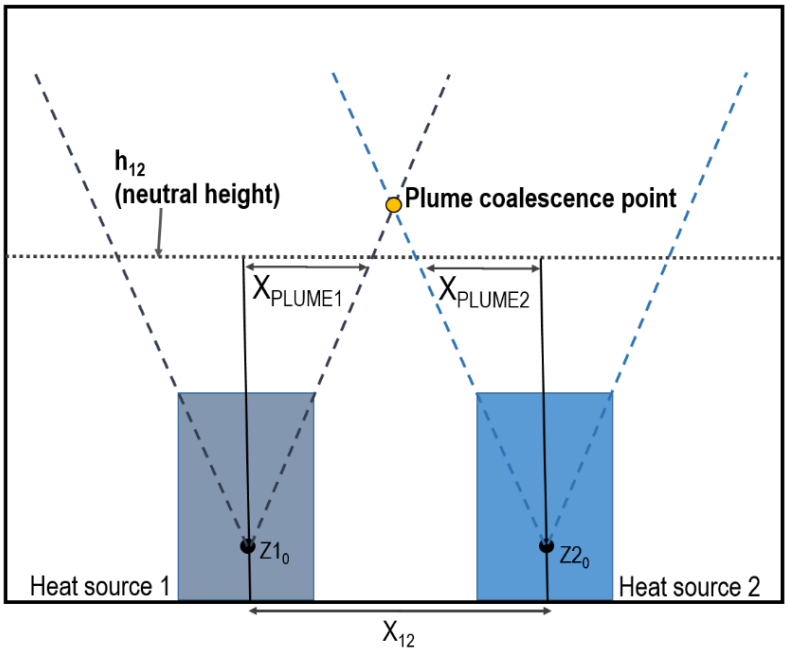

Figure 4. Geometric method to test plume coalescence.

2.1.1 Methodology for predicting the neutral height from temperature profiles

To develop the methodology i will use three independent experimental studies with simultaneous measurement of CO_2 concentration and temperature (shown in table 3). Analysis of the temperature profile shown in figure 3 can provide hints for a successful quantitative methodology to locate the neutral height: the rate of temperature increase between the floor and the lower part of the mixed layer is markedly higher than in the rest of the room height. The proposed method locates the point in the region of this gradient transition that matches the neutral height obtained from concentration gradients. I start by defining the average normalized temperature gradient along the total room height (NTG):

$$NTG = \frac{T_{z_{ceiling}} - T_{z_{floor}}}{Z_{ceiling} - Z_{floor}} \qquad (5)$$

Next, all experimental temperature profiles are discretized using one hundred, equally spaced points (along z, from floor to ceiling) and a rolling average smoothing with a ± 0.1m vertical averaging interval is applied to avoid false results due to local inflections in the experimental profiles. Starting from the floor, the method uses a forward marching logic check to identify the first point with a local gradient, defined using points z+1 and z, that is larger than NTG by a factor that will be calculated using the three cases where both profiles are available:

$$(1+C_{NH}) \times \frac{T_{z_{total}} - T_{z_0}}{Z_{total} - Z_0} > \frac{T_{z+1} - T_z}{(Z+1) - Z} \qquad (6)$$

To find the value of the coefficient (C_{NH}) that result in the best agreement between temperature and pollutant profile based neutral heights the method was applied to the profiles measured in three independent experimental studies shown in table 3. The best fit was obtained when: C_{NH} = 0.3. Figure 5 shows the results of applying the method to one of the three studies used (Brohus et al [20]).

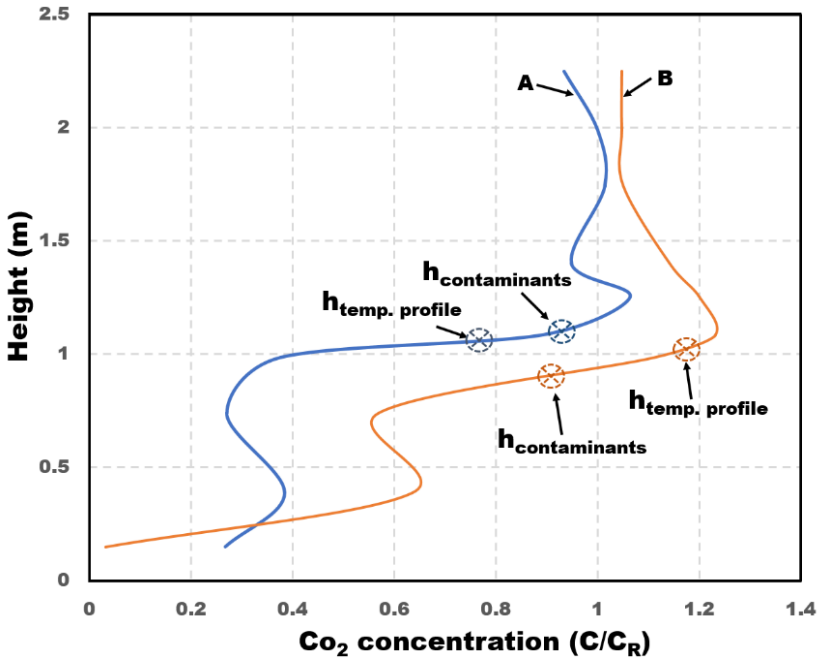

Figure 5. Comparison between the neutral height obtained from contaminant profiles (by visual inspection) and thermal profiles (applying the proposed algorithm). Measurements by Brohus et al. [20].

To quantify the differences between the neutral heights predicted by the two methods the following error indicators were used:

$$\text{Bias (m)} = h_{\text{temp. profile}} - h_{\text{comtaminants}} \quad (7)$$

$$\text{Error (\%)} = 100\% \times \left| \frac{h_{\text{temp. profile}} - h_{\text{comtaminants}}}{h_{\text{temp. profile}}} \right| \quad (8)$$

Table 4 - Comparison between concentration and temperature neutral heights for three independent studies.

Reference	$h_{temp.\ profile}$	$h_{contaminants}$	Bias (m)	Error (%)
Brohus et al. [20]	1.04	1.06	-0.02	1.7
	1.01	0.91	0.10	9.8
Bouzinaoui et al. [40]	3.98	3.83	0.15	3.8
Trzeciakiewicz, et al. [41]	0.83	0.91	-0.08	9.6
Average indicators			**0.04**	**6.2**

The results presented in table 3 confirm the validity of the proposed method: the bias is negligible (4cm) and the maximum error is less than 10%.

2.1.2 Validation of neutral height prediction

The method developed in the previous subsection can be used to evaluate the precision of expressions 4 and 5 using a larger set of experimentally measured temperature profiles, shown in table 1, including different heat gains densities, airflow magnitudes and type of heat gain. Still, not all studies presented in table 1 can be used to validate the model since, in some cases, not all the test cell dimensions, airflow rate, temperature and heat gain information is available. Further, the heat gains must be static and not unrealistically small: Cases with internal heat gains of less than 7.5 W/m^2 should be avoided since typical office buildings have at least 20W/m^2. Cases with very small heat gains display large effects of heat loses in the envelope that, in some cases, can exceed 10% of the total heat gains [42]. Application of these rules resulted in three selected studies that will be used to validate the model presented in this paper: Brohus et al. [20], Yuan [21], Mundt [22] (the first three cases in table 1, signaled with a "*").

The results shown in table 4 and figure 6 confirm the applicability of expressions 4 and 5 to predict the neutral height. The average error obtained is 14%, and the correlation coefficient, R^2, is 0.69.

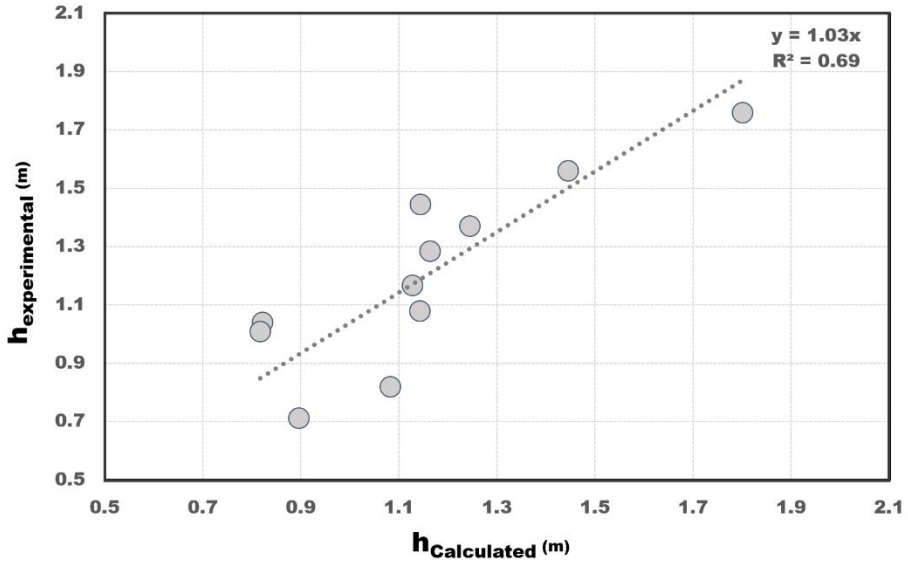

Figure 6. Correlation between calculated and experimental neutral heights.

Table 5 - Comparison between calculated and experimental neutral heights.

Reference	$h_{calculated}$ (m)	$h_{measured}$ (m)	Bias (m)	Error (%)
Brohus et al. [20]	0.82	1.04	0.22	21.0
	0.82	1.01	0.19	19.1
	1.14	1.45	0.30	20.9
	1.16	1.29	0.12	9.5
	1.14	1.08	-0.06	5.8
	1.44	1.56	0.11	7.4
	1.80	1.76	-0.04	2.4
Yuan [21]	1.13	1.16	0.04	3.3
Mundt [22]	0.90	0.71	-0.18	25.7
	1.08	0.82	-0.26	32.0
	1.24	1.37	0.13	9.2
Average indicators			**0.18**	**14.2**

2.2. A simplified three node DV model

The proposed model extends the perfectly mixed room air single node approach to three nodes located along the room height (shown in figure 7). The model considers fully mixed air in each node and a linear air temperature variation between nodes. The three model nodes represent three distinct room regions:

- The floor level air temperature node (T_{Af}) characterizes the temperature of the air that is entrained by the plumes into the occupied zone. This point is located at 0.1m height.
- The occupied zone air temperature node (T_{OC}) is located in the center of the occupied zone (0.65m for seated occupants and 0.9m for standing occupants).
- The mixed layer air temperature node (T_{MX}) characterizes the exhaust/mixed layer temperature and represents a region that begins above the neutral height and ends at the ceiling. In the model, this region is isothermal.

All plumes are modeled as point sources of buoyancy. The floor level temperature is obtained by imposing energy conservation to the balance between the heat that is exchanged with the floor, convected to the occupied zone (with the flow rate *F*), and the portion of air that is mixed with the air of the occupied zone. Measurements by Fatemi et al. [43] show that, at a distance of 3.5m from a DV corner diffuser there is as an entrainment generated accumulated flow rate increase of approximately 60% (I_M = 0.6 in equation 9). This mixing between inflow and room air is not modeled in any of the three existing models and will be introduced in the improved model. Finally, the neutral height is predicted using expression 3 or 4 (for single or multiple plumes). The energy conservation equations for the three model nodes are the following:

$$\rho.Cp.F.T_{in} + I_M.\rho.Cp.F.T_{OC} + A_f.h_f.(T_f - T_{Af}) = (1+I_M).\rho.Cp.F.T_{Af} \quad (9)$$

$$(1+I_M).\rho.Cp.F.T_{Af} - I_M.\ \rho.Cp.F.T_{OC} + F_{MO}\ .F_{GC}.G + A_{wl}.h_{wl}.(T_{wl} - T_{OC}) = \rho.Cp.F.T_{OC} \quad (10)$$

$$\rho.Cp.F.T_{OC} + F_{GC}.G.(1 - F_{MO}) + A_c.h_c.\ (T_c - T_{MX}) + A_{wu}.h_{wu}.(T_{wu} - T_{MX}) = \rho.Cp.F.T_{MX} \quad (11)$$

The parameter F_{MO} characterizes the fraction of the convective heat gains that is mixed into the occupied zone, and, therefore, not convected directly to the mixed layer ($0< F_{MO} <1$). This lower level mixing does not occur in an ideal displacement system (F_{MO} =0). As discussed above in the existing three-node model [32] the value of this parameter was not known, yet, as shown in figure 3, its effects on the results are relevant. The database that will be used to validate the model in the next section will be used to obtain the best-fit value for F_{MO}.

Heat transfer from internal surfaces is evaluated using convection coefficients developed for DV heat transfer (Novoselac et al. (2006) [44]) and the air temperature of the room node that is in direct contact with the surface: the floor surface is coupled to T_{Af}, the ceiling is coupled to T_{MX} and the lateral surfaces are coupled to T_{oc} or T_{MX} (depending on their vertical location). For lateral surfaces that are in contact with the occupied zone and

mixed layer an area weighted room air temperature is used. Radiation heat exchange between surfaces is evaluated using exact view factors that are available for rectangular cavities [45]. The room surface energy conservation equations are the following:

$$h_c(T_c - T_{MX}) + h_{rc}\left(T_c - \frac{T_f A_f + T_{wl} A_{wl} + T_{wu} A_{wu}}{A_t - A_c}\right) = F_{GR}\, G/A_t \quad (12)$$

$$h_f(T_f - T_{Af}) + h_{rf}\left(T_f - \frac{T_c A_c + T_{wl} A_{wl} + T_{wu} A_{wu}}{A_t - A_f}\right) = F_{GR}\, G/A_t \quad (13)$$

$$h_{wl}(T_{wl} - T_{OC}) + h_{rwl}\left(T_{wl} - \frac{T_c A_c + T_f A_f + T_{wu} A_{wu}}{A_t - A_{wl}}\right) = F_{GR}\, G/A_t \quad (14)$$

$$h_{wu}(T_{wu} - T_{MX}) + h_{rwu}\left(T_{wu} - \frac{T_c A_c + T_f A_f + T_{wl} A_{wl}}{A_t - A_{wu}}\right) = F_{GR}\, G/A_t \quad (15)$$

This seven equation system (equations 9-15) is nonlinear due to the temperature difference dependent convective heat transfer correlations. As in other models implemented in EnergyPlus, coupling between the energy balance equations (9-15) and the convection correlations is indirect: air and surface temperatures from the previous time step are used to calculate heat transfer coefficients that are used in the following time step. This coupling approximation has no effect on the steady state validation cases presented below: the solutions algorithm ran until the solution stabilized (typically in 10 iterations).

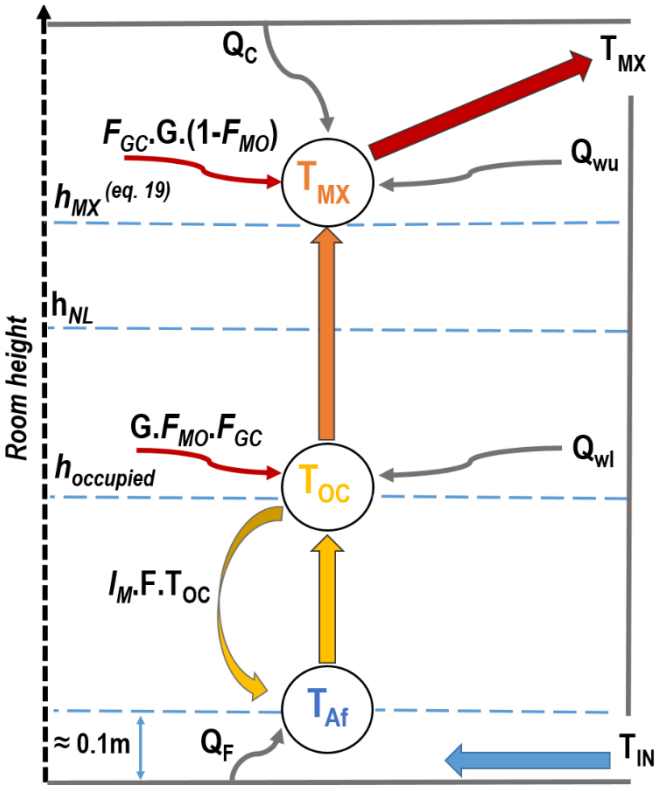

Figure 7. Proposed model structure.

2.3. Model validation

This section presents an assessment of model precision based on experimental data from the first three studies shown in table 1 (for a total of nine different cases). In addition, this database will be used to define the height of the mixed layer node (T_{MX}) as a function of neutral height as well as finding the best-fit value for the parameter that characterizes heat gain mixing (F_{MO}). The model predictions will be evaluated using the following average error indicators:

The average norm of the error: Avg. Dif. (K) = $\frac{\sum_{i=1}^{9}|Sim._i-Meas._i|}{9}$ (16)

The average bias: Avg. Bias (K) = $\frac{\sum_{i=1}^{9} Sim._i-Meas._i}{9}$ (17)

The average percentage error: Avg. Error (%) = $\frac{100\%}{9} \times \sum_{i=1}^{9} \left|\frac{Sim._i-Meas._i}{Meas._{Max.}-Meas._{Min.}}\right|$ (18)

The first application of the experimental database is to define the height of the mixed air node (T_{MX}). As shown in section 2.1, in all temperature profiles analyzed, the neutral height is lower than the bottom of the boundary of the room region where the vertical temperature gradient tends to zero. The upper mixed layer model node (T_{MX}) should be positioned in the lower edge of this nearly zero gradient region. Analysis of the portion of the nine profiles that is above the neutral height revealed that the zero gradient region begins at the height:

$$h_{T_{MX}} = h + \frac{h_{ceiling}-h}{3} \quad (19)$$

The second application of the experimental database and error indicators is to obtain the best-fit value for the parameter that models convective mixing of internal heat gains into the occupied zone (F_{MO}). For this purpose, model runs with F_{MO} varying between zero and one were performed. The results of these simulations show that the best-fit value is 0.4 (figure 8). This value is identical to the value found by the same authors when comparing the model predictions with CFD simulations of the large concert hall [46].

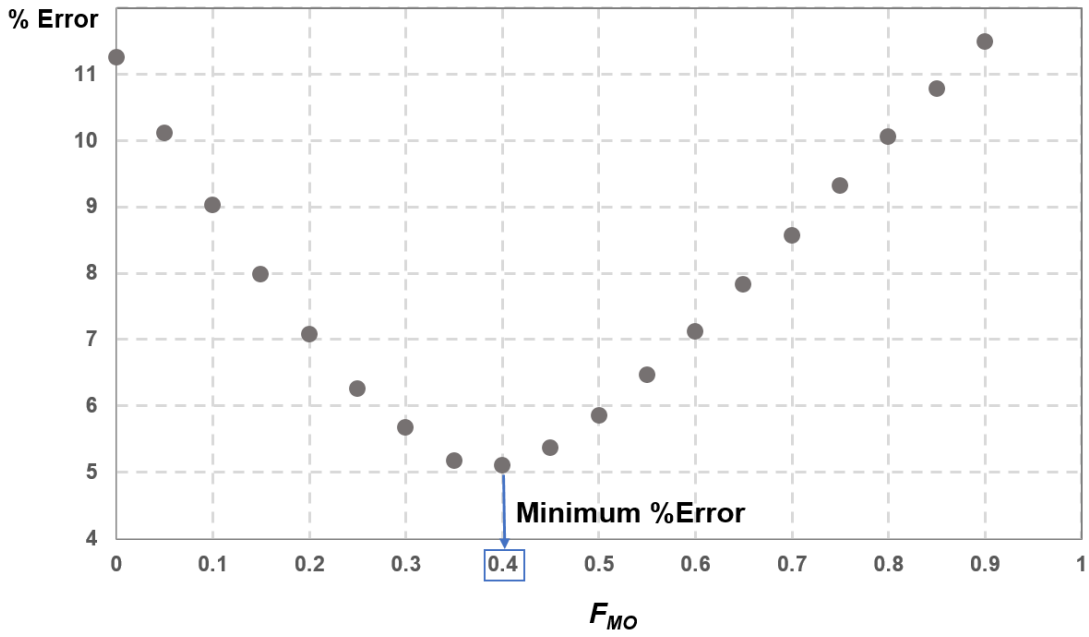

Figure 8. Convective mixing of internal heat gains into the occupied zone (F_{MO}) determination.

Figure 9 shows the results of the model simulation of the nine cases in the database. In light of the model simplicity the results are encouraging: general agreement is good in all nodes. The discrepancies found in some cases were expectable given the large amount of model simplifications used and uncertainties in the experimental boundary conditions (in most experimental studies the boundaries can be best described as “nearly adiabatic” [26]). Figure 10 shows a comparison between the existing and improved model. The improvements are clear, particularly in the floor level and occupied zone temperature predictions.

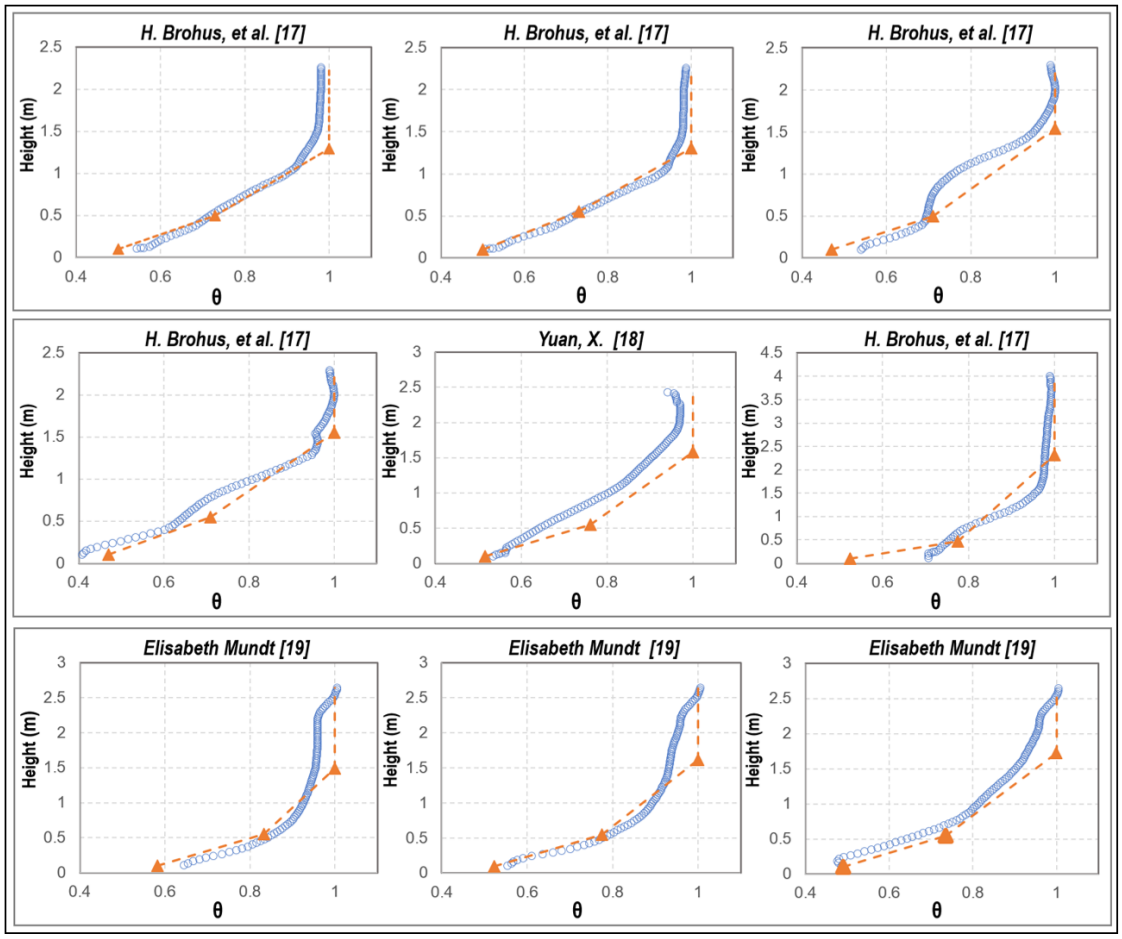

Figure 9. Results of the model simulation for the cases in the database and comparison with measured data.

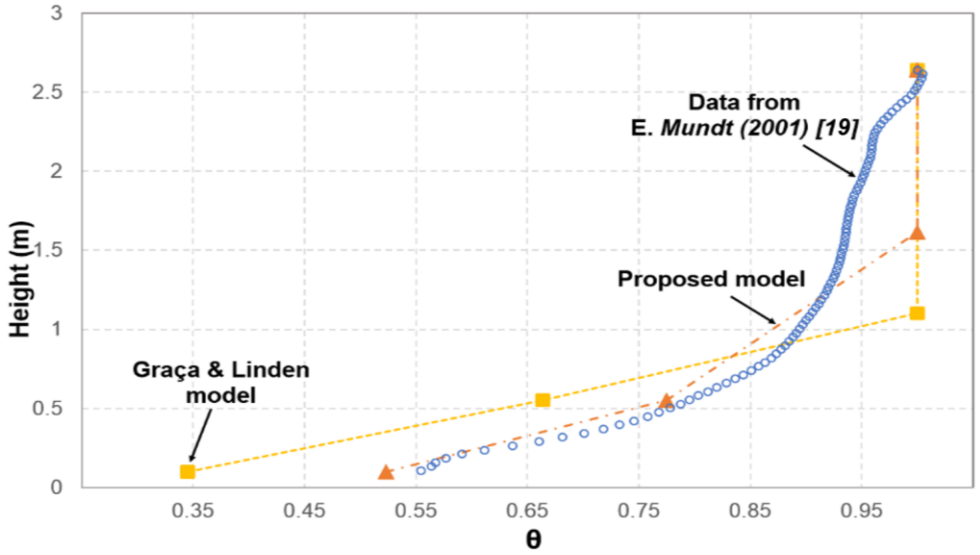

Figure 10. Comparison between proposed model, Graça and Linden [33] DV model and measured data.

Table 5 shows the values of the average error indicators for the nine temperature profiles. The overall average simulation error of 5%. The node with the largest average

error is T_{af} (6%) with a bias towards under prediction. The average temperature error is 0.3K in a dataset that has an average temperature difference between inlet and outlet of 5K. Table 5 also includes the error indicators for the existing model: the improvement is clearly visible in the overall reduction of 17% in model error.

Table 6 - Validation of proposed model and comparison with Graça & Linden [33] model results.

Node	Dif. (K)		Bias (K)		Error (%)	
	Proposed model	Graça& Linden model	Proposed model	Graça& Linden model	Proposed model	Graça& Linden model
T_{af}	0.3	1.5	-0.2	-1.5	6.2	31.4
T_{OC}	0.2	1.7	0.1	-1.7	3.7	28.6
T_{MX}	0.3	0.4	0.1	-0.4	5.3	5.6
Average	**0.3**	**1.2**	**0.0**	**-1.2**	**5.1**	**21.9**

Model limitations

In light of the approximations used in the model, it is expectable that the modeling precision will be greatly reduced in the following cases:

- Internal gains split into several highly asymmetric plumes: these cases generate a stratification profile with several neutral levels that is not captured by the current model.
- Internal heat gains that are predominantly radiative: in these cases convective heat transfer in the room surfaces heated by the radiative gains can compete with the convective heat gains in the occupied zone, creating a more linear temperature gradient with no identifiable neutral level.
- Spaces that are dominated by facade heat gains: ideally the total heat exchange with the building envelope must be one order of magnitude lower than the total occupied zone internal gains (as in the test chamber studies that were used to validate the model). This topic will be analyzed in Chapter 4.
- When high-level lighting loads, currently not explicitly included in the model, are comparable to the occupied zone heat gains.
- Rooms with chilled ceilings or chilled floors.

This last limitation is not due to the physics of the model since heat transfer from a chilled ceiling or floor is considered in the model equations. Still, additional research on this

topic to investigate the chilled ceiling capability to disrupt the stratification and the effects of a chilled floor on ankle level temperature will be addressed in Chapter 3.

2.4. Conclusions

A simplified three-node model for prediction of temperature gradient and neutral level location in DV rooms was successfully developed and validated using three independent experimental studies. In addition, a methodology for locating the neutral height in temperature profiles was developed and a verification of the applicability of Taylor's plume flow equation to predict the neutral level in DV rooms was performed. The proposed model provides significantly improved precision when compared to existing DV nodal models, in particular in the floor level and occupied zone temperatures.

Tests of the Taylor point plume flow equation using a database composed of eleven cases from three independent studies showed that, when applying the total plume flow to inflow matching approach, using Taylor's expression to model plumes generated by real heat sources, the average error in neutral level prediction is 14%. The same database was used to validate the temperature predictions of the model, revealing an average error in the three room node temperatures of 0.3K (5%).

The proposed model is easy to use when implemented in a whole year building thermal simulation tool. Model inputs are limited to the height, number and magnitude of the heat sources in the occupied region. The capability of the model to predict the effect of inflow rate on the location of the neutral height allows for straightforward fine-tuning of DV designs.

3. Simplified modeling of Displacement Ventilation systems with Chilled Ceilings

In the HVAC design community DV systems are known to be an effective air distribution strategy for office buildings due to its potential to reduce room air velocities, ventilation induced noise and HVAC energy consumption [47]. In spite of these well-established qualities these systems do not have widespread use due to poor heating performance and limited space cooling capability (25-35W/m^2 [48,49,50]). Continuous improvement in building envelope insulation has greatly decreased the need for space heating. Still, in many office buildings conventional DV cannot remove the maximum cooling load that often exceeds 50W/m^2. To overcome this cooling limitation the HVAC design and research community has developed two DV system variants: under floor air distribution (UFAD [51]) and the combination of DV with chilled ceiling systems (CC/DV [52,53]). In UFAD systems air is inserted into the room from an under floor plenum using swirl diffusers that induce more mixing than standard DV diffusers, allowing for a higher differential between inflow and room air temperature difference (10ºC) and, consequently, higher cooling capacity. In the CC/DV approach, shown in Figure 11, DV inflow air removes the latent loads and a portion of the sensible load, while the CC system removes the remaining sensible load (mostly by radiative heat transfer). With this combined approach the cooling capacity can reach 100 W/m^2 [54,55] while maintaining the use of standard low velocity DV diffusers. In a successful CC/DV system, the CC is able to add cooling power without compromising the stratified DV flow.

Design of stratified ventilation systems is more complex than conventional overhead mixing systems since the perfectly mixed room air approximation cannot be used to predict internal conditions. In fact, the main goal in DV modeling is to predict the vertical temperature gradient in the room and also manage the position of the lower boundary of the upper layer of room air where indoor pollutants are concentrated. These seemingly simple tasks are difficult as many flow and room geometry features contribute to the stratification: room height, airflow rate and temperature, type, location and strength of the buoyancy sources. Accurate prediction of the vertical temperature gradient is key for fine tuning of system design and sizing as well as accurate predictions of energy consumption and thermal comfort. The inclusion of a CC system increases the complexity of the design by adding the need to use its cooling power without compromising the stratified environment of the DV system. An excessively low CC surface temperature can destroy the stratification and even create condensation in the

CC surface. The stratification is disrupted when the upper mixed layer temperature approaches the occupied zone temperature, creating a mixed room air environment. Condensation occurs when the CC surface temperature drops below the dew-point temperature, a problem that is more likely to occur in rooms with a high portion of latent heat gains [53].

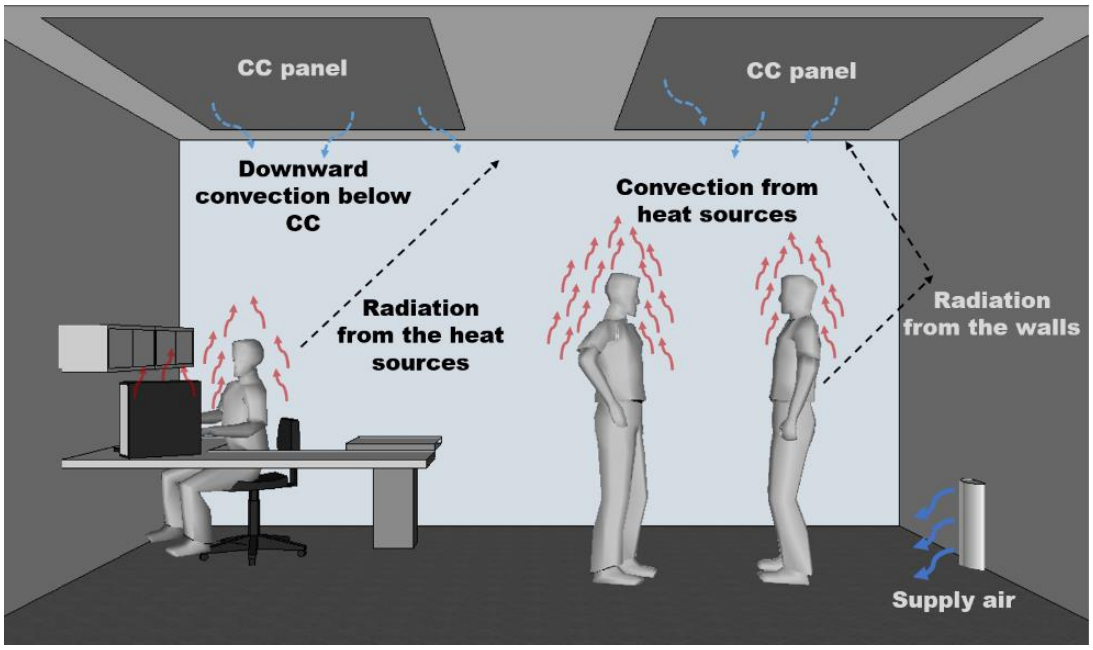

Figure 11. Scheme of CC/DV system driving mechanism.

To size and predict energy consumption of CC/DV systems designers can use three approaches: simplified design methods [56], computational fluid dynamics simulations (CFD, [57]) and room air stratification models implemented in dynamic thermal simulation tools. Simplified sizing methods are useful in early design but cannot predict whole year energy consumption (a common requirement for building energy certification [58]). Reynolds averaged Navier Stokes CFD simulations are increasingly used in design but remain a computationally heavy tool for CC/DV design analysis. Further, in these applications, CFD is hampered by errors in the estimation of mixed convection that have been known for a long time [59] but are still being resolved [60,61]. Further, designers are often faced with the task of simulating multiple rooms, occupation and outside weather scenarios, making CFD simulation very time consuming. In this context, simplified models implemented in dynamic thermal simulation tools are the preferred option.

Although there are several models available for DV, none of the models was tested and validated for CC/DV with variable geometry and internal gains. This chapter presents a simplified model for CC/DV systems that is based on DV model presented on Chapter 2.

The model characterizes the room stratification using three nodes that characterize a CC/DV temperature profile: floor level, occupied zone and mixed upper layer. The next section presents a review of experimental and simulation CC/DV studies. This review is followed by a discussion of the effects of the CC on the vertical variation of the air temperature profile. The following section presents a method to determine the position of the lower interface of the mixed upper layer. This section is followed by a presentation of the assumptions and approximations used in the model. In the validation section a set of twelve experimental measurements is used to assess model precision and compare its predictions with those of the best performing existing model. The last section presents a set of CC/DV design charts that can assist system designers in early design phases.

3.1 Review of existing CC/DV work

Existing research in CC/DV includes experimental and computational modeling studies. Table 7 presents the main characteristics of existing experimental CC/DV studies. All studies listed are performed in nearly adiabatic test chambers. In order for an experimental study to be used for model validation the dataset obtained must include all of the following data: test cell dimensions, airflow rate, supply air temperature and heat gains. This complete dataset in only available for three of the studies shown in the table (labeled with "*" in the last column of the table).

Table 8 shows a list of existing computational modeling studies. The two modeling approaches that are commonly used for CC/DV are nodal models and CFD. Among the existing nodal models, the model developed by Rees and Haves [62] is the most complete and precise. This model represents room air and surface temperatures using a set of 10 temperature nodes. The model can successfully predict the flow and temperature field for geometries the limited set of geometries used in its development. To deal with other geometries it is not clear that the flow coefficients used in the model are applicable or why they can be used since plumes, the fundamental driving mechanisms of the displacement flow are not explicitly modeled. None of the models listed in the table is currently implemented in whole year building energy simulation tools.

Table 7 - Dimensions, internal gains and operating conditions of CC/DV test chamber experimental studies.

Reference	Test chamber dimensions		Plume type	Flow rate ($\frac{m^3}{h.m^2}$)	Internal gains ($\frac{W}{m^2}$)	% Area with CC panels	$T_{chilled}$ (ºC)	Complete Dataset
	Height (m)	Area (m^2)						
S.J Rees, et al. [62]	2.8	17	vv , 🖥	14	48	88%	16	*
Simon J. Rees, et al. [63]	2.8	17	vv , 🖥	8-14	27 - 72	88%	14 - 18	*
A.H. Taki, et al. [64]	2.8	16	Vv , 🧍	20	62	88%	12 - 21	*
M. Behne [54]	3	46	Vv , 🖥	9	40 - 65	45-90%	-	X
W. Chakroun, et al. [65]	2.8	23	v , 🧍	26	52	80%	16	X
M. Kanaan, et al. [66]	2.8	7	vv , 🧍	-	58	-	18	X
S. Schiavon, et al. [67]	2.8	35	Vv , 🖥, 🧍	0.3–1.5	68-137	73%	17 - 23	X
S.G. Hodder, et al. [68]	2.8	16	vv, 🖥, 🧍	0.9	62	90%	13 - 22	X

v – single plume; vv - multiple symmetric plumes; Vv - multiple asymmetric plumes; 🖥 – computer; 🧍 - person simulator; * - used to validate the model.

Table 8- Approach used, main focus and typical precision of CC/DV modelling studies.

Reference	Modelling approach	Main focus	Typical precision
S. J Rees, et al. [57]	CFD	Flow and heat transfer	-
S. J Rees, et al. [62]	CFD and Nodal model	Air and surface temperature gradients	-
A.H. Taki, et al. [64]	CFD	Analysis of convection currents	-
W. Chakroun, et al. [65]	Nodal model	IAQ in breathing zone – CO_2 level	± 25ppm
M. Kanaan, et al. [66]	CFD and Nodal model	Bacteria distribution; air velocity; temperature	±10.4 CFU/m^3 0.0016 m/s 0.3 K
M. Ayoub, et al. [69]	CFD and Nodal model	Air temperature; stratification height	0.27 K ± 0.05 m
M. Kanaan, et al. [70]	Nodal model	CO_2 concentration and air temperature	< 30 ppm

3.2. Effects of the CC on the DV flow

This section analyzes the effects of the CC on the DV flow by comparing two average temperature profiles: CC/DV and DV only. The CC/DV profile that will be used in this comparison is the average from the three complete datasets shown in Table 7. In order to calculate an average temperature profile using different experimental studies the room temperature data is non-dimensionalised (by equation 1).

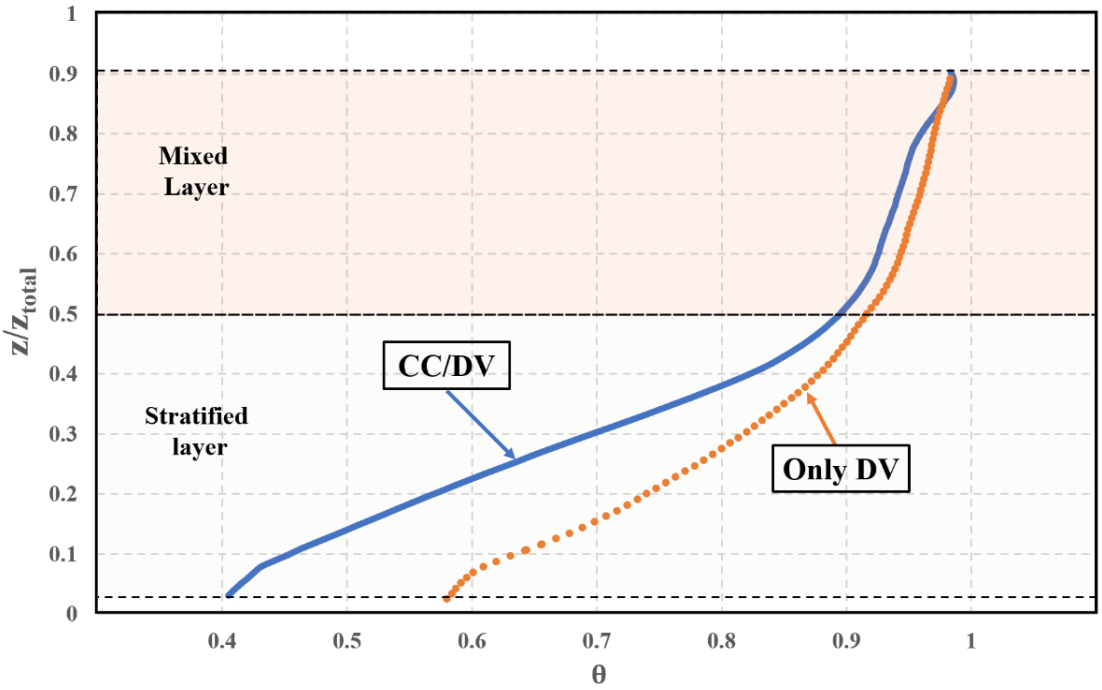

Figure 12. Experimental average temperature profile of CC/DV and DV [71] systems.

The resulting average profile is shown in Figure 12, along with a similar profile, previously obtained for studies with DV only. Analysis of the figure reveals the following:

- Both profiles have a nearly linear temperature increase in the occupied zone.
- CC/DV displays a colder floor and foot level temperature ($z^* \approx 0.03$). This difference is likely to be caused by increased radiative cooling of the floor by the chilled ceiling.
- In CC/DV there is larger temperature difference between the occupied zone ($0.2 < z^* < 0.4$) and the upper mixed layer.
- Both profiles show a nearly isothermal mixed upper layer.

Although the two profiles are different, it seems likely that the existing DV model can be adapted so that it can model the effects of the CC. In particular by adjusting the coefficient that represents the fraction of the convective gains that mix into the occupied zone. The next section presents the structure of the model and the model equations.

3.3 A three-node model for CC/DV systems

The structure of the proposed model for CC/DV systems is the same that was considered for DV systems model on Chapter 2 (see Figure 13). The nodes represent the following flow regions:

- The floor level node (T_{Af}), represents the average temperature of the air near floor, felt by the occupants at foot level. Air from this layer is entrained by the plumes into the occupied zone. This node is located at approximately 0.1m height.
- The occupied zone node (T_{OC}), characterizes the average air conditions felt by the occupant's body. This node is located in the center of the occupied zone (approximately 0.65m for seated occupants and 0.9m for standing occupants).
- The mixed layer node (T_{MX}), represents the average air temperature in the mixed layer, located near the room ceiling. The temperature of this node is the exhaust air temperature.
- The figure shows two heights that are inter-related but different: the lower boundary of the mixed layer (h_{MX}) is slightly higher than the neutral height (h_{NL}) due to the smoothing of the temperature profile transition caused by convective heat transfer in the occupied zone (the flow is driven by the plumes but there are other heat transfer processes).

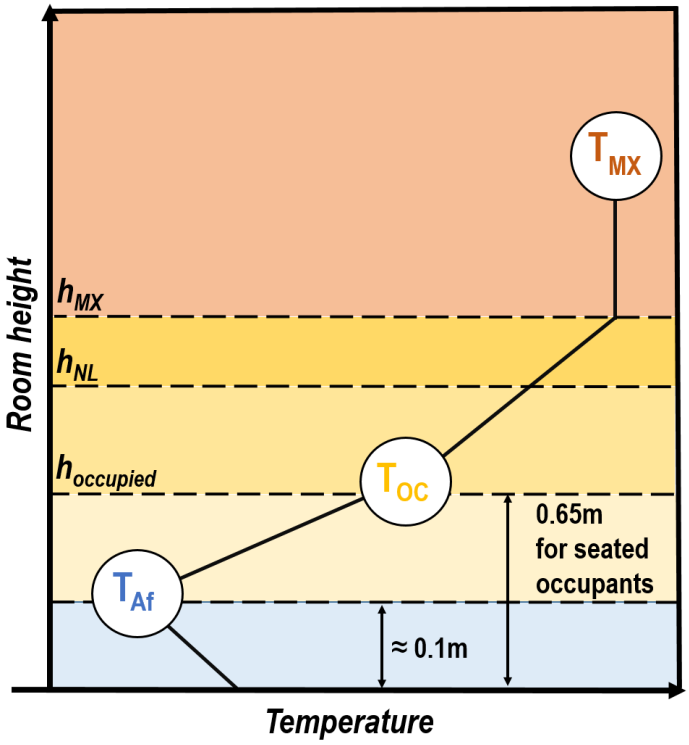

Figure 13. Schematic representation of three temperature points and temperature gradients.

Figure 14 shows the energy and air mass fluxes considered by the model. The inclusion of CC panels in the DV flow does not change the surface heat transfer process. For this reason the proposed model uses convection coefficients developed for DV systems by Novoselac et al. [44]. As discussed above, interaction between heat sources, furniture and wall driven flows promotes a certain degree of mixing of the internal gains into the occupied zone. This mixing is included in the model in the heat gains fraction parameter (F_{MO}) that characterizes the fraction of convective heat gains that mixes into the occupied zone and is not convected directly to the mixed layer ($0< F_{MO} <1$). The value of this parameter will be defined in the section 3.4. The model energy conservation equations and the equations for room surface energy conservation are already presented on Chapter 2 (equations 9-15).

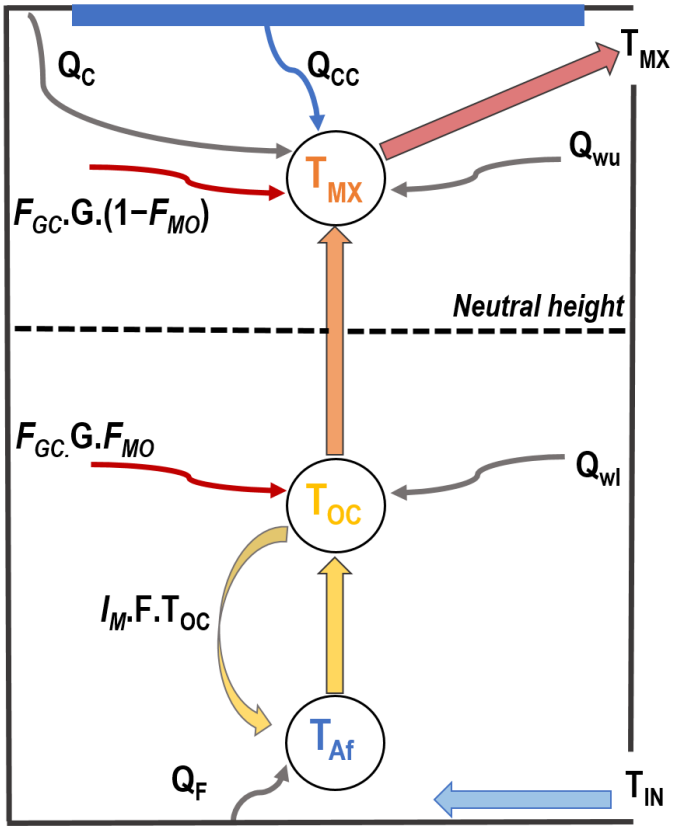

Figure 14. Schematic representation of model structure.

In order to consider the CC effect on energy balance, the ceiling surface temperature (T_c) is an area weighted average between the temperatures of the CC and the non-chilled part of ceiling (A_{NCC}):

$$T_c = \frac{T_{CC}.A_{CC}+T_{NCC}.A_{NCC}}{A_c} \qquad (20)$$

3.3.1 Prediction of the position of the neutral height

In DV flows the neutral height is defined as the point above which air entrained into the plumes recirculates, creating a mixed upper layer with a uniform temperature [11,39]. The neutral height (h_{NL}) as the height for which the inflow is equal to the total plume flow. This subsection tests the possibility of using this hypothesis define this height by modeling the plume flows using Taylor's equation [35]. In the experimental profiles, this height is defined as the point where the linear temperature gradient transitions into the nearly vertical profile that characterizes the mixed upper layer (Figure 15).

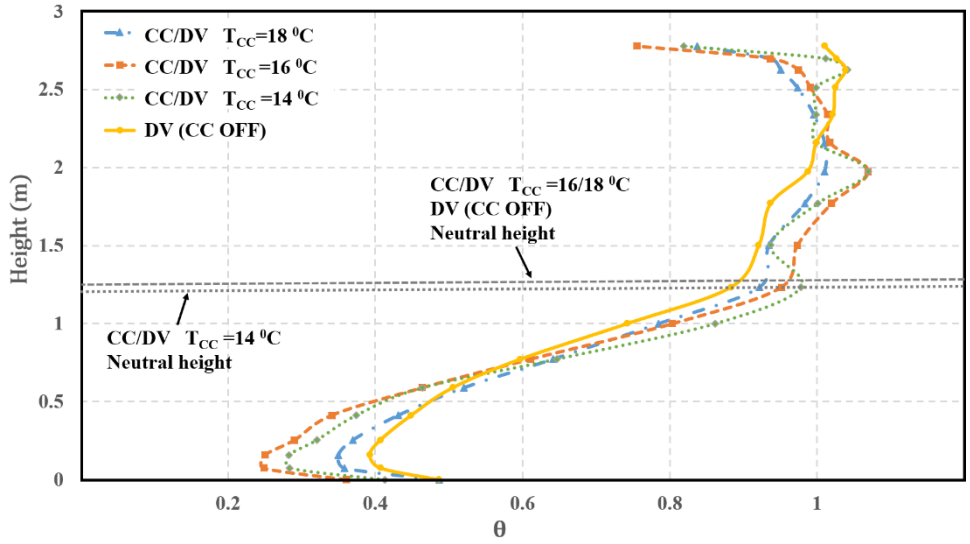

Figure 15. Neutral height position of temperature profiles presented by Rees, et al [63].

We will begin by assessing whether downward convection air currents caused by the CC change the neutral height. After this analysis i proceed to verify that the neutral height location can be determined using the "total plume flow matches inflow" hypothesis. The quantitative method to predict the location of the neutral height validated in the previous chapter will be used to determine the location of the neutral height in temperature profiles.

Figure 15 shows four temperature profiles obtained by Rees, et al [63], on a test cell operating with a CC/DV system with fixed inflow rate and internal gains but variable CC temperatures (between 14ºC and 18ºC). For each temperature profile the neutral height position was calculated using Equation 10. The results show that, in a stratified CC/DV system, the neutral height has a negligible dependence on the CC temperature: the variation between the DV only case and the coldest CC (14ºC) case is approximately 8%. In light of these results, the equation 5 will be used to obtain the neutral height.

The next step is to test the “total plume flow matches inflow” hypothesis. For this, the plume flow was modelled using the equation proposed by Morton et al. [35] (Equation 2). To analyze the validity of this equation to predict neutral height the method described previously (Equation 5) will be used to evaluate the precision of plume flow equation [35] (Equation 2) on CC/DV cases.

Since the vertical flow rate of the plumes increases with height, with exponent 5/3, for any inflow rate in a room, there is always a neutral height (h) where plume driven flow rate matches the inflow rate. Rearranging equation 2, for a given room inflow (F) and point buoyancy source (W), the neutral height could be obtained by:

$$h = 24.15 \sqrt[5]{\frac{F^3}{W}} \tag{21}$$

For cases with *n* non-coalescing plumes the neutral height is given by:

$$h = 24.15 \sqrt[5]{\frac{F^3}{W\, n^3}} \tag{22}$$

Analysis this equation provides hints on the difficulties of maintaining a set of desired conditions in the occupied zone of a displacement ventilated room, such as: average temperature, temperature gradient, and height of the mixed layer. The difference between expression 4 and 5 is the $n^{-3/5}$ multiplying factor. The exponent reflects a dampened reaction of the mixed layer height to changes in the number of plumes. The mixed layer height will decrease by 35% when doubling the number of plumes. The asymmetric dependence of the mixed layer height with inflow rate and convective gains contributes to the stability of DV flows: when the heat flux in the plume increases by one order of magnitude, *h* is only reduced by one third. In light of this, the flow rate should be defined based on the average heat gains and a fixed flow rate system can be used. The problem then is that, as a result of energy conservation, the temperature in the occupied zone will have a linear dependence on the internal gains. One way to control the resulting temperature increase is to reduce the inflow temperature, but this will result in occupant complaints due to cold draft discomfort at feet level. In this scenario, the CC can have benefits that go beyond the increase in cooling power: the CC temperature can be controlled to meet room comfort temperature requirements while the DV system remains fixed flow and inflow temperature mode.

To validate the applicability of expressions 21 and 22, the experimental data from the three complete studies presented in Table 7 was used. The differences between the neutral height predicted by the two described methods are quantified using the following error indicators defined by equations 23 e 24.

$$\text{Bias (m)} = h_{\text{temp. profile}} - h_{\text{numerical}} \quad (23)$$

$$\text{Error (\%)} = 100\% \times \left| \frac{h_{\text{temp. profile}} - h_{\text{numerical}}}{h_{\text{temp. profile}}} \right| \quad (24)$$

The results shown in Table 9 confirm the applicability of plume flow equation [35] to predict the neutral height position in a CC/DV system. The average error obtained is less than 10%.

Table 9 - Comparison between calculated and experimental neutral heights.

Reference	$h_{calculated}$ (m)	$h_{measured}$ (m)	Bias (m)	Error (%)
S.J Rees, et al. [62]	1.49	1.44	-0.05	3.6
Simon J. Rees, et al. [63]	1.31	1.21	-0.10	7.5
	1.31	1.32	0.01	0.8
	1.31	1.29	-0.02	1.3
	1.32	1.37	0.05	3.5
	1.46	1.34	-0.12	8.2
	1.44	1.10	-0.34	23.5
A.H. Taki, et al. [64]	1.37	1.15	-0.22	16.3
	1.37	1.15	-0.22	16.3
	1.37	1.18	-0.19	14.2
	1.37	1.41	0.04	2.8
	1.37	1.18	-0.19	14.2
Average indicators			**-0.11**	**9.3**

In any DV flow, the room surfaces are heated by radiative exchange with the internal gains. This heating results in a smoothing of the temperature profile due to the effect of the natural convection wall currents [11]. A nodal model with a limited number of nodes cannot reproduce this smooth profile. In order to improve the fit between model perditions and measured profiles was proposed to locate the lower boundary of the mixed upper

layer zone in the model slightly above the neutral level. To determine the relation between this newly introduced mixed layer height (h_{MX}) from the existing neutral height (h_{NL}), the smooth transition in the twelve temperature profiles available from the three complete studies in Table 7 was analyzed. This analysis resulted in the following relation between the two heights (the same obatined for DV systems standalone):

$$h_{MX} = h + \frac{h_{ceiling} - h}{3} \qquad (25)$$

3.4 Validation

This section presents an assessment of the accuracy of the proposed model, based on the twelve experimental datasets that have been selected in section 3.2 (signaled with a "*" in Table 7). The accuracy of the model will be assessed using the average error indicators defined by equations 16, 17 and 18.

The model has a single adjustable parameter, F_{MO}. This parameter will be set to the value that minimizes the average error for the twelve cases in the experimental database. The average error obtained for each value of F_{MO} in these runs is shown in Figure 16. The optimal value, 0.2, is one half of the value previously determined for standard DV systems on Chapter 2 (F_{MO}=0.4). Clearly, the addition of a CC reduces the average surface temperatures in the room and, consequently, the magnitude of the convective wall currents effect that generates the increase in temperature in the occupied zone. This effect is incorporated in the model as a lower F_{MO} value.

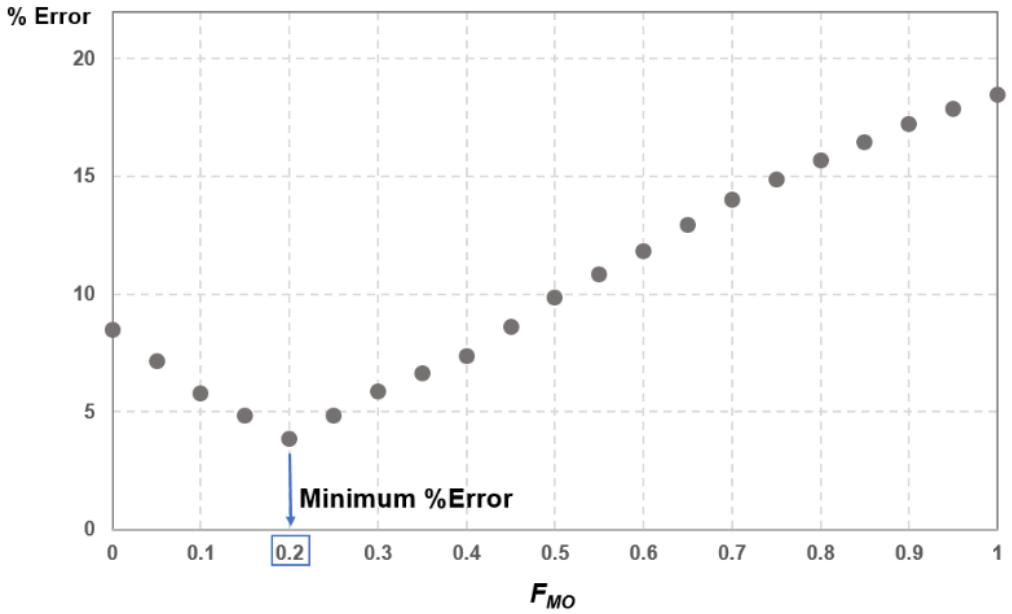

Figure 16. Convective mixing of heat gains into the occupied zone (F_{MO}) determination.

Figure 17 shows the results of the comparison between the twelve experimental temperature profiles of the database and the simulation for each case (all with F_{MO}=0.2)**.** Table 10 presents the overall average error indicators. Approximately half of the cases shown display a model under prediction at 2m heights and above. This error can be attributed to the use of a fully adiabatic boundary condition in the simulation models. In the test chamber studies there are small heat losses that reduce the air temperature (the air inside the chamber is usually warmer than the labs were the chambers are installed due to the heat gains used to generate the DV flows). Overall, the results show very good agreement between measurements and simulations: the average overall bias is negligible and the average error is less than 5%.

Table 10 - Validation of the proposed model.

Node	Dif. (K)	Bias (K)	Error (%)
T_{af}	0.2	0.0	5.7
T_{OC}	0.2	0.0	4.0
T_{MX}	0.3	0.3	4.3
Average	**0.2**	**0.1**	**4.7**

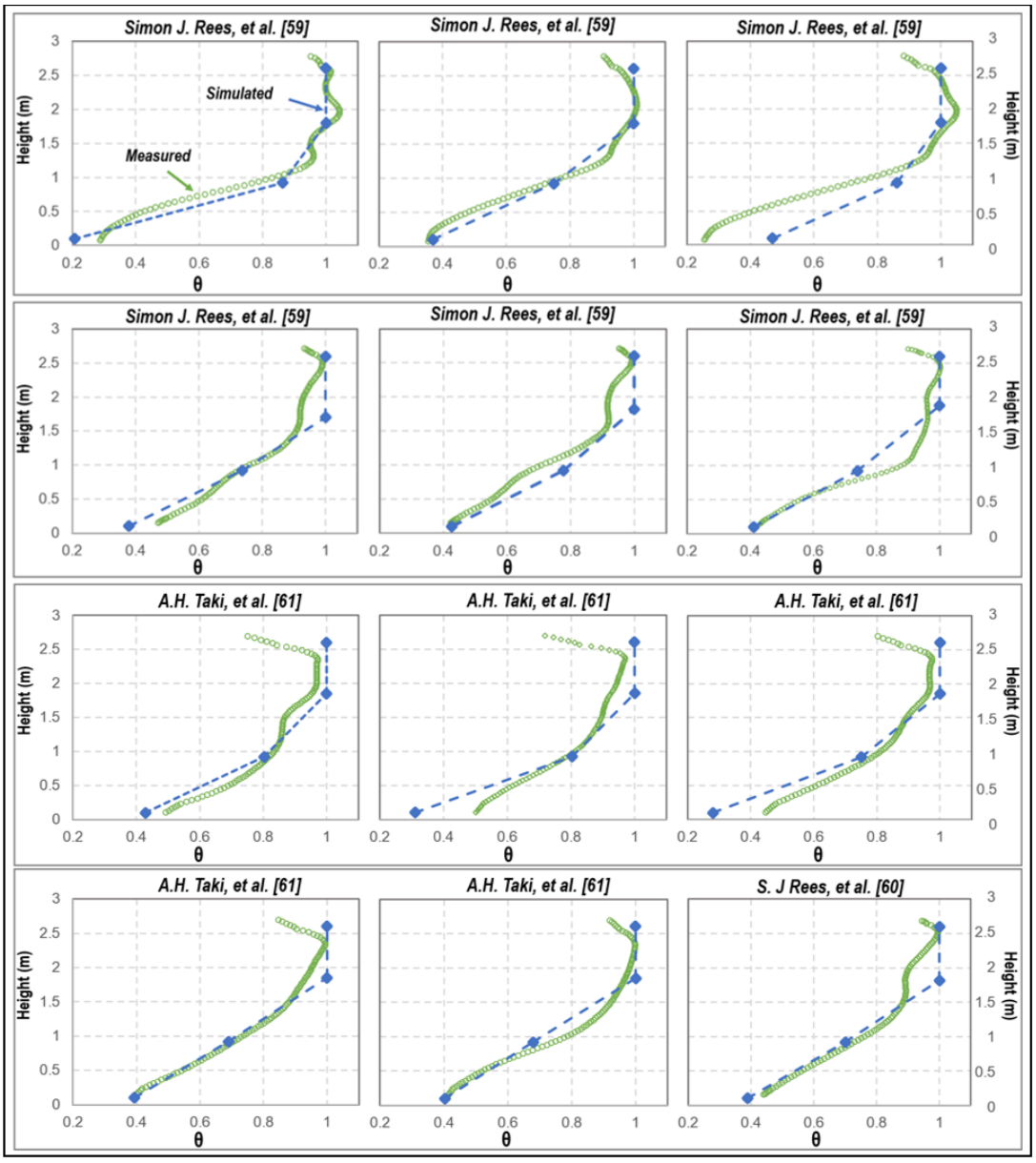

Figure 17. Results of the model simulations and comparison with measured data.

3.5 Comparison with existing model

This section presents a comparison between the proposed model and the best performing existing CC/DV model (Rees&Haves [62]) and CFD. This comparison will use two experimental data sets that were also used by Rees&Haves, shown on Figure 18. Table 11 presents the average percentage of error obtained for the simulated cases.

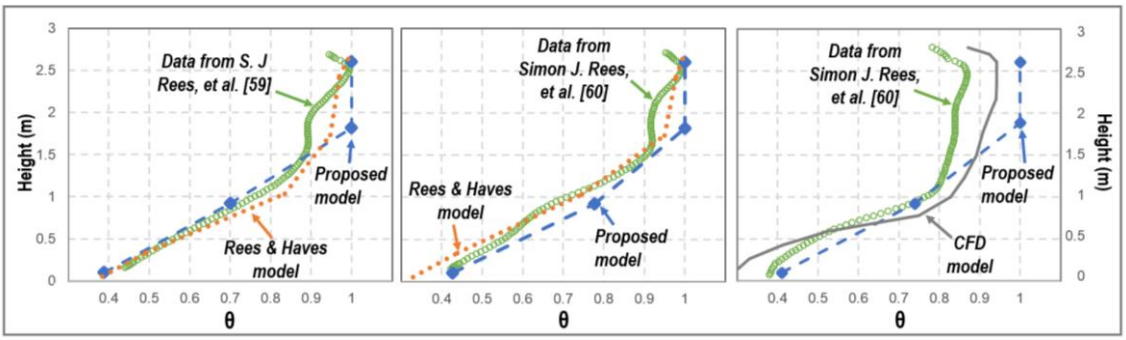

Figure 18. Comparison between proposed model, Rees & Haves CC/DV model, CFD and measured data.

Table 11 - Comparison of models precision.

Node	Error (%)	
	Proposed model	**Rees & Haves model**
T_{af}	7.2	15.3
T_{OC}	9.0	1.8
T_{MX}	1.5	2.6
Average	**5.9**	**6.6**

Table 12 - Proposed model and CFD precision comparison.

Node	Error (%)	
	Proposed model	**Rees & Haves model**
T_{af}	6.9	26.7
T_{OC}	2.0	9,1
T_{MX}	21.9	13.8
Average	**10.3**	**16.3**

The results of both models, shown in figure 18 and table 12, are similar (5.9 versus 6.6 average percentage of error). As a result of the larger number of nodes used the Rees & Haves model is slightly more accurate in the occupied zone. In the floor level temperature the proposed model is more accurate due to the inclusion of measured

inflow degree of mixing (I_M). The exhausted air temperature (T_{MX}) is well calculated by both models through the imposed overall energy balance. It is important to note that, in order to run the Rees & Haves model for the two cases shown in figure 18 the user must perform a separate CFD simulation for each case (to generate the inter-cell airflow coefficients). The proposed model is much simpler: three versus ten nodes, and does not use of auxiliary simulations (CFD simulations) to determine model parameters.

The right hand side of figure 18 and table 6 show the results of a comparison between the proposed model and a CFD simulation for one of the cases in [63] (using a RANS approach with a two-equation eddy viscosity model of Launder and Spalding). For this case the proposed model displays a lower error. Still, CFD can provide a much more detailed result and can be used to analyze 3D flow effects. Unfortunately, CFD has not reached a stage where it can be used in hourly annual energy simulations that typically have a time step of 10-20min.

These results contribute to increased confidence in the proposed model. Since there are no relevant differences in the simulation results, the two models can only be distinguished by their complexity.

3.6 Model application to CC/DV system design

In this section, the model is used to develop design charts that can assist designers in initial sizing of CC/DV systems. Separate charts were developed for low and high internal gains. The results presented can provide simple initial guidance on the appropriate inflow and ceiling temperature conditions that result in a given target temperature in the occupied zone. In addition, the charts provide information on the lower limits of the CC temperature that preserve the stratification and avoid condensation. The supply airflow rates used in each scenario maintain the neutral level above the seated occupants head.

3.6.1 Methodology

The tables are developed for the core zone of an office space with 100m^2 floor area and 3m floor to ceiling height. The large majority of the ceiling area is covered by CC panels (90%). Table 13 presents the two loads and airflow scenarios considered.

Table 13 - Simulated heat gains scenarios.

Scenario	Occupants (W/m2)	Equipment (W/m^2)	Lights (W/m^2)	*Total Loads (W/m^2)*	*Airflow ($(m^3/h)/m^2$*	*Room CO_2 concentration (ppm)*
Low	10	15	10	35	12	510
High	15	30	10	55	21	490

The space available to install the DV diffusers limits the maximum airflow rate. For the two cases was considered circular diffusers, 0.2m diameter [72], evenly spaced on the room floor with a 2m separation. In each case, the supply airflow rate was determined solving the Equation 22, assuming the neutral height is kept above seated occupant's height (1.2m).

Simulations were performed for all possible combinations of CC (16-27 ºC) and supply air (18-22ºC) temperatures, resulting in one CC/DV design chart with the predicted occupied zone temperature (T_{OC}) for each heat gain scenario. In order to make the role of each system clearer, in each case was defined a cooling loads ratio ($0.1< R <1$) as the portion of the total sensible gains that is removed by the supply air provided by DV (Q_{DV}):

$$Q_{DV} = \rho.Cp.F.(T_{MX} - T_{in}) \quad (26)$$

$$R = \frac{Q_{DV}}{G} \quad (27)$$

To predict the CC condensation risk vapor pressure in the system was predicted, beginning with an air condition after the cooling coil of 90% saturation and a temperature that is 2K lower than inflow. The room air dew point temperature was determined by the balance between the supply air moisture and the moisture generated by the active sources in the room (occupants). To determine the room humidity ratio was considered that 1/3 of generated heat by the occupants is latent and the remaining corresponds to sensible heat (for office activity [73]).

3.6.2 Results

The design charts, shown in figuresFigure 19 and Figure 20, define three system operation zones:

- The optimal operation of CC/DV zone (shown in green) is defined by the area in the design chart where: the thermal comfort of the occupants is achieved (T_{OC} between 20-25ºC [74]) and the cooling loads ratio above 0.1 (less is not possible due to minimum outdoor air requirements).

- DV zone (shown in orange) is an area where the thermal comfort also can be obtained without the CC.
- The CC condensation risk zone (shown in blue) represents the system operation zone where the ceiling surface temperature is lower than room air dew point temperature (inflow air plus occupants). System operation in this zone should be avoided.

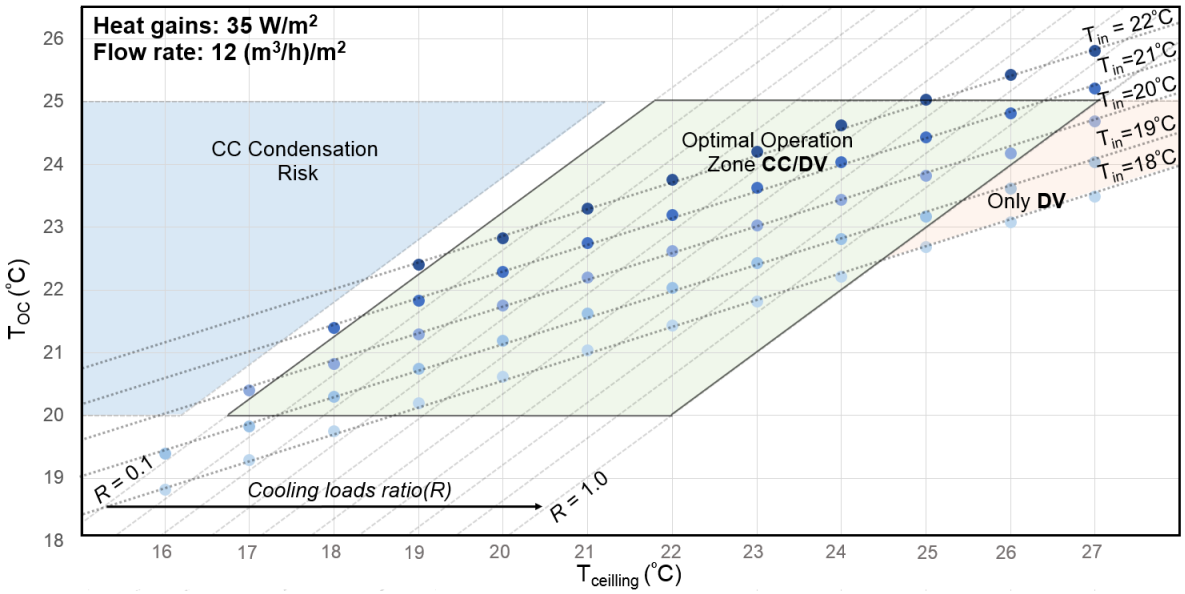

Figure 19. CC/DV system design chart – low heat gains scenario.

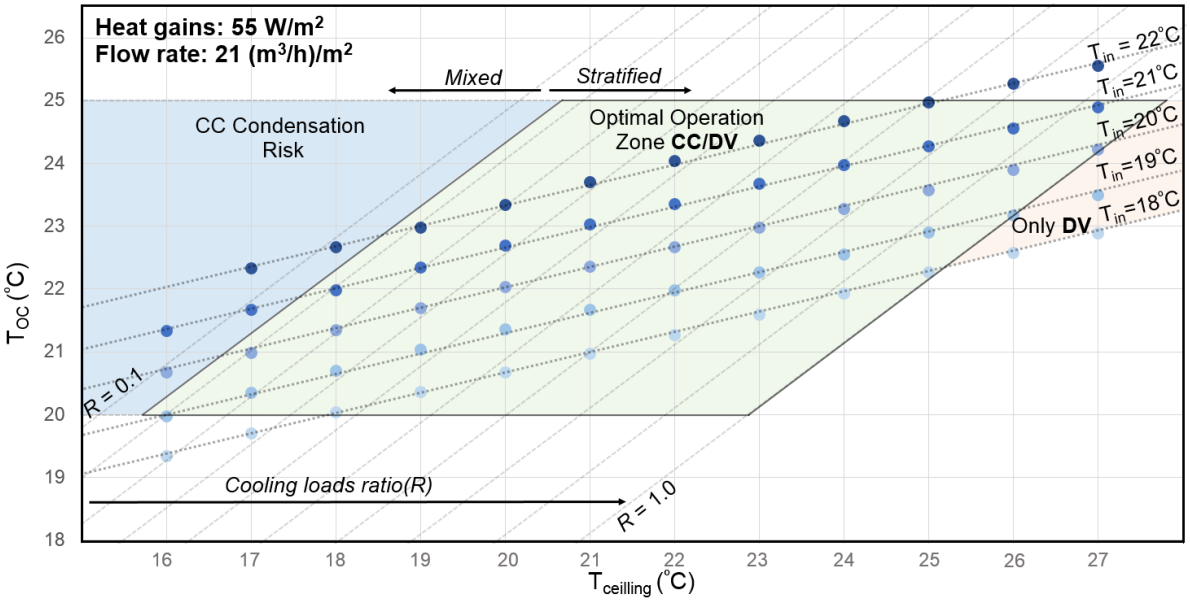

Figure 20. CC/DV system design chart – high heat gains scenario.

The results shown on the design charts are representative of the typical performance of a CC/DV system. Analysis of the charts shows that:

- The maximum and the minimum temperature on occupied zone was obtained for low heat gains scenario that have the lower ratio airflow per heat gains ((m^3/h)/W).
- As the flow rate and the heat gains increases (from low to high scenario) the CC condensation risk area is bigger, and for low CC panels temperature some of the simulated points are on this zone.
- The number of simulated points in optimal operation zone is bigger in high heat gains scenario. As expected the DV zone is higher on the low heat gains scenario.

Based on this analysis the following system operation temperatures shown in Table 14 were recommended.

Table 14 - CC/DV recommended operating parameters.

	T_{in} (^{0}C)			$T_{ceiling}$ (^{0}C)		
	Min.	***Optimal***	*Max.*	*Min.*	***Optimal***	*Max.*
Low gains	19	**20**	21	18	**22**	24
High gains	18	**19**	20	18	**21**	25

3.7 Conclusions

Combining a CC with DV can be an effective strategy to increase the cooling power of standard DV while retaining a low airflow velocity stratified room environment. To preserve thermal comfort in a DV flow while avoiding condensation the CC temperature must be carefully adjusted. The design and control of the combined CC/DV system is complex and cannot be modeled using the fully mixed room air approach.

This chapter presents a simplified model three-node model that is able to predict the vertical temperature profile and the location of the mixed layer in rooms with DV systems supplemented by CC. The proposed nodal approach provides significantly improved accuracy when compared to existing perfectly mixed flow models. The model is able to accurately predict vertical temperature variation and heat transfer with room internal surfaces for cases where the dominant heat fluxes in the room are a set of *n* equal plumes located in the room occupied zone.

The model was validated using 12 measured temperature profiles. The average prediction error for the three room node temperatures was 0.2 K. The proposed model

is simple enough to be implemented in a whole year building thermal simulation tools. Required model inputs are limited to the strength, height and number of heat sources in room. The model can easily predict the occurrence of two of the main problems of CC/DV systems, namely, the disruption of the thermal stratification and the occurrence of condensation in the CC surface.

4. Comparison of measured and simulated performance of natural displacement ventilation systems for classrooms

Children spend the majority of their weekdays in classrooms that often have low indoor air quality (IAQ) due to insufficient outdoor airflow [75,76]. There are several studies that link low IAQ to reduced effectiveness of schoolwork and learning outcomes [77,78,79,80,81]. In response to this problem current classroom ventilation standards and guidelines recommend a minimum fresh air amount of 7-8l/s per occupant [82,83] and an indoor-outdoor CO_2 concentration differential of less than 700ppm [83,84]. Achieving these airflow rates with a mechanical ventilation system inevitably increases energy consumption and maintenance costs in schools that, in the majority of cases, have a limited budget. In many climates, a well-designed natural ventilation (NV) system can provide adequate IAQ with no running costs.

Implementing effective NV systems in schools is difficult due to the intense use of the classroom spaces and the dependence of NV on building geometry and outdoor conditions (weather, pollution and noise). NV airflow is driven by pressure differences generated by buoyancy effects, wind or a combination of these two mechanisms. These pressure differences drive airflow from high to low pressures zones, across different zones inside the building or between indoor and outdoor environment. To naturally ventilate a space there are three main approaches that can be employed: single-sided ventilation (SS), cross-ventilation (CV) and displacement ventilation (DV). SS ventilation is the most common NV system due its simplicity: it requires openings in a single façade [85]. Unfortunately, these systems often struggle to provide sufficient airflow away from the façade. CV uses openings in opposite façades and has the potential to provide large flow rates [86] but is difficult to implement in schools due to potential draft induced discomfort, noise propagation and the prevalence of single sided room configurations. In DV systems air is introduced near the room floor with low velocity. Buoyancy forces induced by temperature differences between inflow and room air heated by internal gains promote airflow across the floor towards the heat sources where the ventilation air expands and moves upward. Ideally, the air movement induced by buoyancy is capable of transporting heat and pollutants away from the occupied zone, promoting stratification, creating a warmed mixed layer in the upper part of the room [11]. In order for the buoyancy forces to be effective, DV systems require a height difference between inflow

and outflow that is difficult to achieve without chimneys. For single story buildings chimneys can be placed in the roof, any other configurations require internal voids or individual chimneys that may be difficult to integrate in the building.

The performance of NV in schools can be evaluated using thermal and occupant comfort simulations, field questionnaires or measurements. In 2004, a questionnaire based study [87] performed in two schools confirmed that, when NV is used, there is a higher tolerance to elevated indoor temperatures, exceeding the thermal comfort limits imposed by building regulations. A recent study analyzed the impact of the type of ventilation system on student performance, concluding that a well-designed NV system can as good as a mechanical ventilation system [88]. When the room CO_2 sources are known, the CO_2 concentration differential between indoor and outdoor can be used as an indirect method to determine room airflow change rates, this bulk airflow measurement approach is often used in schools [89]. In 2008, a large field study measured CO_2 concentration and airflow rates in 62 classrooms [90], showed that in 77% of the time the airflow rates were below 8l/s/occupant. Further, as expected, in the NV systems measured, high indoor CO_2 concentrations occurred predominantly when the windows were closed. This trend was also observed by other authors, mainly during winter when outside air is too cold to allow for open windows without cold draft discomfort [91]. It is increasingly consensual that window operation is predominantly driven by thermal comfort and not IAQ [92]. Existing IAQ problems may be aggravated in schools located in cold climates that are retrofitted with envelopes that have very low infiltration [93].

The world population is increasingly urban and, therefore, the majority of schools are located in dense or semi-dense urban areas. Using wind driven ventilation in dense areas is difficult due to the wind velocity attenuation that characterizes these environments. In response to this limitation, designers often prefer buoyancy driven systems in SS or DV configurations that can still benefit from winds effects but are mostly driven by temperature difference between indoor and outdoor of at least 2-3ºC. This requirement restricts the use of these systems to outdoor temperatures below ≈25ºC [94]. To extend the outdoor temperature range for buildings NV designers can use chimneys that increase the vertical distance between inlet-outlet and decrease the indoor-outdoor temperature difference in the occupied zone [95,96]. An effective chimney lowers room temperatures, reduces outdoor noise ingress and increases safety (windows can be a safety hazard, especially at night).

In a successful natural DV system the indoor environment is stratified forming a layer of warm air and pollutants above the occupants. The stratified environment cannot be

adequately described using a single room air node: additional temperature nodes are needed to correctly simulate the vertical temperature gradient. The most detailed simulation tool that can be used in these cases is Computer Fluid Dynamics (CFD) [97]. CFD is being increasingly used due its capability to predict complex airflow patterns, but remains computationally heavy and time consuming [98], particularly in cases of multiple rooms with variable occupancy that need to be tested in variable weather conditions. For these multi-room cases and in building design phases when time and budget are limited, the use of a simplified dynamic thermal simulation is still the best option. One of the most complete dynamic thermal simulation tools is EnergyPlus [99,100]. EnergyPlus includes a simplified model for DV systems [15,71] that has been validated in mechanically ventilated rooms but is yet to be tested in NV rooms with DV. This chapter presents a set of detailed measurements of NV systems in three classrooms located in two different buildings. The rooms have different buoyancy driven natural DV systems: with and without a chimney and with two different chimney heights. These measurements are used to validate the three-node DV model presented on Chapter 2 that was implemented in EnergyPlus. The chapter begins with a review of existing validation studies of NV systems followed by a discussion of the basic physics of natural DV. The next section presents a description of experimental setup. Section 4.4 presents the experimental results, including a comparison of simultaneous measurement of two similar NV rooms with different chimney heights. Finally, in sections 4.5 and 4.6, the predictions of thermal and airflow simulation models are compared with the measurement results.

4.1 Existing comparisons between measurements and simulations of NV systems

Validation of NV simulation models requires detailed data sets comprising multiple sensors to monitor temperature, internal gains, operable window position, tracer gas concentrations and air velocity. In many cases, the need to control boundary conditions leads to the use of test chambers with nearly adiabatic boundaries. NV systems are highly dependent on boundary and outside weather conditions and therefore, in most cases, require measurements in real buildings. Unfortunately, detailed measurements in real buildings are rare due to difficulties in controlling and measuring boundary conditions. As a result, there is only a limited number of validation studies of NV systems.

Table 15 presents a summary of the results obtained in existing NV simulation validation studies of five types of NV system. Several studies focus on double skin façades (DSF). The complexity of these façade systems makes the use of CFD simulations a common

approach. In the case of CFD validation studies based on weather exposed test cells [102,104] the heat transfer through the walls can have a large impact on the results. In order to reach a higher level of precision the use of low-Reynolds wall functions is essential [101], making the CFD simulations even more time consuming. Further, assessing the impact of DSF in building energy consumption during the building design phase requires whole-year energy simulations that only can be performed in a timely manner using thermal simulation tools. The DSF validation studies that use EnergyPlus identified the quality of the weather data that is used as input to the simulation and the uncertainties related to the airflow modelling as the potential causes for discrepancies between simulations and measurements [108,109]. Studies based on systems driven by wind [103,106,107] tend to display larger deviations between measurements and simulations. In part, these differences can be attributed to difficulties in measuring the wind on site. Ideally, the wind direction and velocity sensor should be installed as close as possible to the building. The impact of this problem is higher in CV systems [110].

For the cases in Table 15, the most common approach is nodal modelling based on the EnergyPlus thermal simulation software. The maximum error of the CFD cases is comparable with the remaining approaches. The higher complexity CFD does not lead to lower simulation errors (although it clearly allows for a higher analysis detail). Overall, the results presented in Table 15 reveal an acceptable accuracy for engineering simulations: the mean error considering all models with available data is 1.2ºC (between 0.3-2.9ºC) and 6.6ºC for the maximum error (1.0-21.9ºC). Several of the cases presented on Table 15 reveal a common trend in NV studies: difficulties in determining user operation of doors and windows lead to inconclusive results.

Table 15 - Existing measurement and simulation studies of NV flows.

Reference	Building type	Driving mechanisms	System config.	Simulation tool (approach)	Error (ºC)	
					Average	Typical Max.
Z. Zeng, et al. [102]	Test cell	Buoyancy &wind	DSF	CFD	-	2.0
Y. Wang, et al.[103]	Classroom	Buoyancy &wind	DV	CFD	-	1.2
I.Khalifa, et al.[104]	Test cell	Buoyancy &wind	DSF	TRNSYS& CONTAM (nodal+CFD)	0.5	3.0
F.R. Mazarrón, et al.[105]	Wine cellar	Buoyancy	Chimney	EnergyPlus (nodal)	0.3	-
Z. Zhai, et al.[106]	Office	Buoyancy &wind	Chimney	EnergyPlus (nodal)	-	3.3
Taleghani, et al.[107]	Apartment	Buoyancy &wind	SS	EnergyPlus (nodal)	0.9	1.1
Mateus, et al.[108]	Test cell	Buoyancy	DSF	EnergyPlus (nodal)	1.4	2.5
D. Kim, et al. [109]	Test cell	Buoyancy &wind	DSF	EnergyPlus (nodal)	2.9	21.9
C. J. Koinakis, et al. [85]	Apartment	Buoyancy &wind	SS & CV	Custom (nodal)	0.5	1.0
E.H. Mathews, et al. [110]	Horse stable	Buoyancy &wind	CV	Custom (electrical analogy)	-	1.2
Average					**1.2**	**6.6**

4.2. Simplified modeling of natural DV

This analysis begin with a discussion of the principles of DV and then proceed to analyze the special case of natural DV systems. In all DV systems, the point that separates the lower part of the room from the upper mixed layer is called neutral height [35]. In a DV room with occupation most of the vertical variation of temperature and CO_2 concentration

occurs between floor and the neutral height [111]. Predicting and controlling this height is a unique challenge in the design of natural DV systems.

In the case of adiabatic test chambers, like the DV cases studied in [20], the neutral height found in CO_2 and temperature profiles is similar because the high level of insulation of the test chamber walls minimizes the disturbances in temperature profile caused by heat exchange between air and surfaces. This heat exchange has a smoothing effect on the temperature profile [112], making the identification of the neutral height more difficult. CO_2 concentration profiles are less affected by surface exchanges, allowing for a clearer identification of the neutral height point by visual inspection, even in buildings with uncontrolled boundary conditions [24].

Both in natural and mechanical DV systems, as shown in previously chapters, increasing the room airflow rate raises the neutral height by raising the point where the total thermal plume flow matches inflow. The total flow from a point plume is approximately equal to [35]:

$$F = \frac{6}{5}\,\alpha^{\frac{4}{3}}\,\sqrt[3]{\frac{9}{10}}\;\pi^{\frac{2}{3}}\,\sqrt[3]{\frac{g\,\beta\,W}{\rho\,Cp}}\;h^5 \qquad (28)$$

Rearranging the Equation 28 to predict the neutral height (h), we obtained:

$$h = 23.95\,\sqrt[5]{\frac{F^3}{W}} \qquad (29)$$

When there are *n* non-coalescing plumes with equal strength the neutral height is given by:

$$h = 23.95\,\sqrt[5]{\frac{F^3}{W\,n^3}} \qquad (30)$$

The case of natural DV is different from mechanical DV because the flow rate (F) depends on the total stack that, in rooms with no wall heat transfer, depends on the height and temperature of the mixed upper layer [95]. To simplify the analysis of natural DV systems we introduce the effective opening area, A* [95]. For the simplest case of a room with two openings, this area corresponds to the effective area of the top and bottom openings, described by the Equation 31 while the resultant natural airflow rate could be calculated through the Equation 32:

$$A^{*} = \frac{C_d\,a_t a_b}{\left[\frac{1}{2}\left(\frac{C_d}{c}^2 a_t^2 + a_b^2\right)\right]^{\frac{1}{2}}} \qquad (31)$$

$$F = A^{*}[g'(H - h)]^{\frac{1}{2}} \quad (32)$$

Where g' corresponds to the buoyancy, H is the height of the room, C_d is the discharge coefficient, c the pressure loss coefficient associated to the inflow, a_t and a_b are the areas of the top (outlet) and bottom openings (inlet), respectively.

Contrarily to what occurs in a mechanical DV, in NV systems driven by plumes of equal strength, the relative neutral height position (h/H) is independent of the buoyancy flux generated by the plumes. The relative neutral height position depends on A^*/H^2 and the number of thermal plumes: decreasing the A* lowers the natural airflow rate and consequently the neutral level, while lowering the number of plumes increase the neutral height position.

4.3. Experimental Setup

The measurements were performed in two educational buildings located in Lisbon (Portugal): a municipality kindergarten and a University of Lisbon classroom. Subsections 4.3.1 and 4.3.2 describe the rooms and NV systems measured. Subsection 4.3.3 describes the experimental procedures and instrumentation. The final subsection, 4.3.4, describes the experimental configurations tested.

4.3.1. CML kindergarten

The kindergarten is a small two-story building with a total area of 680 m^2 distributed in two floors with 3m floor to ceiling height. Construction finished in 2013. Driven by the need to lower maintenance costs, the building is naturally ventilated and does not have a mechanical cooling or ventilation. Heating is provided by passive convectors, feed by a heat pump. Figure 21 shows exterior and interior views of the kindergarten classrooms. With the goal of maximizing thermal inertia, the walls are made of exposed concrete and have external insulation (Table 16). Summer solar heat gains are limited by horizontal overhangs and low-emissivity double glazed windows with external shading (λ=0.9 W/m.K; τ=0.75). NV air is introduced into the space through low level grilles on the façade (shown in the center of Figure 21) and is exhausted in the center or back of the room, through one or two chimneys (depending on the size of the room, shown on the left side of Figure 21).

Figure 21. Inside and exterior views of the CML Kindergarten.

Table 16 - Kindergarten building material properties (from [113]).

		Material	Thickness (m)	Conductivity (W/m.K)	Density (Kg/m3)	Specific Heat (J/Kg.K)
Exterior Wall	Outside ↓ Inside	*Plaster*	0.01	1.30	2000	653
		Polyethylene	0.08	0.04	40	2200
		Heavyweight Concrete	0.13	2.30	2300	900
Interior Wall	Outside ↓ Inside	*Gypsum board*	0.025	0.25	900	1090
		Air space	0.05	0.03	1.16	1007
		Rockwool	0.07	0.04	40	840
		Gypsum board	0.025	0.25	900	1090
Exterior Roof	Outside ↓ Inside	*Aluminum*	0.01	15.1	8055	480
		Rockwool	0.1	0.04	150	840
		Air space	0.05	0.03	1.16	1007
		Rockwool-gypsum board	0.065	0.04	40	840
Interior Roof	Outside ↓ Inside	*Rockwool-gypsum board*	0.065	0.04	40	840
		Air space	0.05	0.03	1.16	1007
		Heavyweight concrete	0.2	2.30	1375	400
Floor	Outside ↓ Inside	*Soil*	1.70	1.14	1000	1282
		Riprap	0.25	1.20	1000	800
		Heavyweight concrete	0.2	2.30	2240	400
Air flow grilles		*Aluminum*	0.02	160.00	2800	2800

Measurements were performed in two similar west-facing classrooms with identical gains and different chimney heights (see Figure 22):

- Ground floor with 4m chimney (labeled KD0, with a total of ≈6.5m stack)
- First floor with a 1m chimney (labeled KD1, with a total of ≈3.5m stack)

Figure 22 shows the dimensions of the classrooms and the location of the sensors used. To measure the stratification, a column of six air temperature sensors were installed in the middle of the room. In addition, the measurement setup included CO_2 concentration sensors in the room inlet and outlet, allowing for accurate indirect measurement of the bulk airflow (using the methodology discussed in subsection 4.3.3, below).

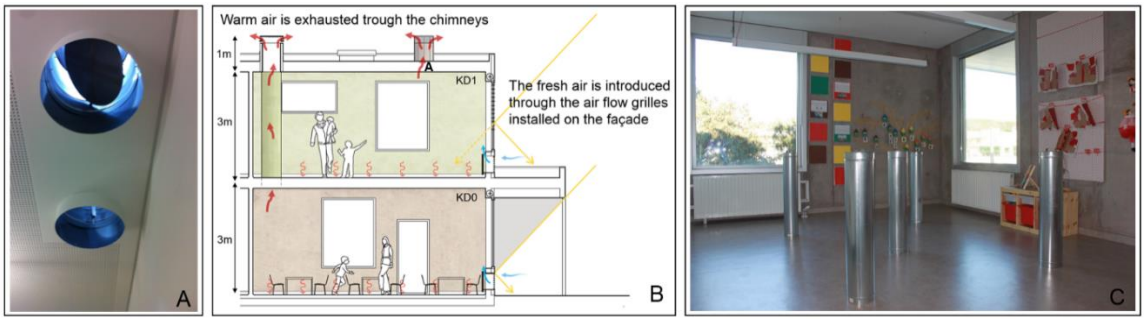

Figure 22. A- Chimneys and dampers; B- kindergarten NV system scheme; C- interior view of a kindergarten room with the heated cylinders used in the measurements.

The measurements used constant internal gains inserted by heated galvanized steel cylinders (shown in Figure 22), disposed as shown in Figure 23 (for 5 plumes cases), while in one plume cases (KD1_1_1P and KD1_2_1P) the cylinders are all grouped in position number 1. CO_2 was inserted at mid height in each cylinder, feed by a large container located outside the room. To accurately determine the CO_2 flux the canister was weighed before and after each experiment.

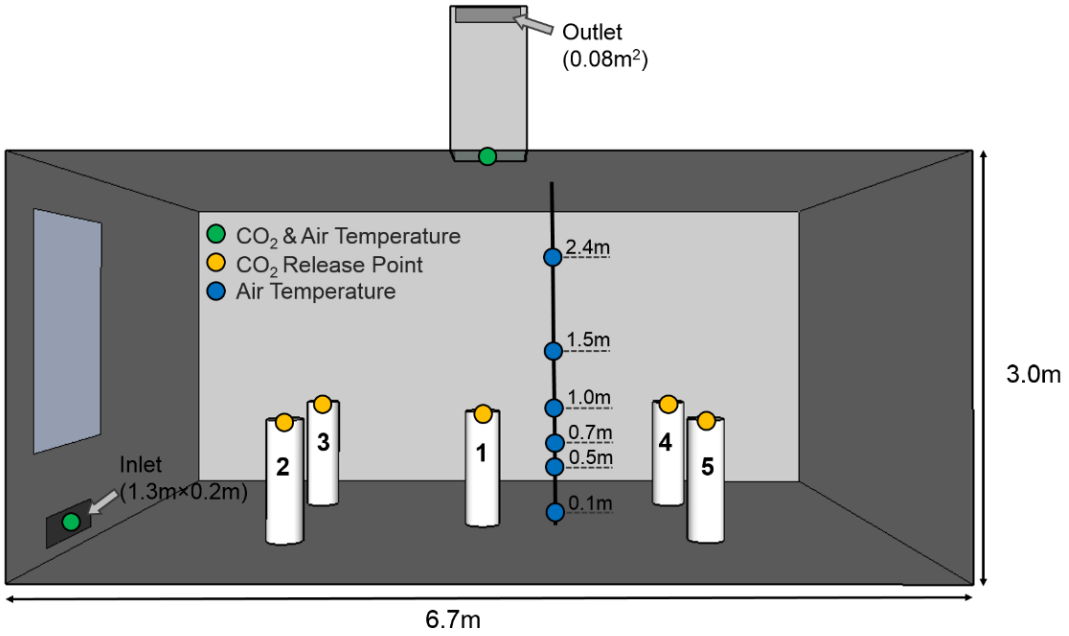

Figure 23. Locations of the sensors used in the Kindergarten measurements.

4.3.2. UL Classroom

The third room used in this study is a classroom in the University of Lisbon (UL) campus. Figure 24 shows an aerial view and two interior views of the space. The classroom is in a five-story southeast oriented building, built in the late 80's, with a heavy concrete based construction (no insulation), single glazing (λ=1.2 W/m.K; τ=0.84) and external shading to avoid direct solar heat gains. Table 17 presents the building construction and material properties [113] used in the thermal simulations.

Figure 24. Aerial and interior views of the UL classroom.

The NV system uses an outflow window in the façade (see center of Figure 24), combined with a low-level inflow inlet on the entrance to the space. The air that enters the room comes from a large corridor that is connected to the outside and has a temperature that is within 1ºC of the outdoor. Figure 25 shows the measurement setup used in this case (similar to the one described in the previous section).

Table 17 - UL classroom material properties.

		Material	***Thickness (m)***	***Conductivity (W/m.K)***	***Density (Kg/m3)***	***Specific Heat (J/Kg.K)***
Exterior Wall	**Outside** ↓ **Inside**	*Brick*	0.11	0.89	1920	790
		Heavyweight Concrete	0.11	2.3	2450	900
		Plaster	1.5	1.15	1950	653
Interior Wall	**Outside** ↓ **Inside**	*Plaster*	0.15	1.15	900	1090
		Brick	0.11	0.89	1920	790
		Plaster	0.15	1.15	900	1090
Roof and Floor		*Heavyweight concrete*	0.2	2.3	2240	400

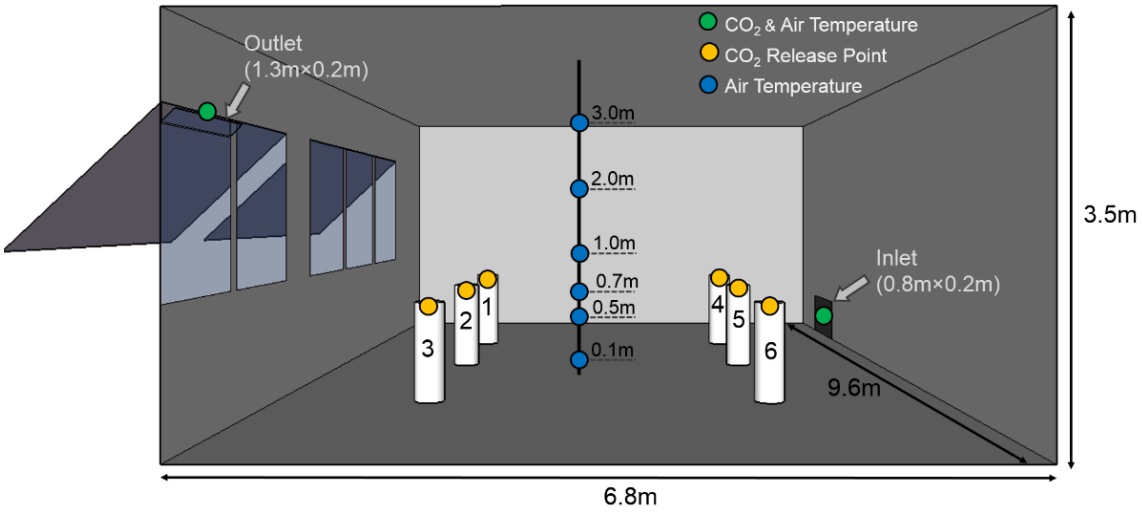

Figure 25. Locations of the sensors used in the UL classroom measurements.

4.3.3. Measurement procedure

The measurements focused on the main features of the natural DV systems, namely: vertical temperature and CO_2 profiles, and bulk airflow rate. Constant sensible gains were used in the rooms, provided by heated cylinders (sensible heat gains, split in 65% convective and 35% radiative) with a constant CO_2 release (3.72×10^{-5} kg/s per simulator, in all cases). For each measurement, the bulk airflow rate was determined when steady state conditions are reached solving the mass balance described by the equation 33 [114], using CO_2 released by near the cylinders as a tracer gas [115], according to:

$$F\ (m^3/s) = \frac{CO2_{simulators}\ (mg/s)}{[CO2_{outlet}]\text{-}[CO2_{inlet}]\ (mg/m^3)} \qquad (33)$$

Table 18 shows the specifications of the measurement equipment used. The weather station is located in the UL campus and measures air temperature, humidity, wind speed and direction, as well as global, diffuse and direct solar radiation. This weather station is in the same location as the UL classroom and less than 3km from the kindergarten. The weather data was measured in ten-minute intervals and is included in the EnergyPlus weather file used in the simulations presented below.

Table 18 - Specifications of the measurement equipment used.

Sensor		Measurement	Specifications	
Lufft *(Weather Station 500)*		Temperature	Range	-50 to 60 º C
			Accuracy	± 0,2ºC (-20 to 50ºC)
		Relative humidity	Range	0 to 100% RH
			Accuracy	± 2% RH
		Wind direction	Range	0 to 359.9º
			Accuracy	± 3º
		Wind speed	Range	0 to 60m/s
			Accuracy	± 0.3 m/s
EKO Instruments	***(MS-802 Pyranometer)***	Global Horizontal Irradiance	Range	0 - 4000 W/m^2
			Accuracy	± 2 W/m^2
		Diffuse Horizontal Irradiance	Range	0 - 4000 W/m^2
			Accuracy	± 2 W/m^2
	(MS-56 Pyranometer)	Direct Normal Irradiance	Range	0 - 4000 W/m^2
			Accuracy	± 1 W/m^2
CO_2 Meter *(K-33 ELG)*		Carbon dioxide (indoor)	Range	0 – 10000 ppm
			Accuracy	± 30ppm ± 3%
		Temperature (indoor)	Range	-40 to 60C
			Accuracy	± 0.4ºC at 25ºC

4.3.4. Measurement configurations

There were a total of seven measurement periods, allowing for variations in the number of thermal plumes, heat gain density and ventilation opening area. Table 19 presents a summary of the settings used in each period (five in kindergarten and two in the UL classroom). The experimental setup of the kindergarten cases allows for the evaluation of the impact of A*, number of plumes and chimney height on neutral height position and room air temperature. All measurements are used to validate the EnergyPlus DV model proposed on Chapter 2. The model outputs that will be analyzed are: floor level air temperature (0.1m), occupied zone temperature and mixed layer temperature.

Table 19 - Natural DV measured cases.

Cases		Nº of plumes	W/plume	W/m²	Opening Area (%)		A*
					A_{in}	A_{out}	
CML Kindergarten	KD0_1_5P	5	400	66	100	100	0.07
	KD1_1_5P	5	400	66	100	100	0.07
	KD1_2_5P	5	400	66	50	100	0.06
	KD1_1_1P	1	2000	66	100	100	0.07
	KD1_2_1P	1	2000	66	50	100	0.06
UL Classroom	CLR_1_6P	6	308	28	100	50	0.09
	CLR_2_6P	6	308	28	50	50	0.07

4.4 Experimental results

Figure 26 and 27 show the results of the temperature and CO_2 measurements from the kindergarten cases (KD0 and KD1). On the left chart in Figure 26 we can see the impact of a reduction of 50% in the inflow area (15% reduction in A*): as the inflow rate decreases the indoor air temperature rises. The right chart of Figure 26 displays the effect on natural DV system performance of increasing the number of plumes (1 to 5): higher flow rate and, for the same outdoor temperature, lower indoor air temperature.

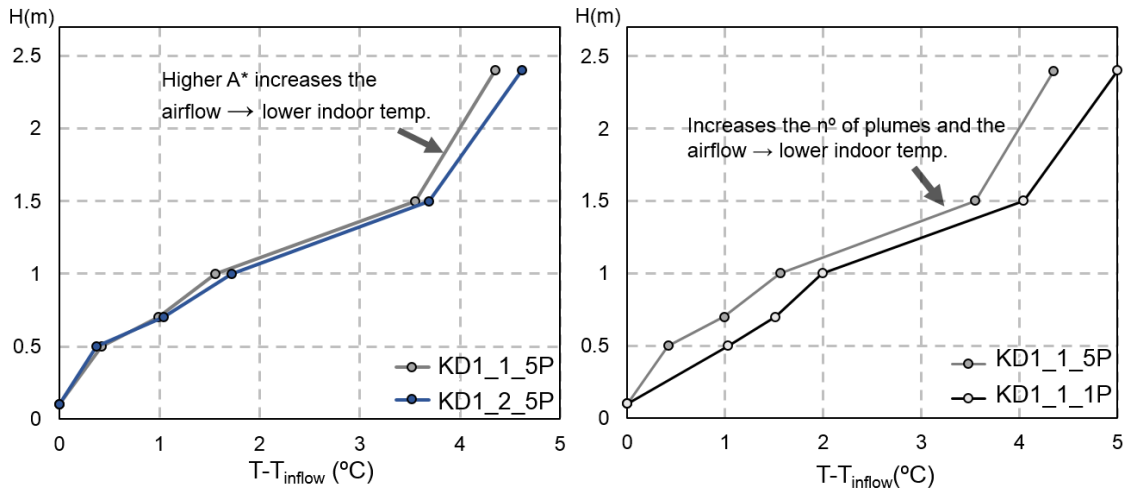

Figure 26.Kindergarten measurements results: A* and number of plumes impact on indoor air temperature profile.

Figure 27 presents the impact of room stack height on indoor air temperature profile. The two lines shown in the figure were measured simultaneously in the 3m and 6m stack rooms using similar internal gains (cases KD0_1_5P and KD1_1_5P in Table 19). These results confirm that, as expected, doubling the stack height increases the airflow rate and lowers the indoor air temperature (≈1ºC at 1m). Similar measurements performed in multi-story naturally ventilated library also showed that, in comparison with lower floors, the upper floors tend to be warmer due to reduced chimney height [116]. For these cases, the temperature increased between indoor and outdoor is 5-6ºC. This large value is partially due to the high internal gains used in the tests (66W/m^2). In the next section of this paper, these measurements will be used to assess the simulation precision of EnergyPlus for natural DV rooms.

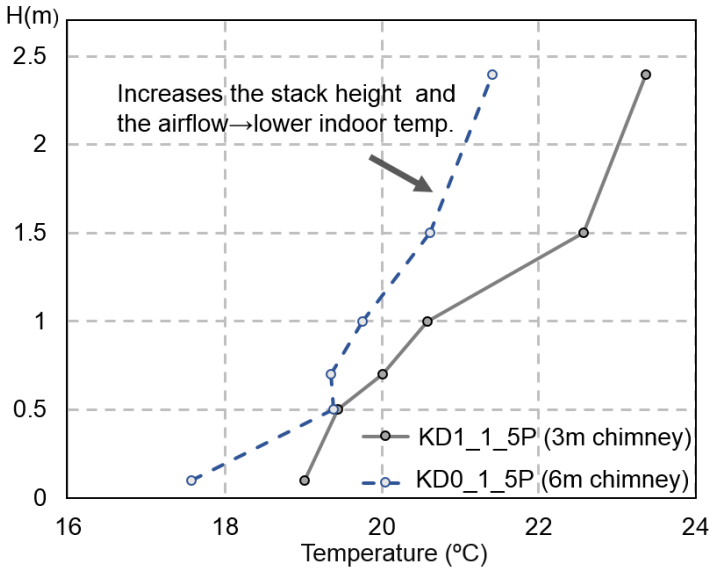

Figure 27. Kindergarten measurements results: impact of chimney height on indoor air temperature profile (outdoor air temperature =13.7ºC).

4.5. EnergyPlus thermal and airflow simulation

The simulations were performed in EnergyPlus, version 8.3.0 [99,100]. The thermal zoning strategy used in simulation models impacts the results and must be carefully defined. In the present case, both room simulation models used two thermal zones (Figure 28). The UL room model included, in addition to the classroom, the interior corridor that connects to the outside (the supply airflow comes from this corridor). In the UL simulations the air temperature of the corridor is set to the measured air temperature for this space. In the CML kindergarten the second zone is the thermal chimney. The two thermal zones are connected by a virtual horizontal opening.

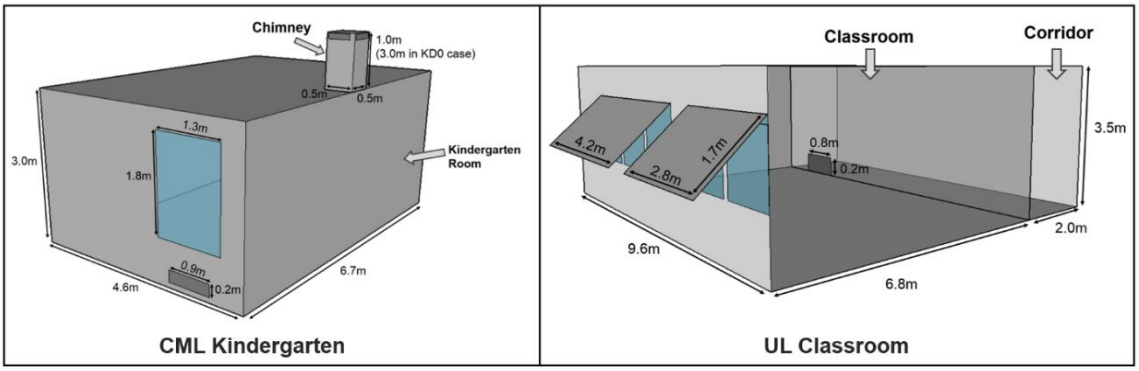

Figure 28. Kindergarten and UL classroom thermal zones (geometric model).

NV flow was simulated using the airflow network model [100] that has the capability to simulate multizone buoyancy and/or wind driven airflow. This model allows for manual introduction of wind driven pressure coefficients or automatic generation. In the present case, the buildings are located in an urban environment influenced by several surrounding buildings, resulting in low wind driven surface pressures. Further, during the measurement period the average wind velocity was ≤0.5m/s. This effect combined with the opening configurations, designed to reduce wind driven shear ventilation effects, makes the impact of wind on NV airflow negligible. In this context, the simulation flows are driven exclusively by buoyancy. The adequate discharge coefficient [117] associated with each aperture is one the parameters that must be defined in the airflow network model. This coefficient directly affects the magnitude of the airflow. In the case of the UL classroom, the openings installed are commercially available and a 0.6 value was used. In the Kindergarten case, the complex configuration of the inlet (grilles plus radiator) and outlet (chimney with perforated plates) creates the need to use CFD simulations to determine the discharge coefficients. The methodology used and the CFD simulations performed are presented and discussed in subsection 4.5.1. Solar heat gains were modeled using “Full Interior and Exterior” setting, taking into account the shadowing effect of the exterior obstructions (such as overhangs). Internal convection was simulated using TARP algorithm [118], that selects the adequate surface natural convection correlation depending on the surface orientation and the average air to surface temperature difference.

According to what was showed on Chapter 2, in order to correctly model the stratification in DV flows a minimum of three-air temperature nodes must be used. In this context, the DV proposed model, presented on Chapter 2 (Figure 29) was implemented in EnergyPlus source code and was used in the simulations presented in this chapter.

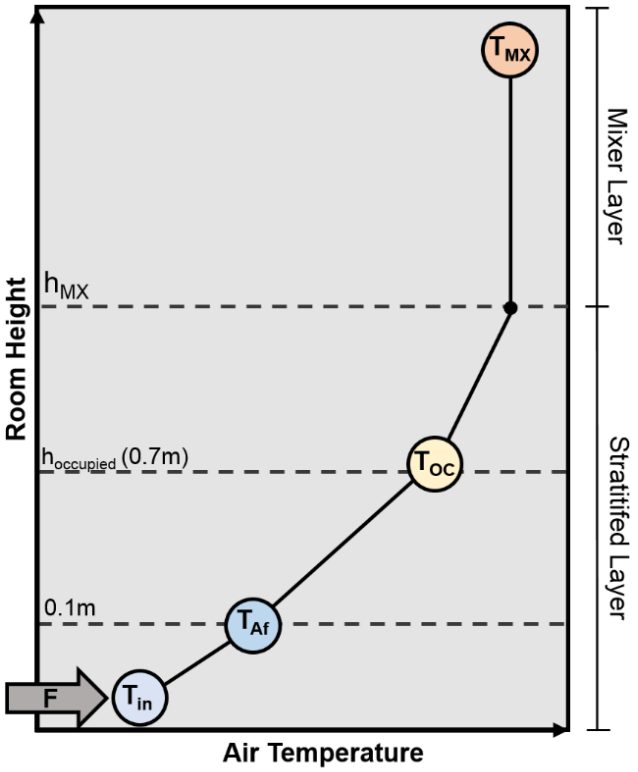

Figure 29. Three-node DV model structure implemented on EnergyPlus.

4.5.1. CFD calculation of discharge coefficients

This section presents the CFD simulations of the inflow and outflow opening geometries of the kindergarten NV systems. These simulations were required to determine the discharge coefficients (C_d) that result from complex inlet and outlet configurations. Particularly in the inflow opening, the system is difficult to characterize due to the succession of elements that compose this inflow systems: the inflow grille, the plenum and the opening in the back of the radiator. The CFD simulations were performed in PHOENICS (2015) [119], using the standard k-ε turbulence model. Figure 30 shows the geometry used in the inlet. The right side of the figure shows, for illustrative purposes, the air velocity obtained in the simulations.

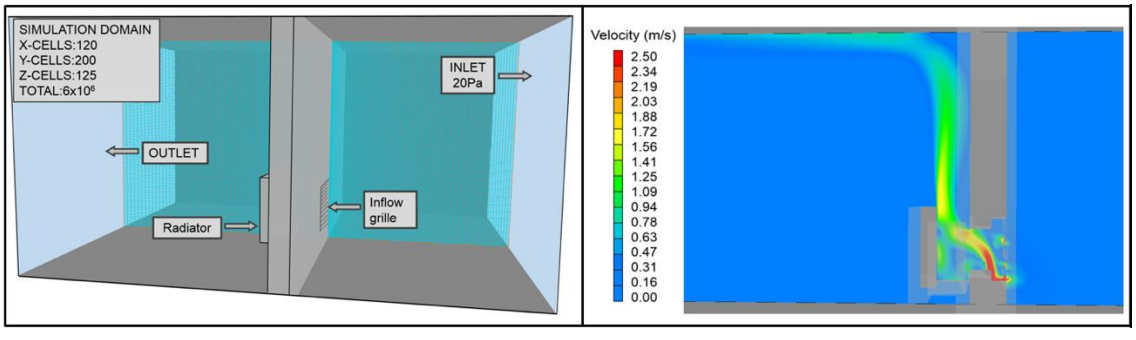

Figure 30. Inlet CFD simulations: geometry and results.

The discharge coefficient was calculated using the flow (F) obtained in the CFD simulations by imposing a 20Pa pressure in the inflow:

$$C_d = \frac{F}{A_{opening} \times \sqrt{2 \times \rho \times \Delta P}} \quad (34)$$

Where $A_{opening}$ is the opening area that will be used in the EnergyPlus simulations. For each case, a grid sensibility analysis was performed, using an increasing number of simulation cells, shown on the left side of figure 30 and 31. The results of grid sensibility analysis are presented on Table 20, confirming the grid independence of the results obtained. This methodology was also used to calculate the outlet discharge coefficient. The left side of the Figure 31 shows the geometry considered. The perforated metal plates on the top of the chimney were characterized using the CIBSE model [120] with an airflow permeability of 15%. The discharge coefficients obtained were 0.50 for the outlet and 0.32 for the inlet.

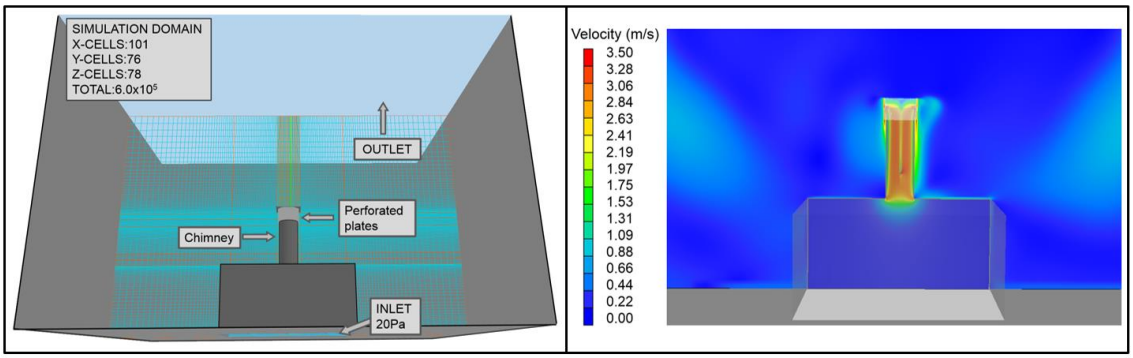

Figure 31. Outlet CFD simulations: geometry and results.

Table 20 - Grid sensibility analysis: discharge coefficient results.

Opening	Number of cells	Discharge coefficient
Inlet	$3.0x10^6$	0.30
	$6.0x10^6$	0.32
	$9.0x10^6$	0.32
Outlet	$3.0x10^5$	0.49
	$6.0x10^5$	0.50
	$9.0x10^5$	0.50

4.6. EnergyPlus validation results

This section presents the evaluation of the thermal simulation precision for the experimental cases shown in Table 19. The simulations are evaluated by comparing two sets of parameters: bulk airflow rate and DV model temperature nodes. The differences between the predicted and measured airflow rates were quantified using the following error indicators:

$$\text{Bias (l/s)} = F_{simulated} - F_{measured} \quad (35)$$

$$\text{Error (\%)} = 100\% \times \left|\frac{F_{simulated} - F_{measured}}{F_{measured}}\right| \quad (36)$$

Figure 32 presents the comparison between the simulated and measured bulk airflow rate. Overall, there is a good agreement (r^2=0.77), negligible bias (10l/s) and the average error of 16%. The comparison between kindergarten cases KD1_1_5P and KD0_1_5P (3.5m and 6.5m stack height, respectively) shows, as expected, an increase of 170% in the airflow rate of higher chimney case.

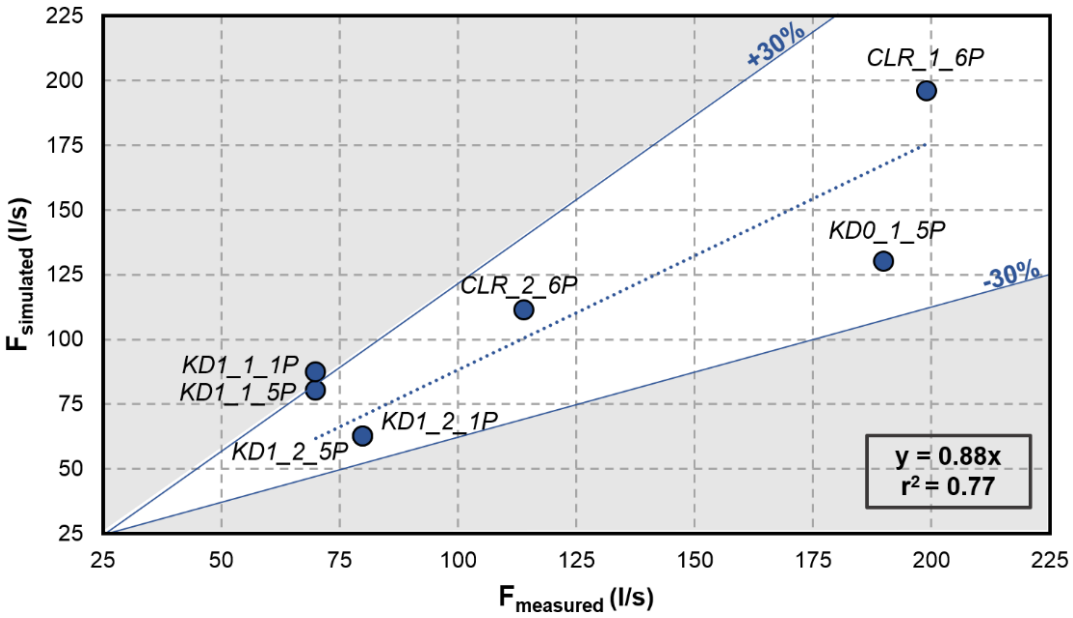

Figure 32. Bulk airflow rate results: measured vs simulated.

The simulation results for the air temperature are evaluated using the following average error indicators:

The average norm of the error: Avg. Dif. (K) = |Simulated - Measured| (37)

The average bias: Avg. Bias (K) = Simulated - Measured (38)

The average percentage error: Avg. Error (%) = $\left|\frac{\text{Simulated - Measured}}{\text{Measured}_{max.}\text{-Measured}_{min.}}\right|$ (39)

Table 21 shows the values of the average error indicators for the node temperatures in the temperature profiles of the seven experimental cases. The average simulation error is 4%, corresponding to an average difference of 0.7ºC. In the node with the largest average error, T_{af} (8%), there is a systematic under prediction. This problem was also previously observed in simulation validation on mechanically conditioned rooms presented on Chapters 2 and 3 and will be addressed in future research. The overall agreement in the other two air nodes, T_{MX} and $T_{OC,}$ is very good: the maximum error achieved is less than 6%. Figure 33 show the results of the temperature obtained in the three-node model simulation. As expected, the agreement in T_{MX} node is higher due to the imposed mass/energy balance on the model structure.

Table 21 - Comparison between measured and simulated node temperatures: T_{AF}, T_{OC} and T_{MX}.

Case\Node	**Avg. Dif.(ºC)**			**Avg. Bias (ºC)**			**Avg. Error (%)**		
	T_{AF}	***T_{OC}***	***T_{MX}***	***T_{AF}***	***T_{OC}***	***T_{MX}***	***T_{AF}***	***T_{OC}***	***T_{MX}***
KD0_1_5P	1.4	1.0	0.2	-1.4	-1.0	-1.0	7.7	5.1	0.8
KD1_1_5P	1.2	1.0	0.3	-1.2	1.0	0.0	6.3	5.2	1.3
KD1_2_5P	2.3	0.8	0.4	-2.3	0.8	0.0	11.6	4.1	1.5
KD1_1_1P	1.8	0.1	0.4	-1.8	-0.1	0.0	11.7	0.3	1.9
KD1_2_1P	2.1	0.6	0.0	-2.1	0.6	0.0	12.1	3.2	0.1
CLR_1_6P	0.5	0.1	0.4	-0.5	0.1	0.0	2.4	0.5	1.6
CLR_2_6P	0.9	0.1	0.1	-0.9	-0.1	0.0	4.1	0.3	0.4
Average indicators	**1.4**	**0.5**	**0.2**	**-1.4**	**0.2**	**-0.1**	**8.0**	**2.7**	**1.1**

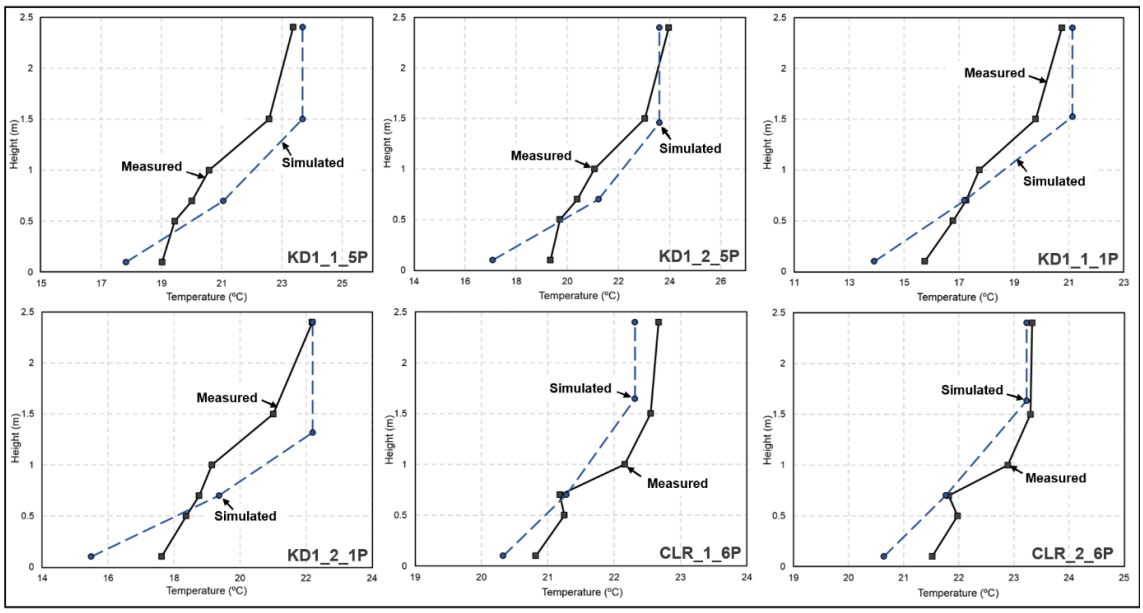

Figure 33. Three-node DV model temperature results comparison.

The kindergarten classroom simulations presented in section 4.6 use discharge coefficients calculated using CFD simulations. In many engineering design contexts CFD simulations are not available due to lack of time or access to a CFD code. In these cases, designers use tabulated or measured values that are typically obtained for particular geometries that do not fully match the cases that are being simulated. This subsection analyses the impact of using tabulated discharge coefficients in the simulation results.

The tabulated values used in this comparison were: inlet, C_d of 0.5 (obtained for ventilation dampers [121]), outlet, C_d of 0.52 (measured for chimneys [122]). The impact is shown in Table 22 using the error indicators presented in the previous section.

Table 22 - Sensitivity analysis: impact of discharge coefficient on three-node DV model simulation results.

Case\Node	**Avg. Error (%)**					
	T_{AF}		***T_{OC}***		***T_{MX}***	
	CFD	*Tabulated*	*CFD*	*Tabulated*	*CFD*	*Tabulated*
KD0_1_5P	7.7	9.2	5.1	7.2	0.8	1.7
KD1_1_5P	6.3	11.9	5.2	3.1	1.3	5.7
KD1_2_5P	11.6	17.4	4.1	5	1.5	7.8
KD1_1_1P	11.7	19.3	0.3	10.2	1.9	6.6
KD1_2_1P	12.1	18.5	3.2	6.2	0.1	6.7
Average indicators	**9.9**	**15.3**	**3.6**	**6.4**	**1.1**	**5.7**

The impact of using tabulated values is clearly visible in the increased error for all temperature nodes. The larger is in the air temperature near the floor (T_{AF}, increasing from 8% to 15%). The impact in the T_{OC} and T_{MX} nodes is lower but still noticeable. These results indicate that, with the exception of the air temperature near the floor, it is possible to use tabulated discharge coefficients and still achieve errors below 10%.

4.7. Conclusions

This chapter presents a validation of the proposed three-node DV model implemented on the open-source thermal building simulation software EnergyPlus. The model was used to predict bulk airflow rates and the vertical temperature gradient in three rooms located in two educational buildings, a kindergarten and a university, with different buoyancy driven natural DV systems (with and without chimneys).

The comparative measurements performed in the two kindergarten rooms results revealed, that as expected, increasing chimney height from 1 to 4m has a significant positive impact in NV system performance. For the internal convective gains used in the measurements, 66W/m^2, the larger chimney increases the bulk flow by 170% and reduces the occupied zone temperature by 1.2ºC. The performance of natural DV systems depends on the number of thermal plumes in the room. For the same sensible heat load, increasing the number of plumes from one to five lowers the average occupied zone air temperature (0.6ºC) and increases the bulk airflow rate (9%). All measured temperature profiles showed clear stratification and were not significantly disrupted by envelope heat transfer effects.

The validation results show that the building thermal simulation model tested is able to predict bulk airflow rate with an average error of 16% resulting in a correlation factor of 0.77 (r^2). In addition, a good agreement is also obtained for the vertical temperature prediction: an average error of 4% corresponding (average deviation of 0.7ºC). The largest temperature deviation occurs near the floor (T_{af} node, 8% error), future model development work will investigate the energy balance and air mixing that occur in this node. The sensitivity analysis performed showed that the use of tabulated discharge coefficients instead of coefficients obtained using CFD has a negative impact on modeling precision. Still, the average error obtained with the tabulated discharge coefficients is acceptable for typical engineering calculations (9%). In light of the complexity of the cases tested, NV with uncontrolled boundary conditions, the results of the comparisons performed between measurements and simulations should contribute

to increase confidence in the use of EnergyPlus to simulate buoyancy driven natural DV systems.

5. Measured performance of a displacement ventilation system in a large concert hall

DV systems were initially developed as an efficient buoyant pollutant removal strategy for Scandinavian high ceiling industrial halls (in the 70´s [5]). In the 80's these systems started being used in the mechanical cooling of office buildings, taking advantage of its recognized potential to reduce room airflow velocities, ventilation induced noise, HVAC energy consumption and remove heat efficiently [47]. Despite these advantages, the application of DV in office buildings is limited by system geometry constraints that limit cooling capacity. Limited space to install relatively large diffusers in the floor or office walls, combined with the obstacles created by office furniture that limit the airflow rate and consequently the cooling capacity to 25-35W/m^2 [48,49,50] (see Figure 34). In contrast, in large rooms, such as concert halls or theatres, there is more space to install inflow air diffusers under the seats, and the fresh inflow air is supplied directly to the occupied zone (Figure 34), leading to a possible increase of the cooling capacity up to 180W/m^2 (up to five times more than the typical office buildings removal heat loads capacity).

Most large rooms are characterized by highly variable and a non-permanent use that can range from a nearly empty room to a completely full audience plus high lighting loads. Therefore, low energy consumption may not be the main priority but rather high comfort levels for the occupants and low HVAC noise levels that in most cases can only be achieved using low velocity supply of DV diffusers.

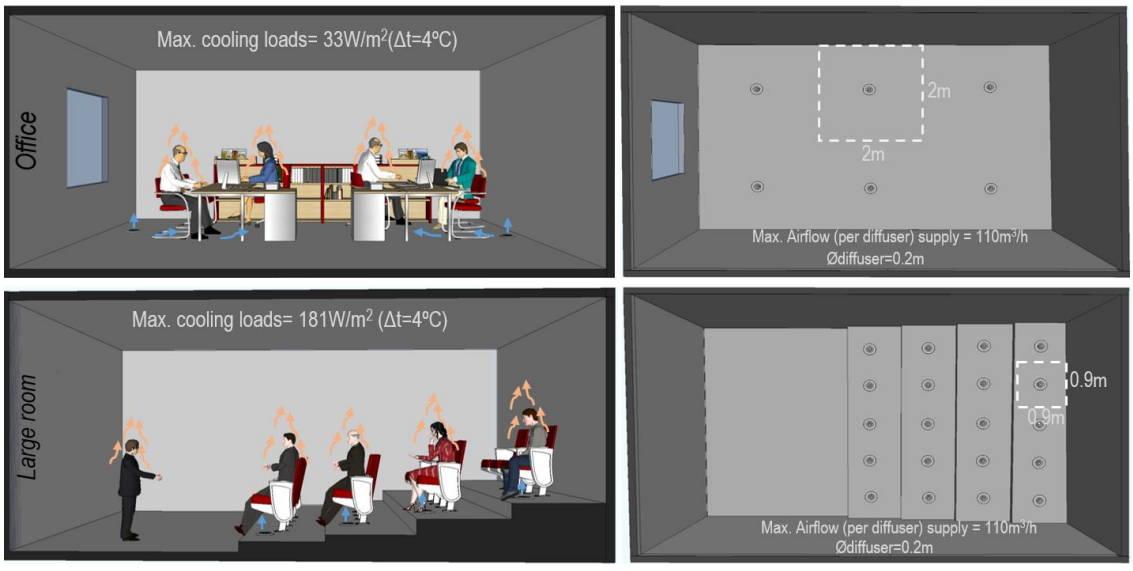

Figure 34. Typical office and large DV rooms maximum cooling loads.

The stratified room environment that characterizes DV systems creates difficulties to designers when sizing or predicting the energy consumption of a space where a single node cannot be used to model the whole room air conditions (approach used to model MX systems). To assist in the design process of DV systems several modelling approaches with different levels of complexity have been developed in the last decades, including simplified design methods, simplified nodal models and CFD simulations. CFD can produce detailed predictions of complex airflow patterns and is the most complete and adequate tool to model DV systems. Alternatively, nodal models can be easily implemented in a dynamic thermal simulation software that is currently a requirement in most of national building regulations and the standard feature in building design. Still, the majority of DV nodal models developed were validated with measurements performed in test cells with controlled boundary conditions what may limit conclusions about model applicability in buildings with active boundary conditions (the most common case). In fact, there is also a lack of measurements that investigate the performance of DV systems in occupied large rooms, leading the authors of this paper to perform a set o measurements in two occupied large rooms with the following goals:

1. How the radiative heat exchanges with the walls could affect the expected temperature and contaminants vertical profiles?
2. Are the thermal stratification profiles in occupied buildings with active boundary conditions similar to the ones measured in test cell cases?
3. Validate the proposed model [71] for large rooms.

To analyze these questions a set of measurements were carried out in two large rooms with active boundary conditions and real occupancy: a large Concert hall and an Orchestra rehearsal room. Further, the results of measurements also allows the comparison with the outputs of a three-node DV model [71] implemented in the thermal simulation tool EnergyPlus [99,100]. The chapter begins to present a review about HVAC systems in large rooms, followed by the presentation of the measurement setup considered. Section 3 presents and analyses the measurement results (DV system performance). Finally, on Sections 4 and 5 the EnergyPlus simulation model used is presented and the expected precision is determined.

5.1 Review of HVAC systems in large rooms

This section presents a review about HVAC systems in large rooms, where are discussed the most common configurations and the approaches used to analyze its performance. Usually, large rooms represent an additional challenge for the designer's

team, not only for the dimension of the space but also for its main purpose, as part of a service building, the occupants comfort is the ultimate goal that need to be ensured. These kind of rooms are characterized by high ceiling height, low ventilation airflow rates and high cooling and/or heating loads [123]. For the analysis performed in this paper, large rooms are defined according with the dimension of the space: minimum of 300m^2 area and a floor-ceiling height of 5m. Table 23 presents the results of the survey performed.

This bibliographic review identified two types of large rooms: educational (lecture hall) and entertainment (concert hall e theatre and cinema). Three types of airflow distribution methods have been used: DV, MX and underfloor air distribution (UFAD). The most common approach used in entertainment rooms is DV airflow distribution method. Initial measurements about DV system performance in real buildings were performed in 1989 [124]. The analysis of the results of these measurements indicated that the air quality and the thermal comfort could be achieved for most of the space. The main problems detected are related to the accumulation of heat and CO_2 on the last rows of the audience and on balcony area [124,125]. In 2008, similar measurements performed in a theatre (in Belgrade) identified the overventilation of the space as a major potential problem for DV system performance, which may result in excessive energy consumption and occupant's cold draft discomfort [126]. To control and predict these potential problems CFD simulations are the most suitable tool, as it can be used to analyze complex airflow patterns of improved modifications against the existing installation [127].

Otherwise, MX are the commonest airflow distribution method applied to lower ceiling height rooms, as the lecture halls. In MX systems, the main problems detected are related to the existence of recirculation zones that promote the accumulation of CO_2 in the occupied zone [128]. Some authors, indicate an intensive early design stage where should be tested and analyzed several HVAC system configurations and constructive solutions as the solution to prevent the identified problems [129,130]. The airflow distribution method less used in large rooms is the UFAD, which principles are similar to DV. In UFAD, the air is supplied from an under floor plenum using swirl diffusers that induce more mixing than standard DV diffusers. This systems allows higher differential between inflow and room air temperature difference (≈10ºC) and, consequently, higher cooling capacity. However, the higher supply air velocity may also induce discomfort by air drafts [131,132,133]. The cases presented on Table 23 reveals that the most used approach to study HVAC systems in large rooms are CFD simulations and the use of dynamic thermal simulation tools has not been an option considered for this purpose.

Table 23 - Large rooms studies references.

Reference	Room type	Heat loads (W/m^2)	Airflow rate ($m^3/h.m^2$)	System config.	Approach used
H. M. Mathisen [124]	Auditorium, theatre, cinema	105-316	31-107	DV	Measurements & CFD
P. Ricciardi, *et al.*[125]	Concert hall	-	-	DV	Measurements & questionnaires
M. Kavgic, *et al.*[126]	Theatre	68	31	DV	Measurements & CFD
A. Scanlon, *et al.*[127]	Concert hall	-	-	MX & DV	CFD
K.W.D. Cheong, *et al.*[128]	Lecture hall	-	55	MX	Measurements & CFD
H. Hangan, *et al.*[129]	Concert hall	-	-	MX	CFD
M.W. Muhieldeen, *et al.*[130]	Lecture hall	81	-	MX	Measurements & CFD
M. H. Fathollahzadeh, *et al.*[131]	Lecture hall	115	-	UFAD	CFD
Y. Cheng, *et al.*[132]	Lecture hall	35	4.4-13	UFAD	CFD
G. Kim, *et al.*[133]	Lecture hall	98	-	UFAD & MX	CFD & questionnaires

5.2. Field monitoring

The measurements were performed in two distinct rooms of Calouste Gulbenkian Foundation building in Lisbon (Portugal): the Concert hall and the Orchestra rehearsal room. The Calouste Gulbenkian Foundation building is one of the most important engineering and architectonic projects of the 20th century in Portugal. However, after more than forty years of intense use, the existing HVAC systems did not meet the current requirements of indoor air quality and thermal comfort creating the opportunity to update the existing systems and improve the efficiency of the HVAC system. The refurbishment of the building was concluded in 2014 and the updated HVAC systems of the new Orchestra rehearsal room and the Concert hall represent an opportunity to analyse a contemporary DV system operating under real usage conditions. In this section, the two rooms and corresponding HVAC systems are presented and the experimental procedures are described.

5.2.1 Concert hall

The Concert hall was part of the initial structure of Calouste Gulbenkian Foundation building built in 1960's. This room has a seating capacity of 1100 on the main floor plus 200 seats on a balcony area and up to 250 artists in the stage (Figure 35).

Figure 35. Concert hall: audience and stage.

The HVAC system (installed during the refurbishment project in 2014, presented on section 6.1), consist in three air-handling units, one for each zone of the room: audience, stage and orchestra pit. The audience area and the orchestra pit is served by a low-velocity DV system while in the stage, the functional requirements of the stage make the use of a DV system with low-level inflow diffusers extremely difficult. For this reason, the stage has a variable configuration consisting in high-level nozzles and low-velocity air supply from the pressurized under-stage. The Figure 36 presents the actual Concert hall HVAC system configuration.

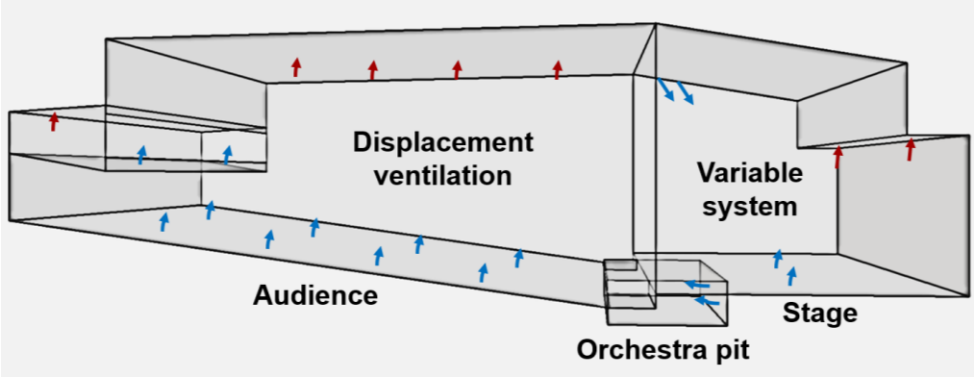

Figure 36. Concert hall HVAC system configuration.

The measurements were performed during a classical orchestra concert: 400 persons in the audience and 70 musicians on the stage. The focus of these measurements was the performance of the DV system in the audience area. To capture the room characteristic temperature and CO_2 vertical profile two vertical columns of 8 sensors (CO_2 meter) were installed in positions 2 and 3 (see Figure 37). To analyze possible localized effects, two sensors at 0.1m and 0.7m were installed in positions 1 and 4. The temperature of each surface was measured before, during and after the concert.

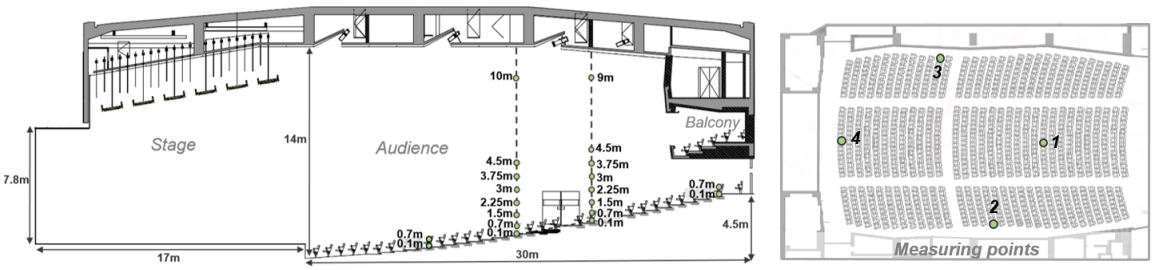

Figure 37. Locations of the sensors used in the Concert hall measurements.

5.2.2 Orchestra rehearsal room

The Orchestra rehearsal room was built in 2014 during the refurbishment of Calouste Gulbenkian Foundation building and consists in a 325m^2 room (7m height) with maximum capacity for 150 musicians (Figure 38). The HVAC system was designed considering the thermal comfort of the occupants but also the acoustic and constructional restraints of an orchestra rehearsal space, thus, a low-velocity DV system supported by a radiant floor was installed. The air is supplied thought wall perforated plate diffusers (hidden by architectural wood panels) and extracted on the ceiling. The hydraulic radiant floor has heating and cooling capacity, but only was used in cases of low occupancy to ensure the users thermal comfort.

Figure 38. Orchestra rehearsal room.

Figure 39 presents the measurement setup used in Orchestra rehearsal room, that as in Concert hall case, display a vertical column of 8 temperature and CO_2 concentration sensors installed near the middle of the room. The remaining occupied zone is monitored by two sensors positioned at 0.7m (as shown on Figure 39). The supply air conditions were also measured by a CO_2 meter sensor. The measurements were performed during a conference lecture with 65 occupants, and only the DV part of the HVAC system is under operation (the room thermal conditions did not require the radiant floor). As in Concert hall measurements, all surfaces temperature were measured before, during and after the room occupation.

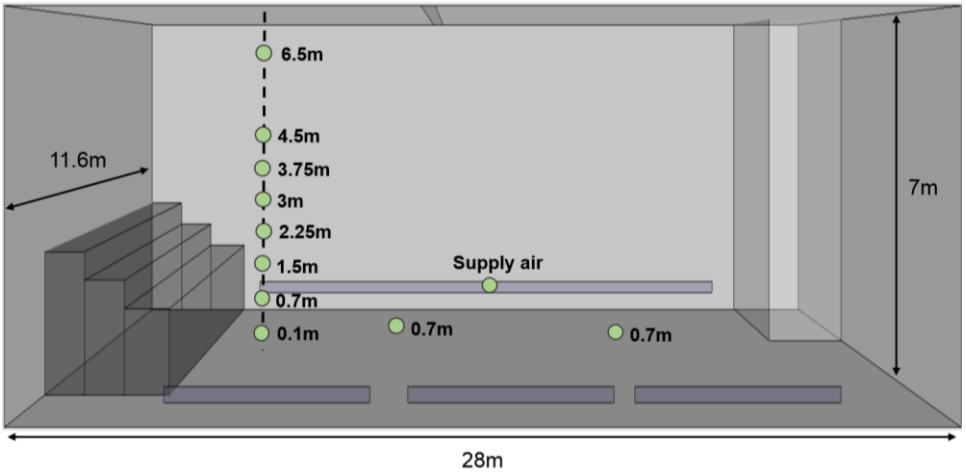

Figure 39. Locations of the sensors used in the Orchestra rehearsal room measurements.

Table 24 shows the specifications of the equipment used in two large rooms measurements. The weather station is located in the Calouste Gulbenkian Foundation garden and measures air temperature and humidity. The setup also included a set of indoor temperature and CO_2 sensors that was used to capture the vertical temperature and CO_2 profiles (CO_2 meter), and an infrared sensor that measure the surfaces temperature (FLIR i7). The weather data was measured in ten-minute intervals and is included in the EnergyPlus weather file used in the simulations presented below.

Table 24 - Specifications of the measurement equipment used.

Sensor	Measurement	Specifications	
Lufft *(Weather Station 500)*	Temperature	Range	-50 to 60 º C
		Accuracy	± 0,2ºC (-20 to 50ºC)
	Relative humidity	Range	0 to 100% RH
		Accuracy	± 2% RH
CO_2 Meter *(K-33 ELG)*	Carbon dioxide (indoor)	Range	0 – 10000 ppm
		Accuracy	± 30ppm ± 3%
	Temperature (indoor)	Range	-40 to 60C
		Accuracy	± 0.4ºC at 25ºC
FLIR i7	Surface temperature	Range	-20ºC to 250ºC
		Accuracy	± 2%

5.3. Analysis of measurement results

The experimental setup used in the Concert hall and Orchestra rehearsal room allows for the evaluation of DV system performance, including the analysis of the temperature and CO_2 concentration vertical profiles, the determination of the neutral height position and the ventilation efficiency of each room DV system.

5.3.1 Neutral height prediction

The neutral height (h_n) position corresponds to the transition height that separates the lower stratified layer from the upper mixed zone and defines the point where the total plume flow matches the inflow air flow rate [35]. The position of this point is determined by the balance between the upwards convective flows generated by the plumes and the descending flows that can be promoted by cold surfaces [134]. Several cases of measurements performed in adiabatic test chambers reveals that the temperature and CO_2 gradient is higher between floor and the lower part of the mixed layer [22, 27], and the neutral height position is approximately located at the transition point where that gradient become markedly lower. In cases like these, where the air-surface exchanges are almost null there is an almost perfect matching between the neutral height position determined in temperature and CO_2 profiles [20]. In CO_2 profiles, due to CO_2 concentration independency from surfaces heat exchanges is easy to determine neutral height position by visual inspection [34]. However, in buildings with active boundary conditions, the effect of the air-surface radiative heat exchanges on temperature profile is unknown and the determination of the neutral height position could be more difficult. To identify this point in a measured temperature profile the numerical method presented on Chapter 2 will be used. This method defines the location of the neutral height as the point where the temperature gradient of two consecutive points is smaller than 1.3 times the total temperature gradient of that room:

$$1.3 \times \frac{T_{z_{total}} - T_{z_0}}{Z_{total} - Z_0} > \frac{T_{z+1} - T_z}{(Z+1) - Z} \qquad (40)$$

Otherwise, to determine the neutral height position numerically it was necessary to identify the type of plumes generated by each heat source (that in the measured cases are persons). Figure 40 presents a schematic representation of the expected vertical temperature variations profiles and the correspondent buoyancy flow rate equation [35]. In the most common cases, like a single person in a room, the thermal plumes are generated by single point sources of buoyancy. However, when several point sources are close enough can coalesce before the beginning of the mixed layer and form one plume with different aspect. The second and third columns of Figure 40 show the

possible result of point source plumes coalescence: linear and horizontal thermal plumes, respectively. For a given room inflow (F) and buoyancy source (G), the expected neutral height position obtained for the horizontal plumes is the lower among the three types of plumes (see Figure 40).

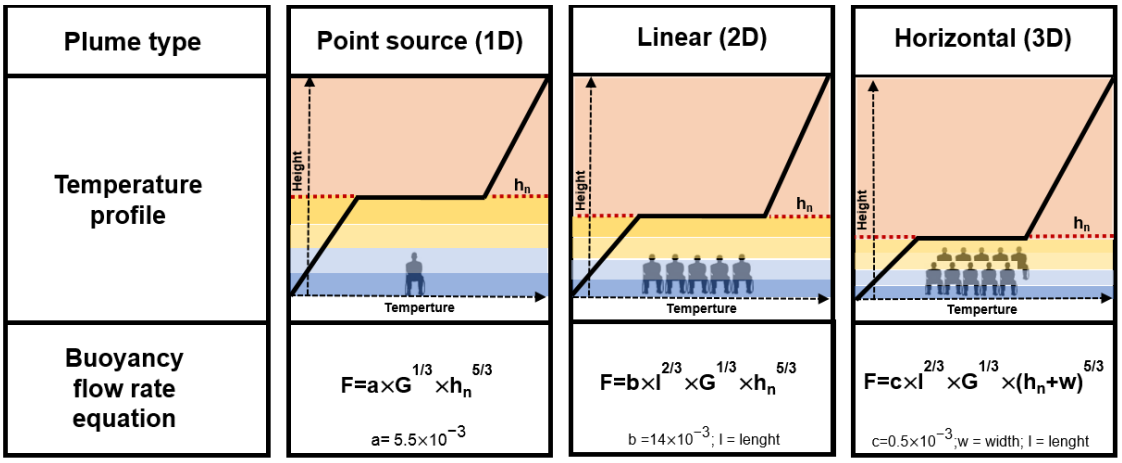

Figure 40. Expected vertical temperature profiles produced from different plume types.

In the measured cases, the plumes coalescence is a relevant question that should be analyzed in detail (determine the number and type of thermal plumes), in order to determine numerically the neutral height position (that was included in DV model implemented on EnergyPlus). To verify thermal plumes coalescence, the minimum approach to locate the virtual origin of the plumes was used (described on Chapter 2). Figure 41 shows the method used to analyzed for plume coalescence: there are no coalescence since $X_{plume1}+X_{plume2} > X_{12}$ is larger than measured neutral height position. The application of this method to the measured cases reveals plume coalescence in both cases, originating six horizontal plumes (corresponding to the six groups of seats showed on Figure 37) in Concert hall and three linear plumes in Orchestra rehearsal room case (matching the three rows of people in the audience, right side of Figure 38).

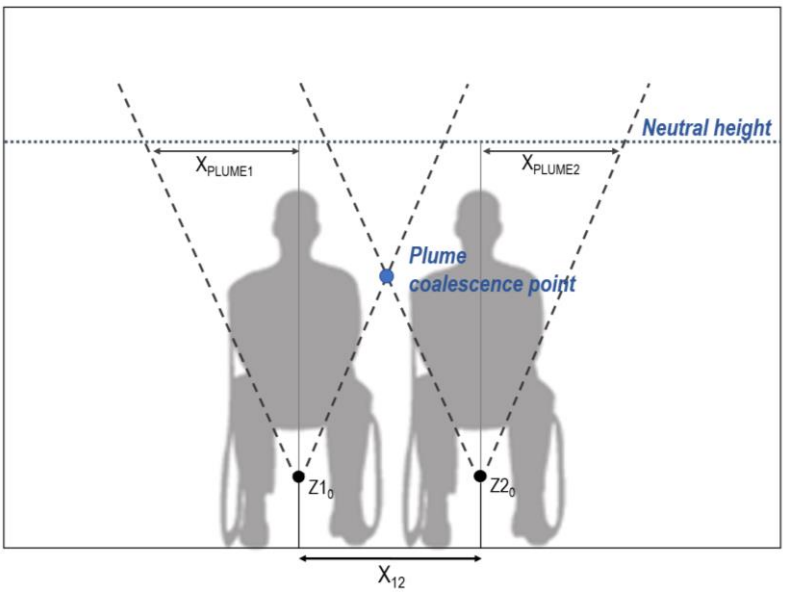

Figure 41. Method used to test plume coalescence.

The next subsections present the results obtained for the temperature and CO_2 vertical profiles that allows the determination of experimental neutral height position for each measured room. Using the methodology described previously, the experimental neutral position was compared with the obtained numerically (using the equations shown on Figure 40).

5.3.1.1 Concert hall

Figures 42-48 presents the evolution of temperature and CO_2 results during the measurement period in the Concert hall. The results show the room dynamics during the concert, the air becomes increasingly warmer and more polluted from the beginning until the end of the concert, increasing approximately 1.6ºC and 600ppm on the higher measured point (10m). In both profiles, it is possible to identify a dedicated comfort zone until 1m height (approximately seated occupants head height), where the air temperature and CO_2 concentration remains almost unchanged along the measurement period. The measured temperature gradient between ankle and head is kept bellow 0.5ºC (that is within the comfort limit of 4ºC/m [135]) and the CO_2 concentration on the occupied zone never exceed 760ppm. During the measurement period, the temperature on occupied zone is maintained bellow 22.7ºC.

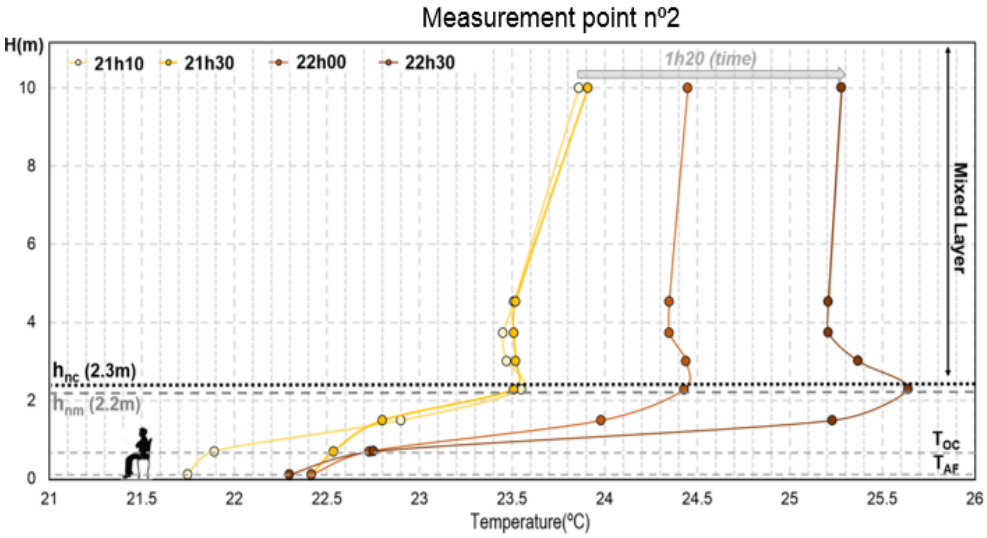

Figure 42. Concert hall dynamics: Temperature vertical profile (measurement point nº2).

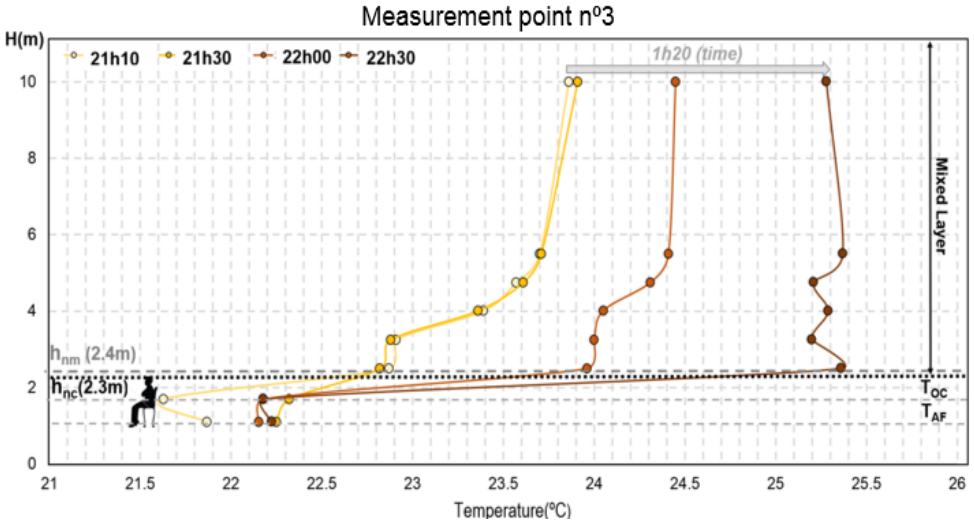

Figure 43. Concert hall dynamics: Temperature vertical profile (measurement point nº3).

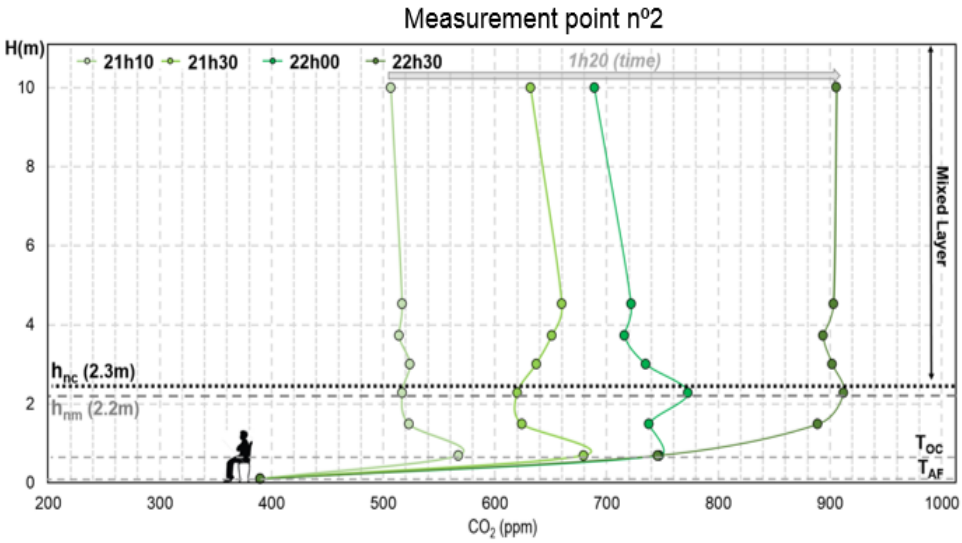

Figure 44. Concert hall dynamics: temperature and CO_2 concentration vertical profile (measurement point nº2).

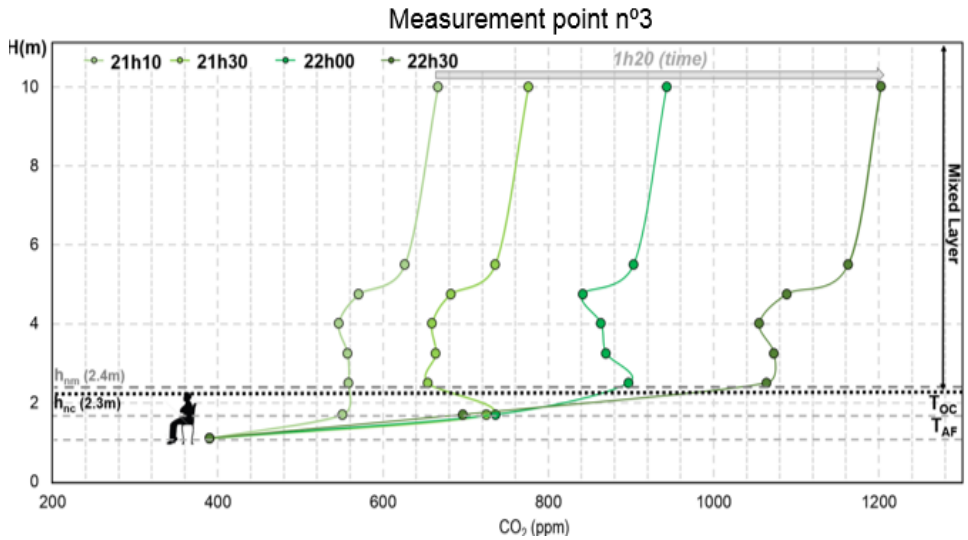

Figure 45. Concert hall dynamics: temperature and CO_2 concentration vertical profile (measurement point nº3).

Due to the slope of the room, it was also important to analyze the spatial variation of temperature and CO_2 profiles (showed on Figure 46 and 47). The profiles obtained for the measurement points 2 and 3 (front and back positions, respectively) presents similar aspect, a stratified ambient until 2.2/2.4m and an mixed layer above that with a maximum gradient of 1ºC. As expected, the back rows are warmer (+0.5ºC) and higher CO_2 concentration levels were measured (+130ppm).

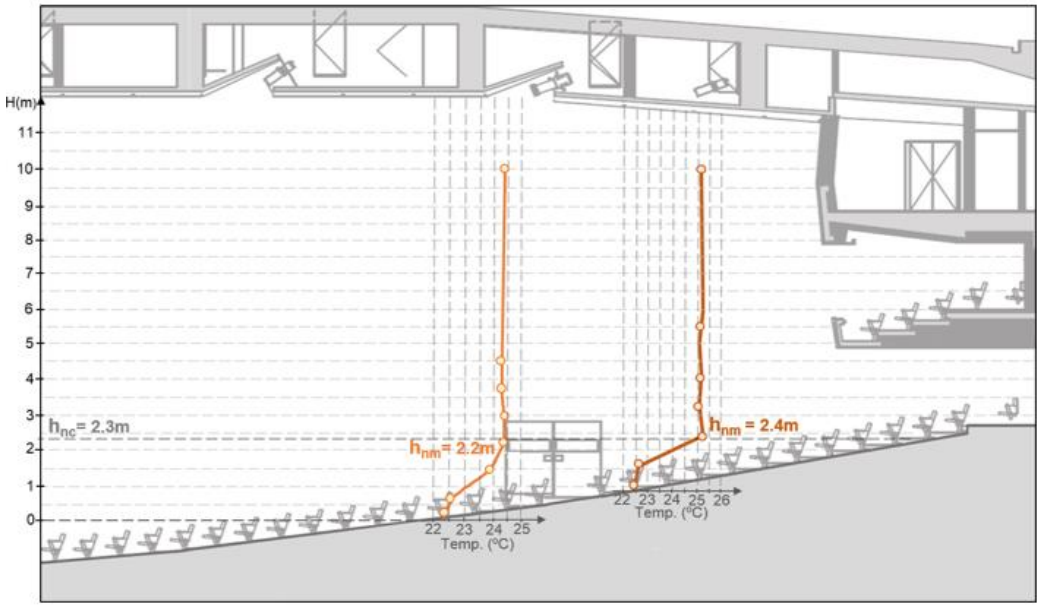

Figure 46. Concert hall spatial analysis: temperature vertical profiles.

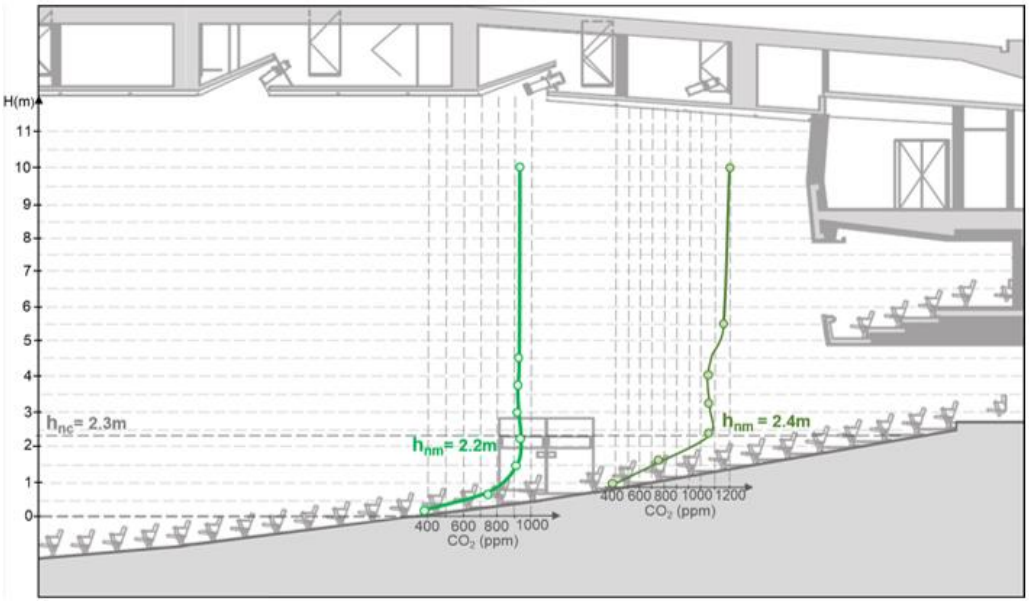

Figure 47. Concert hall spatial analysis: CO2 concentration vertical profiles.

5.3.1.2 Orchestra Rehearsal Room

Figure 48 and 49 shows the results of temperature and CO_2 vertical profiles measured in the Orchestra rehearsal room. The left side of Figure 48 presents the evolution of the room air temperature, a difference of 0.2ºC between occupant's ankles and head was obtained during the measurements. The air conditions obtained in this room are more stable, during the measuring period (1h40minutes) the room air temperature and CO_2 concentration only increased 0.7ºC and 160 ppm, respectively. This fact could be related to the higher airflow rate per heat gains that is 1.5 times higher in Orchestra rehearsal room than in the Concert hall. The comfort of the occupants was achieved during the measurements: temperature range of 21.4-21.6ºC and maximum CO_2 concentration of 680ppm on the occupied zone.

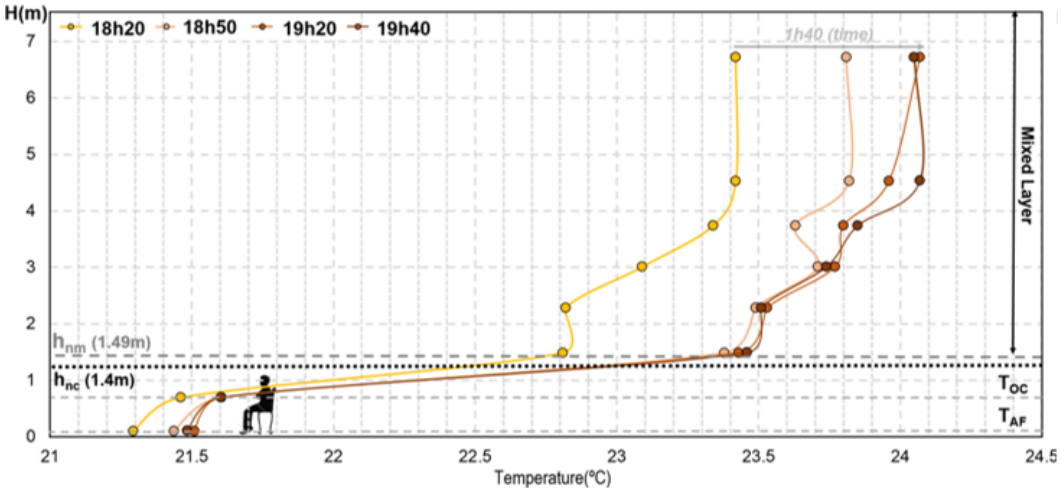

Figure 48. Orchestra rehearsal room dynamics: temperature vertical profile.

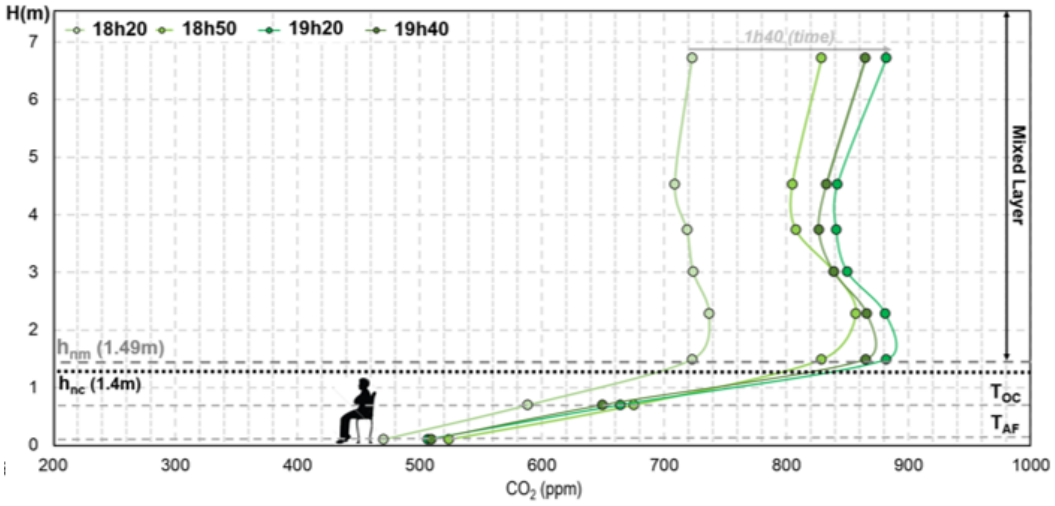

Figure 49. Orchestra rehearsal room dynamics: CO_2 concentration vertical profile.

Initial studies about DV that used scaled salt-water models results to develop a two-layer model for natural DV, identified a clear definition between stratified and mixed layer (that is completely isothermal) and an abrupt transition between the two layers is observed [11]. However, in these experiments the effect of heat diffusion and thermal radiation were completely neglected. Later, in 2002, in contrast to the results obtained in scaled salt-water models, wind tunnel results indicate the existence of a non-isothermal mixed layer in DV rooms, with a maximum gradient of 0.7ºC [136]. These results are also confirmed by the review experimental DV studies in test cells presented on Chapter 2 [71]. Even in well insulated rooms, the air heat exchanges with the room surfaces had impact on temperature profile, displaying a smoother transition between mixed and stratified layer. These results are in accordance with the measurement results obtained in this section, where the active boundary conditions of both rooms produce an even smother transition between stratified and mixed layers (average mixed layer

gradient=0.8ºC) making difficult the determination of neutral height position on temperature profiles.

To validate the applicability of method used to determine numerically the neutral height position (using the equations for linear and horizontal plumes showed in Figure 40), the results obtained were compared with the measured neutral height position. The differences between the neutral height predicted by the two methods are quantified using the following error indicators:

$$\text{Bias (m)} = h_{\text{temp. profile}} - h_{\text{numerical}} \quad (41)$$

$$\text{Error (\%)} = 100\% \times \left| \frac{h_{\text{temp. profile}} - h_{\text{numerical}}}{h_{\text{temp. profile}}} \right| \quad (42)$$

The results shown in Table 25 confirm the applicability of method used to predict the neutral height position in DV systems. The average error obtained is less than 5% corresponding to a under prediction of 4cm. In concert hall case, as expected the measured neutral height in both measuring point present a good match, showing the validity of plume flow theory (total plume flow matches the inflow airflow rate at neutral height).

Table 25 - Comparison between calculated and experimental neutral heights.

Case		$h_{calculated}$ ***(m)***	$h_{measured}$ ***(m)***	***Bias(m)***	***Error (%)***
Concert hall	*Meas. Point 2*	2.30	2.22	-0.08	3.6
	Meas. Point 3	2.30	2.42	0.12	5.0
Orchestra rehearsal room		1.41	1.49	0.08	5.4
Average				**0.04**	**4.6**

Figure 50 presents the comparison between calculated and experimental neutral heights of the 25 temperature profiles analyzed in this thesis, revealing a correlation factor of 0.80 (r^2) that corresponds to an average error of 12%. This overall results confirm the validity of the Taylor point plume flow equation to determine the neutral height position in DV rooms.

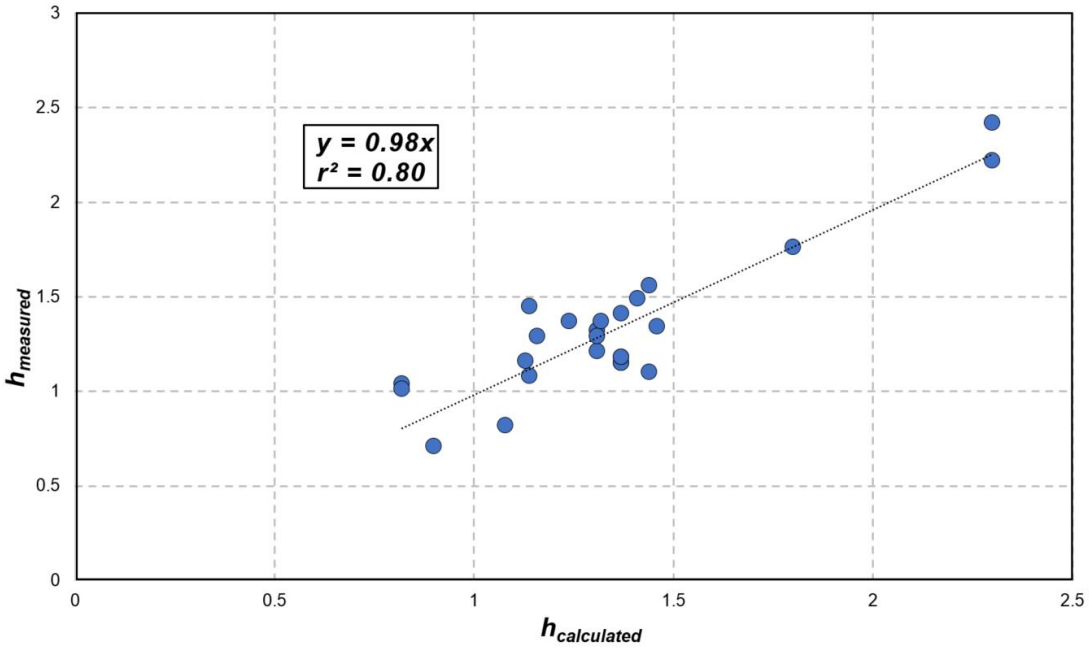

Figure 50. Correlation between calculated and experimental neutral heights of all temperature profiles analyzed.

5.3.2 HVAC system pollutant removal efficiency

The indicator that define the perceived air quality and characterize the effect of the room airflow pattern in the ventilation process is called pollutant removal efficiency (ε_p) [137].This parameter is based on contaminant concentration in the occupied zone ($C_{occupied}$, measured at 0.7m), at supply C_s, and on exhaust zone (C_e):

$$\varepsilon_p = \frac{C_e - C_s}{C_{occupied} - C_s} \quad (43)$$

Figure 51 shows the results of the evolution of pollutant removal efficiency indicator during the measurement periods in the Concert hall and Orchestra rehearsal room. Due to the airflow pattern promoted by DV systems, from low to high level, the pollutants should be removed in ideal way, corresponding to an efficiency equal or greater than one. The results obtained for the two rooms corresponds to the expected results for a DV system, resulting in an average efficiency of 1.7 and 1.2 for Orchestra rehearsal room and Concert hall, respectively. In the Figure 51 is also showed the average pollutant removal efficiency obtained for measurements performed in an auditorium, theatre and cinema (ε_p =1.71) [124] that are similar to the obtained for Orchestra rehearsal room.

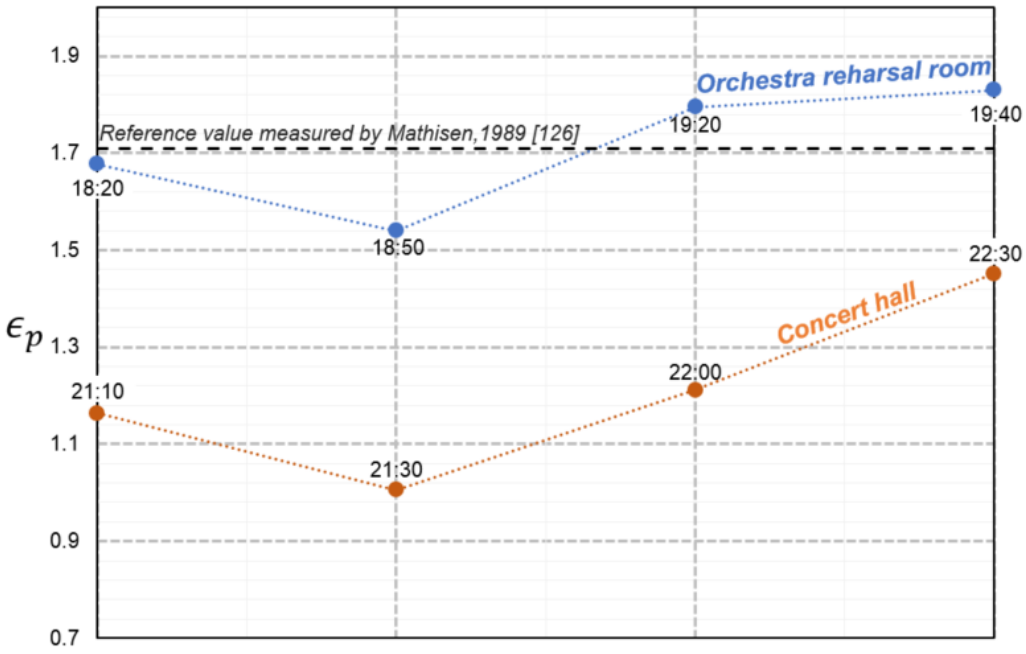

Figure 51. Concert hall and Orchestra rehearsal room pollutant removal efficiency.

5.4 EnergyPlus simulation

The simulations were performed using thermal building simulation software EnergyPlus [99, 100] (version 8.3.0) developed by the United States Department of Energy. This software is based in an open source concept and remains open to new developments by individual programmer's contributions. The EnergyPlus is a whole-building simulation that is capable to model combined heat and mass transfer balance, multizone airflows, HVAC loops, lightning and renewable energies, etc. [99]. This software was already validated by several authors, showing its capability to simulate free running or controlled temperature buildings with an average error below 10% (the expectable error for thermal simulations performed in an engineering design context) [108,138,139].

In Concert hall model, despite the comparisons between measurements and simulations will only be performed for the audience zone, the simulation model includes three thermal zones: stage, audience and balcony. This simulation geometry will allow obtaining the air boundary conditions for the audience (the orchestra pit was closed and for that reason was not modelled). In both simulated rooms, the surfaces were set with the measured surfaces temperature. The two rooms construction it's similar, based on a heavy concrete construction. The floor and walls are made of 0.3m concrete (0.27W/m.K; 750kg/m^3; 1000J/kg.K), the roof consists of 0.3m concrete slab (2W/m.K; 2100kg/m^3; 880J/kg.K) with external insulation (0.04W/m.K; 0.02m).

The HVAC systems were modelled using the EnergyPlus template for a unitary system (one in Rehearsal room case and three on the Concert hall). The DV systems were modelled using the detailed three-node DV model presented on Chapter 2 that was implemented on EnergyPlus source code (see figure 52). According to what has already discussed in Section 5.3.1, in Concert hall case the plumes are modeled as horizontal plumes (3D) while in Rehearsal room are considered as linear plumes (2D), the correspondent equations to determine the neutral height position are used (Figure 40).

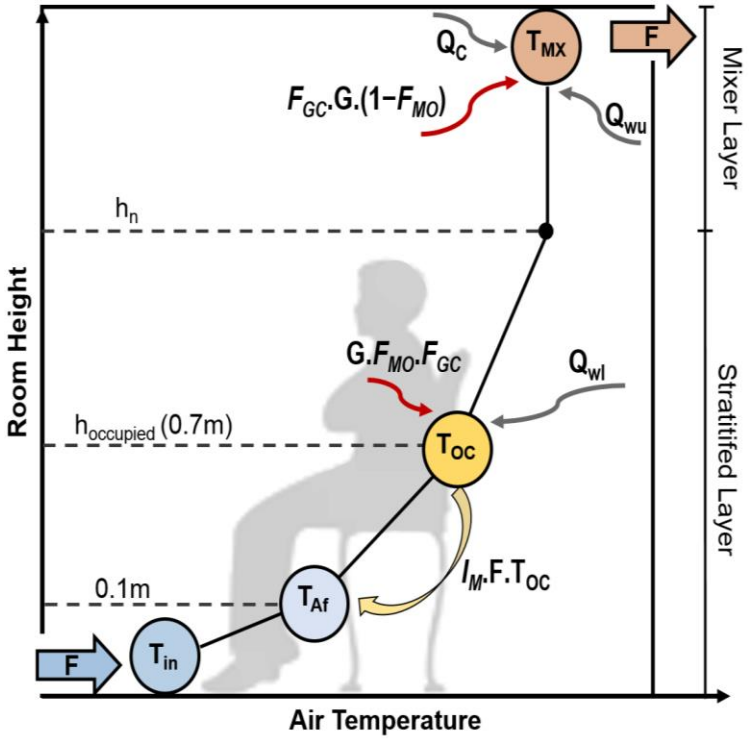

Figure 52. Three-node DV model implemented on EnergyPlus.

Table 26 - EnergyPlus simulation conditions.

Case	Zone	Nºoccup.	$\frac{W}{person}$ [126]	Lightning (W/m^2)	Total Internal gains (W/m^2)	Airflow rate (m^3/h)	Supply air temp. (ºC)
Concert hall	*Audience*	400	120	24	91	39000	19ºC (12:00-20:30) 18ºC (20:30-22:30)
	Balcony	72		10	81	5900	
	Stage	70	167	48	81	8000	18ºC
Orchestra reharsal Room		65	120	41	65	10000	21ºC

5.5 EnergyPlus model validation

This section presents an assessment of model precision based on the measurements performed in Concert hall and Orchestra rehearsal room. The model predictions were evaluated using the following average error indicators:

The average error: Avg. Dif. (ºC) = $\frac{\sum_{i=1}^{n}|Sim._i\text{-}Meas._i|}{n}$ (44)

The average bias: Avg. Bias (ºC) = $\frac{\sum_{i=1}^{n} Sim._i\text{-}Meas._i}{n}$ (45)

The average percentage error: Avg. Error (%) = $\frac{100\%}{n} \times \sum_{i=1}^{n} \left|\frac{Sim._i\text{-}Meas._i}{Meas._{Max.}\text{-}Meas._{Min.}}\right|$ (46)

Figures 53 and Figure 54 presents the comparison between measurements and simulations of Concert hall and Orchestra rehearsal room, respectively. The results show the evolution of the vertical temperature profile along the measurement periods (1h20). In both cases, the results in the first time step present an almost perfect agreement in all nodes, however, during the concert the differences increased: the simulations over predicted T_{AF} and T_{OC} nodes. As expected, higher agreement is achieved for T_{MX} node due to the imposed mass/energy balance.

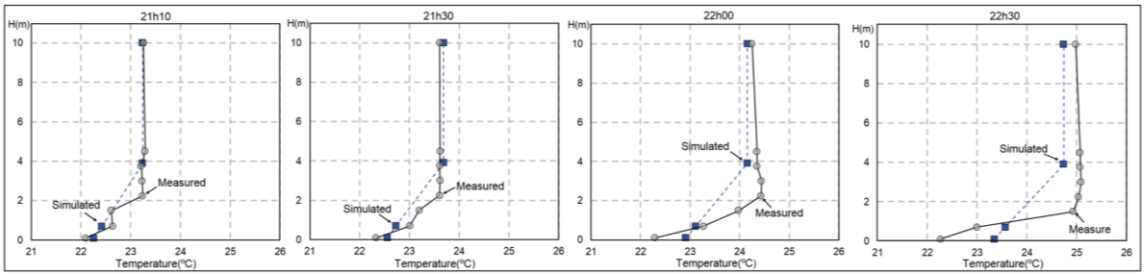

Figure 53. Comparison between measurements and EnergyPlus simulations of the Concert hall.

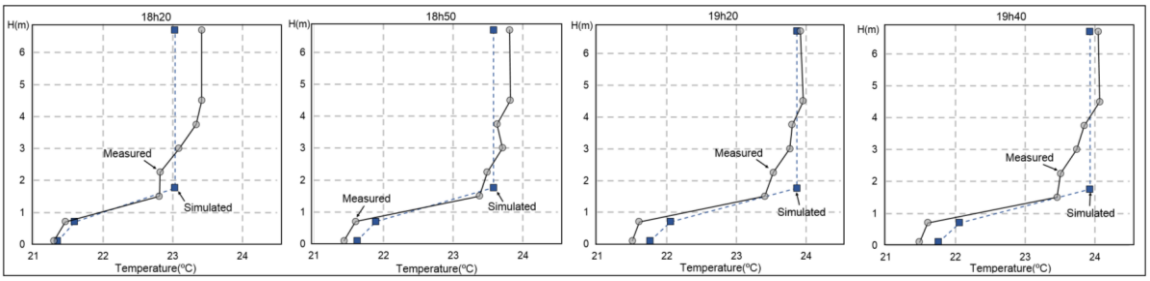

Figure 54. Comparison between measurements and EnergyPlus simulations of the Orchestra rehearsal room.

Table 27 shows the average error indicators results for the two analyzed cases. The overall agreement between all nodes is very good; the average difference between simulation and measurements is 0.3ºC, corresponding to an average error below 6%. The bias indicator reveals that simulation over predicts T_{AF} node and under predicts T_{MX}. The higher comparison differences are obtained for T_{AF} node, reaching 0.5ºC (9.9%) in the Concert hall case.

Table 27 - Comparison between measured and simulated node temperatures: T_{AF}, T_{OC} and T_{MX}.

Case		***Bias (ºC)***	***Difference (ºC)***	***Error (%)***
Great hall	T_{AF}	0.5	0.5	9.9
	T_{OC}	-0.1	0.3	6.1
	T_{MX}	-0.1	0.2	3.1
Rehearsal room	T_{AF}	0.2	0.2	4.3
	T_{OC}	0.3	0.3	6.7
	T_{MX}	-0.3	0.3	5.2
Average		**0.1**	**0.3**	**5.9**

5.6 Conclusions

Modelling DV systems is a complex task, the interaction between the thermal plumes and active boundary conditions could condition the development of the stratified layer leading to poor IAQ level and users thermal discomfort. The determination of neutral height position, as the prediction of the vertical temperature and pollutants profile are the

ultimate goal for DV designers. In this paper, two large rooms were used to conduct a set of measurements under real occupancy conditions that allows the analysis of DV systems and direct comparison with the results obtained from the EnergyPlus simulations.

The analysis of the measurements demonstrate the applicability of the methodology used to predict neutral height position, based on the plume flow equations, with an average error of 4.6% corresponding to an over prediction of 4cm. The performance of DV systems of both measured rooms reveals that the thermal comfort and good IAQ levels were achieve during the measurement periods. As expected, a high pollutants efficiency removal was obtained for the both rooms, resulting in an average efficiency of 1.7 and 1.2 for Orchestra rehearsal room and Concert hall, respectively.

The validation of the results from EnergyPlus simulations shows that the building thermal simulation models tested are able to predict the required variables used in engineer context for a DV building: neutral height position and the vertical temperature profile. The comparison between simulations and measurements reveals a good agreement: the average simulation error in the three-node temperatures is 5.9%, with the largest deviation on the T_{af} node (7.1% ≈ 0.4ºC). Comparisons between the validation results obtained for both rooms reveals that the slope of Concert hall does not affect the results of tested DV three-node model. In light of the results obtained, the EnergyPlus proved be able to simulate DV systems in large rooms (with or without slope) with a good precision.

6. Applications of simplified modelling of displacement ventilation

In this chapter, the concepts of simplified modelling of DV systems developed in previously chapters will be applied in the design of two DV systems case studies. Section, 6.1 presents an application of building thermal and CFD simulation in the refurbishment of the HVAC system of the Gulbenkian large Concert hall (the room was presented on Chapter 5). The thermal simulation tool EnergyPlus was used to size the HVAC system while CFD simulations were used to predict detailed airflow velocity and temperatures in the space.

Finally, on section 6.2, are presented two cases of stack driven ventilative cooling systems implemented in kindergarten schools located in the mild Subtropical-Mediterranean climate of Lisbon (Portugal). The designs were developed and fine-tuned using dynamic thermal simulation (EnergyPlus). The approach used, allowed for straightforward statistical analysis of expected system performance, assessed in terms of thermal comfort and indoor air quality.

6.1. Thermal and Airflow Simulation of the Gulbenkian Great Hall

This section presents the refurbishment project of the HVAC system of the Gulbenkian large concert hall, in Lisbon (Portugal). Built in 1960's, it has a seating capacity of 1100 on the main floor plus 200 seats on a balcony area with up to 250 artists in the stage area (see Figure 55). The hall has four main areas: stage, orchestra pit, stalls and balcony. The existing HVAC system uses a single air-handling unit (AHU) that serves all the areas through an overhead mixing system. After forty years of intense use, the existing HVAC system doesn't meet current requirements for indoor air quality and thermal comfort. The main problems are excessive energy use during rehearsal periods, inefficient mixing of the ventilation system.

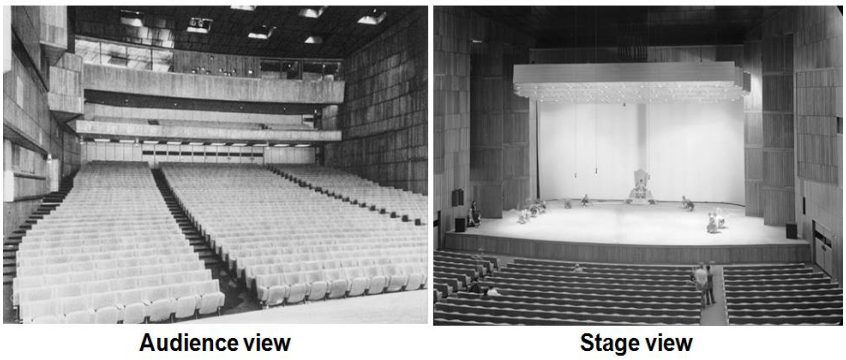

Figure 55. Gulbenkian Concert hall.

After four decades of continuous use there is a need for a complete refurbishment of the HVAC and lighting systems. This need created an opportunity to update the systems, but also to change the airflow pattern from overhead mixing to displacement ventilation (DV). The transition between systems is achieved by transforming the existing air exhaust openings, located under the seats, into inflow openings, allowing the use of a displacement system (the current standard approach in contemporary concert hall design). Figure 56 shows the original ventilation strategy.

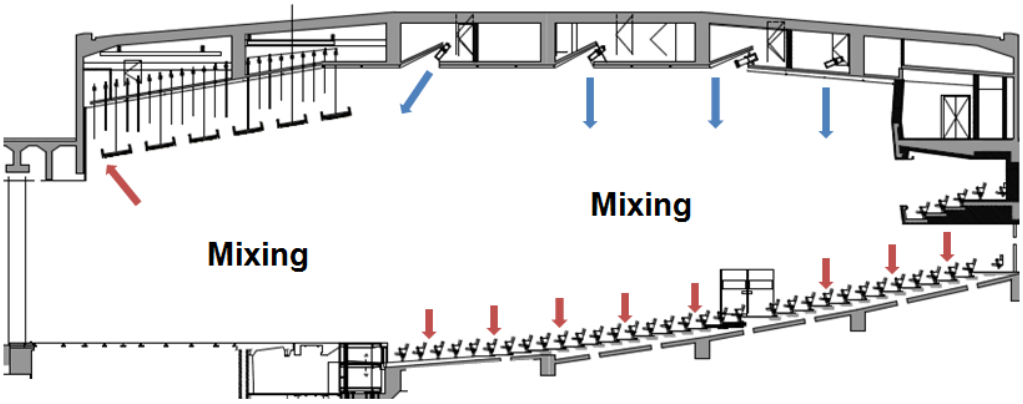

Figure 56. Gulbenkian Concert hall original HVAC system.

For the new system, the coexistence of different indoor thermal comfort requirements in the room dictated the use of three distinct air-handling units:

- Seating area (stalls and balcony).
- Stage area.
- Orchestra pit.

The geometry of the orchestra pit makes the use of an overhead system difficult (there is no ceiling), clearly, in this case, displacement ventilation is the better option. In contrast, the functional requirements of the stage area make the use of a displacement system with low-level inflow diffusers, extremely difficult. For this reason, a variable configuration system is used for the stage. The proposed HVAC system configuration for the refurbishment is shown in Figure 57. In its initial configuration, the system included a potentially problematic interaction between an overhead system (stage system with high momentum nozzles) and a displacement ventilation system (seating area, with low velocity inflow). The HVAC system was sized using the thermal building simulation software EnergyPlus. The complexity of the proposed system and the uncertainty about the interaction of the two different airflow patterns created the need for a computational fluid dynamics simulation (CFD), focusing on the main occupancy and internal load scenarios.

6.1.1 Thermal simulation - EnergyPlus

In order to analyse indoor air conditions of each occupied space, the simulation model includes four thermal zones (stage, orchestra pit, stalls and balcony, shown in Figure 57). The hall has heavy concrete construction. The floor and walls are made of 0.3m concrete (0.27 W/m.K; 750 kg/m^3; 1000 J/kg.K), the roof consists of 0.3m concrete slab (2 W/m.K; 2100 kg/m^3; 880 J/kg.K) with external insulation (0.04 W/m.K; 0.02m).

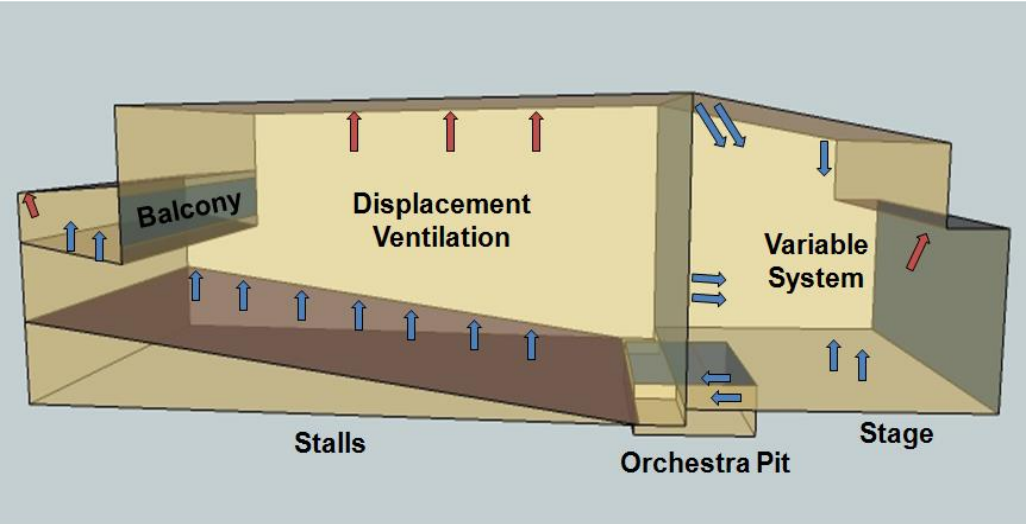

Figure 57. Concert hall thermal zones.

The proposed HVAC system, composed of three air-handling units, was modelled using EnergyPlus template for a unitary system. Table 28 shows the settings used for each air-handling unit. The stalls and balcony thermal zones were modelled using the three-node displacement ventilation model that is presented on Chapter 2 and implemented on EnergyPlus. The other zones, orchestra pit and stage, were treated as perfectly mixed.

Table 28 – UHA's sizing criteria.

UHA	**Setpoints**		**Maximum airflow (m^3/ occupant.h)**	**Maximum airflow (m^3/h)**
	Temperature (ºC)	**HR (%)**		
Stalls and Balcony	20 - 24	35 - 65	35	45000
Stage	21 - 23	40 - 60	35	10000
Orchestra Pit	21 - 23	40 - 60	40	4000

6.1.1.1 Internal loads scenarios

Two typical maximum stage utilization scenarios were defined to size the system, labelled Classical and Modern (see table 29). Both scenarios used the same occupancy schedule, corresponding to the maximum, fully occupied daily utilization (from 10 am to 12 am; from 3 pm to 5 pm; from 7 pm to 9; from 9.30 pm to 11.30 pm).

Table 29 - Sizing criteria – loads considered in different scenarios.

Zone	Scenario	Occupancy	Internal Gains		
			Occupants (W/occupant)	Illumination (W/m^2)	Total (W/m^2)
Stalls	Classical music	1091	104	25	175
	Modern	1091	104	25	175
Balcony	Classical music	163	104	10	150
	Modern	163	104	10	150
Stage	Classical music	200	167	166	310
	Modern	40	167	292	367
Orchestra Pit	Classical music	0	-	-	-
	Modern	60	167	10	206

6.1.1.2 Sizing criteria

The thermal building simulation sizing results are dependent on the weather file used. Since 2009, the Typical Meteorological Year (TMY) became the new standard weather file used in energy based simulations [140]. The weather files used in EnergyPlus simulations were created based on this format through statistical methods, and typically, the extreme weather data were smoothed by average values. Typically, a TMY weather file for Lisbon (EnergyPlus Weather [141]) would be used to run the simulations. Due to the great sensibility of this project, a weather data sensibility analysis was performed to select adequate weather data to size the HVAC system. Two additional sources of sizing weather data were considered: TMY weather data, eight years measured weather data

(airport of Lisbon). A third weather data source was created, based on airport weather data and ASHRAE sizing conditions [142].

Enthalpy values were analysed and a 0.4 and 1 percentile, heating (minimum enthalpy) and cooling design day (maximum enthalpy), for the three sources of weather data were defined.

6.1.1.3 HVAC system sizing results

Figure 58 and 59 show results of the weather data sensibility analysis on HVAC system sizing results. Figure 58 presents sizing results for the three sources of analysed weather data.

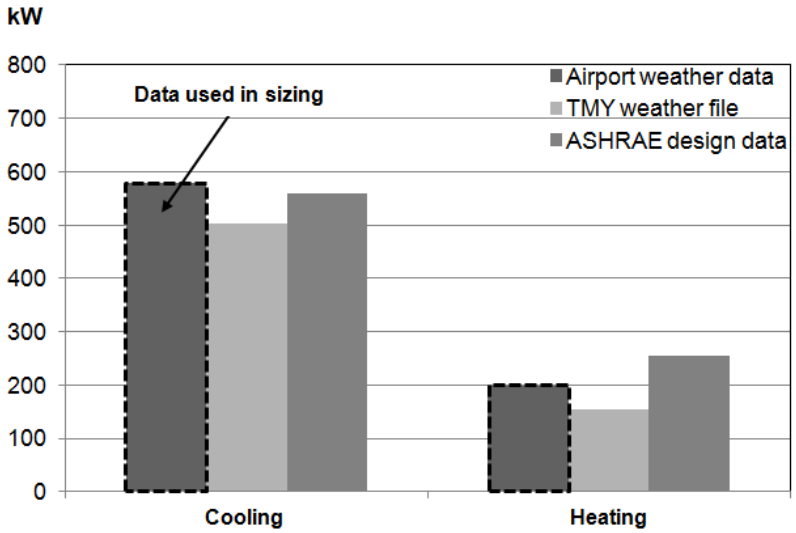

Figure 58. Sizing results: Airport weather data, TMY weather file and ASHRAE design days sizing comparison.

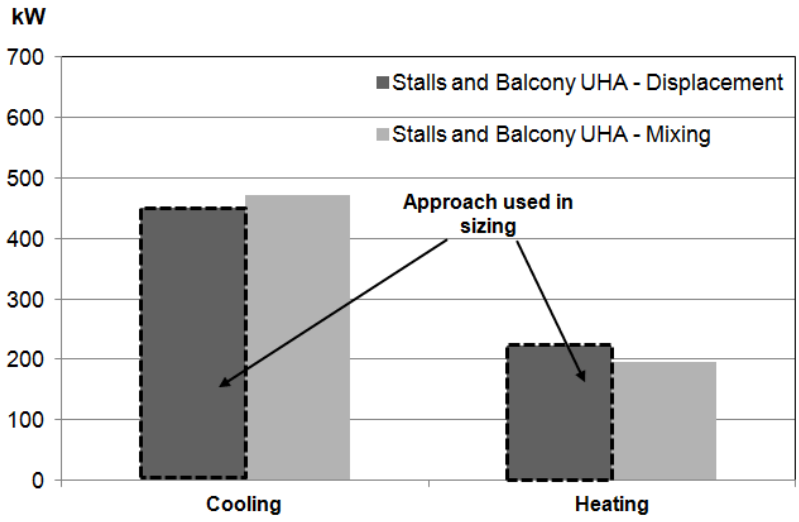

Figure 59. Results: Stalls and balcony UHA sizing - 0.4% Airport weather data.

The Figure 58 shows that the definition of the HVAC system design day has a large impact on the system size. Figure 59 compares sizing results for stalls and balcony UHA, if the airflow pattern of the system is correctly modelled (displacement model) or if mixing model was used. These results demonstrate the influence of modelling properly the airflow pattern on EnergyPlus in order to rightly size the HVAC system.

The difference between the two extreme cases, for cooling and heating, shown in Figure 58 is: 15% (cooling) and 65% (heating). The sizing effects of the ventilation model are lower: 4% (cooling) and 14% (heating).

6.1.2 CFD simulation

In the present case CFD was used to confirm the EnergyPlus sizing results, assess thermal comfort (including average airflow velocity), identify the optimal inflow strategy for the stage, and test the compatibility between overhead (stage) an displacement (seating area) systems.

One of the first examples of the use of CFD to analyze the ventilation efficiency and thermal comfort of overhead mixing systems in two large auditoriums was presented by Hangan et al. (2001) [143]. This study focused on the typical difficulties of overhead mixing systems: preventing overdraft and avoiding still air zones with poor ventilation efficiency. In a more recent applied research paper by Kavgic et al. (2008) [126] CFD is used in a post occupancy assessment of a theatre with a poorly performing natural ventilation system. The usual pitfalls of this ventilation strategy were apparent: excessive inflow velocity (the measured inflow rate per occupant was 50% higher than the value used in the sizing presented in the next subsections) and user complaints of cold ankles. A recent application of CFD in concert hall refurbishment design was presented by Scanlon et al. (2011) [144]. As in the present case, the proposed solution involved inverting existing inflow and exhaust openings in order to convert the existing overhead system into a displacement system. In this case, CFD is used both to fine-tune the design and to facilitate information flow within the design team.

6.1.2.1 CFD model geometry

The geometry used in the simulations is shown in Figure 60. The CFD simulations were performed using PHOENICS [119]. Due to its robustness and adequate capabilities for room ventilation flows, the k-ε turbulence model was used (with the Yap correction for confined spaces). Buoyancy was modelled using the Boussinesq approximation.

CFD simulations are time consuming processes that must be streamlined by introducing simplifications that allow for a converged simulation in adequate time (ideally less than a day for each case). The symmetry of the auditorium along the longitudinal axis enabled for the use of a model of one-half of the room. Grouping of the audience rows was used with each modelled row representing three rows.

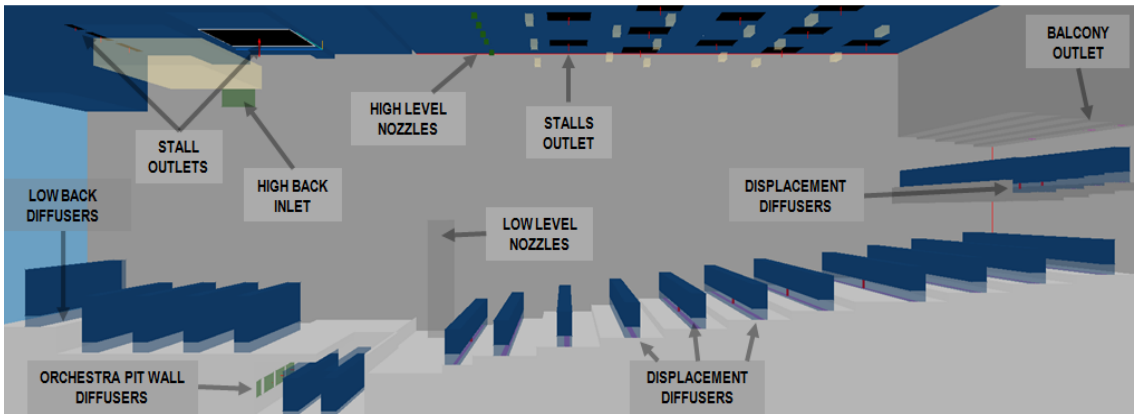

Figure 60. Gulbenkian Concert hall CFD model geometry (half room).

Internal loads, like occupants and lighting were modelled as blocks with a fixed heat source composed of simulation domain material (air). The Figure 61 presents the grid refinement performed along X-axis. In order to facilitate the analysis of the results the airflow velocity and temperature were averaged in control volumes that are coincident with the thermal load volumes shown in Figure 60 (in dark and light blue).

6.1.2.2 CFD simulation scenarios

Four different inflow configurations were created for the stage system (table 30). The inflow boundary conditions tested are shown in Table 31.

Table 30 – CFD simulated scenarios.

Scenario name	***System description***
Classical HN+LN	High Nozzles (5 000m^3/h) + Low Nozzles (5 000m^3/h)
Classical LB+LN	Low Back diffusers (4 000m^3/h) + Low Nozzles (6 000m^3/h)
Modern HN+LN	High Nozzles (5 000m^3/h) + Low Nozzles (5 000m^3/h)
Modern LN+HB	Low Nozzles (6 000m^3/h) + High Back (4 000m^3/h)

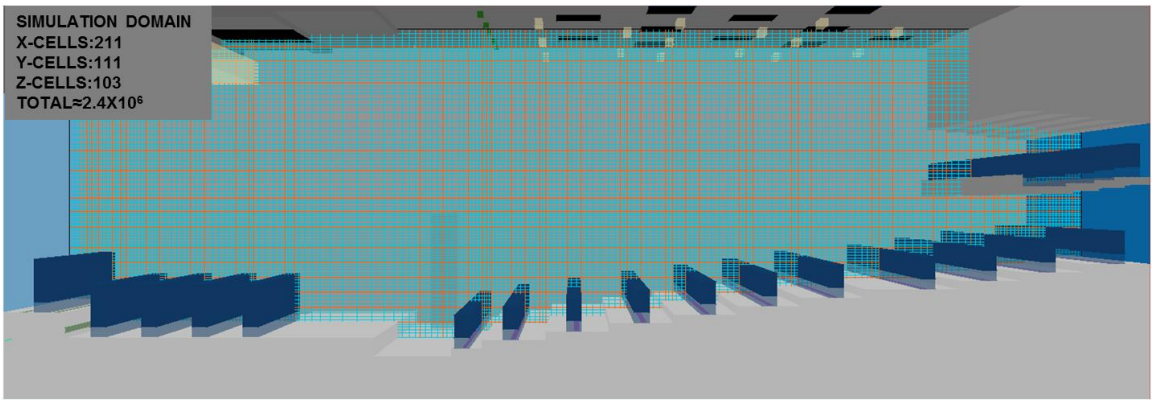

Figure 61. Grid refinement (xx axis) of Gulbenkian Concert hall PHOENICS model.

Table 31 - CFD simulation conditions.

Cases	Zone	Inflow boundary conditions		Airflow volume (m^3/s)
		Velocity (m/s)	Temperature (°C)	
All scenarios	Balcony	0.16	18	1.6
	Stalls	0.18	18	10.6
Modern scenario	Orchestra pit	0.18	19	0.7
Classical HN+LN	Stage	2.87	14	2.8
Classical LB+LN		0.13 (diffusers) 2.87 (nozzles)	14	2.8
Modern HN+LN		2.87	14	2.8
Modern LN+HB		0.13 (High back) 2.87 (nozzles)	14	2.8

6.1.2.3 CFD results

Results of the simulated temperature and velocity in the stage, orchestra pit, balcony and stalls for the four CFD models studied are shown below (Figure 62-65).

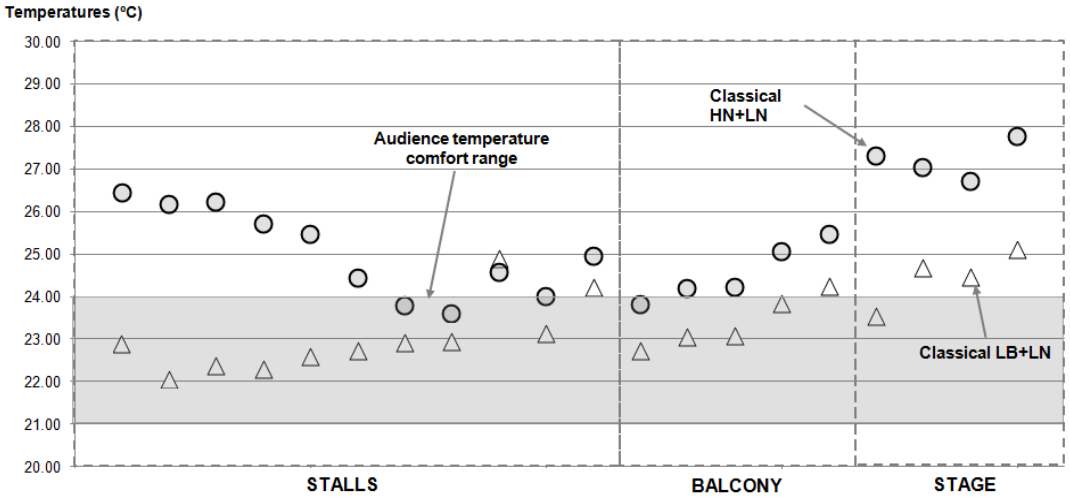

Figure 62. Results: Room temperature Classical scenario.

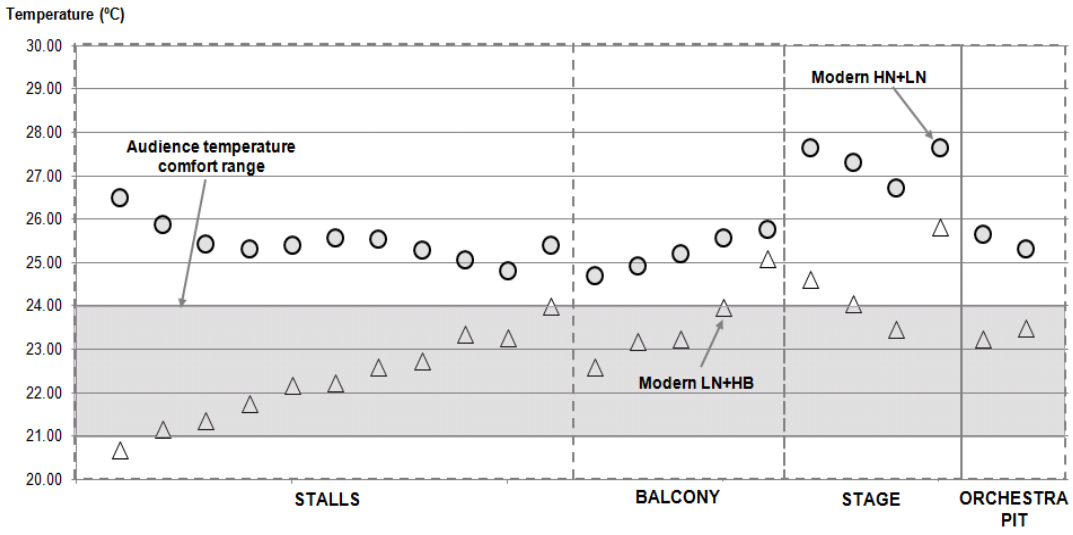

Figure 63. Results: Room temperature Modern scenario.

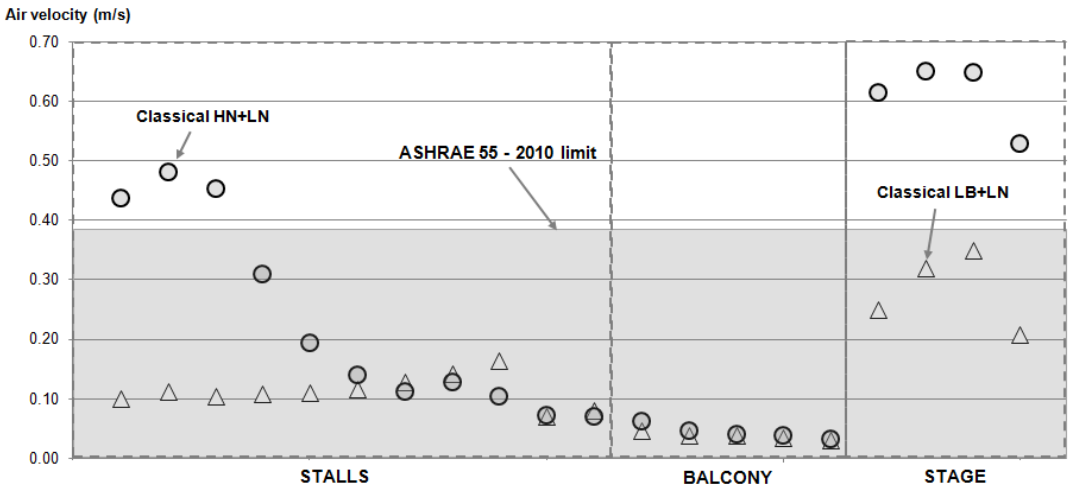

Figure 64. Results: Room velocity Classical scenario.

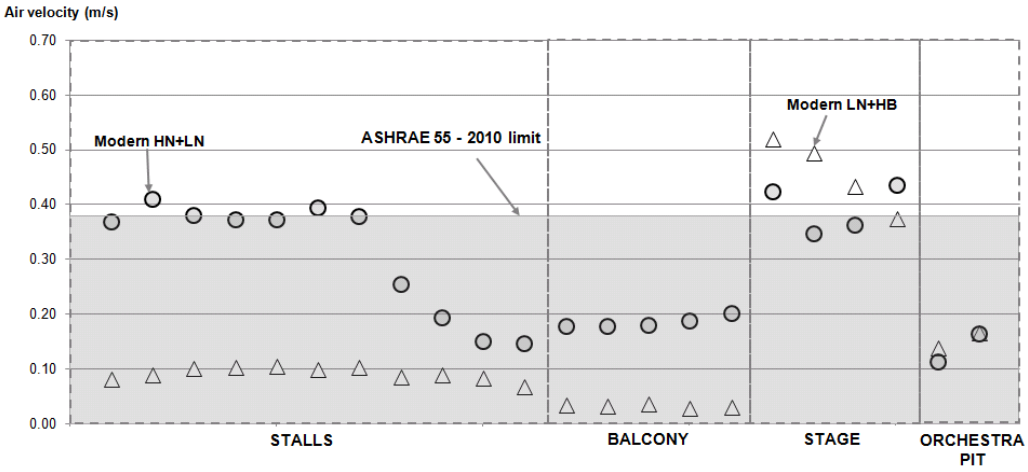

Figure 65. Results: Room velocity Modern scenario.

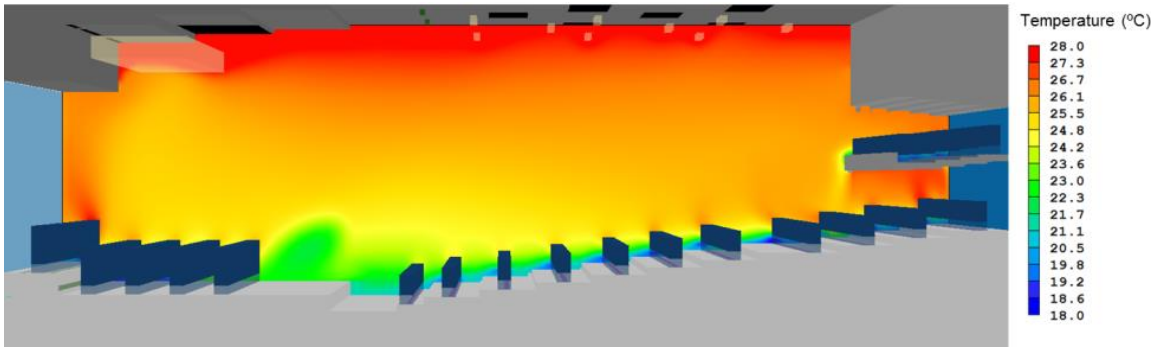

Figure 66. Results: Classical LB+LN scenario - Room temperature profile.

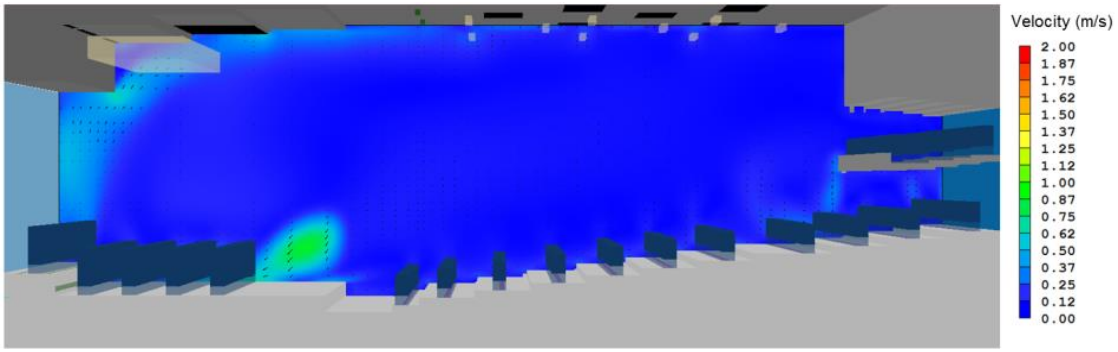

Figure 67. Results: Classical LB+LN scenario - Room velocity profile.

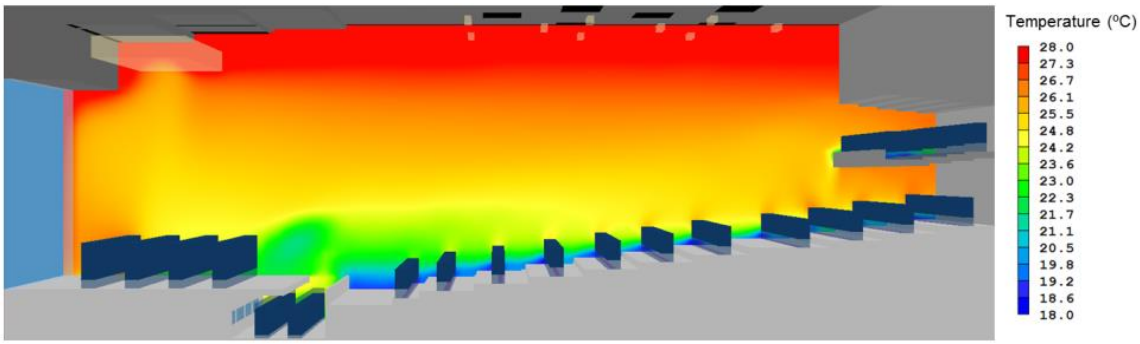

Figure 68. Results: Modern LN+HB scenario - Room temperature profile.

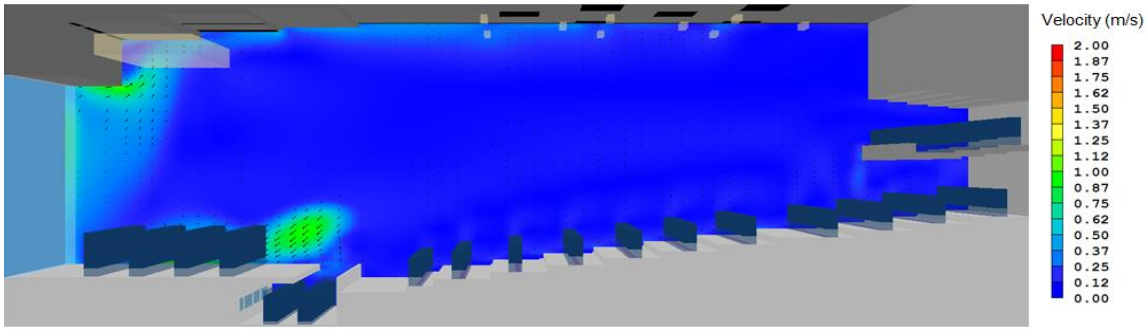

Figure 69. Results: Modern LN+HB scenario - Room velocity profile.

Figures 62-65 show that only two of the four simulated cases (Classical LB+LN and Modern LN+HB) present temperature and air velocity values within the target requirements (shown in grey in the figure). Figures 66-69 show PHOENICS temperature and air velocity results for these two, better performing, scenarios.

Detailed analysis of the CFD results for the two scenarios (Classical HN+LN and Modern HN+LN) that did not perform as expected show that the low velocity airflow along the ceiling (in the positive x direction), caused by the large stage heat gains, greatly reduces the momentum flow from the high level nozzles (that should reach the stage). Due to this effect, the penetration depth of these jets is reduced to approximately ten diameters (2.4 meters, see figure 70). This effect is in agreement with experimental work by Andreopoulos *et al.* (1984) [145] and Chan *et al*. (1998) [146], showing that a high velocity jet perpendicular, or head on, to a uniform airflow with a lower velocity mixes within ten diameters of the outflow nozzle.

Figures 66-69 show that the proposed configuration works well and there is no relevant negative interaction between the displacement ventilation system used for the seating are and hybrid system used for the stage. The back row of the main seating area is affected by heat accumulation under the balcony and may benefit from additional dedicated extraction.

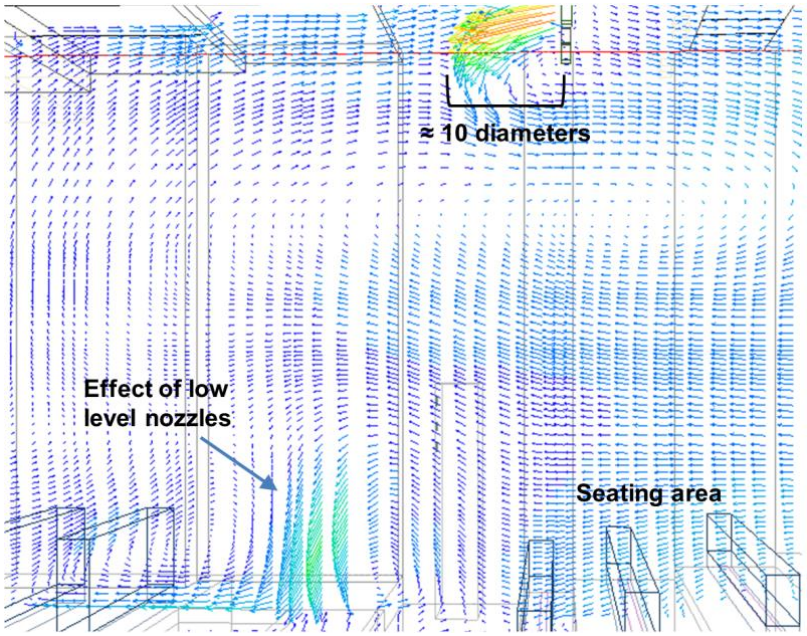

Figure 70. Classical HN+LN and Modern HN+LN: high nozzle velocities profile showing fast velocity decay (and thereby limited cooling effect).

6.1.3 Conclusions

Adequate HVAC system sizing is a complex process involving many variables that can condition final results. The sizing results obtained for the present case show that the definition of the sizing design day and correct modeling of airflow pattern have a significant impact on system size (between 4% and 64%, depending on the case).

The CFD simulations of indoor flow fields and internal temperatures proved invaluable fine-tuning of the design. The stage inflow systems tested in the CFD simulation scenarios Classical LB+LN and Modern LN+HB showed good results and confirmed that the proposed system can meet air temperature and indoor velocity design goals for the main seating and balcony area. The main concern that was initially raised by the proposed design was not confirmed by the simulation results: the stage systems do not increase the airflow velocity in the first rows of the seating area.

6.2 Stack driven ventilative cooling for schools in mild climates

This section presents two case studies of stack driven user-controlled ventilative cooling systems for kindergarten schools in Lisbon (Portugal) that use a combination of DV and SS techniques. The thermal building simulation software EnergyPlus was used in the design and fine-tuning of both natural ventilation systems.

6.2.1 Buildings

This subsection presents the two buildings analyzed: CML Kindergarten (Figure 71) and German School (Figure 72). Both buildings are situated in urban area of Lisbon (Portugal). The CML Kindergarten was built in 2013, with a total built area of 680 m^2 distributed into two floors with 3.1m floor to ceiling height each. The building was south-west oriented, with capacity for 42 children, and each ground floor classroom have direct access to the exterior courtyard, partially covered (courtyard view, Figure 71).

The second case study, the German School of Lisbon, has a main façade facing north (to minimize solar heat gains impact), with two floors, and capacity for 160 children (1200m^2, 3.3m floor to ceiling height). The building structure is concrete, with external insulation, creating a high thermal inertia building. The windows are low-emissivity double glazed with solar control and movable blinds (interior in German school and exterior in CML kindergarten case). In south oriented areas, overhangs were installed to control high solar gains. Both schools were designed with large glazed areas for allow the use of natural lighting.

These two schools are located in the mild Subtropical-Mediterranean climate of Lisbon, Portugal (Figure 73), characterized by mild winters (minimum temperature ≈ 4ºC) and dry summers with high levels of solar radiation (maximum temperature ≈ 37ºC). In spring and summer there are many days with large thermal amplitude (up to 18ºC), that can potentially make a night cooling approach very effective. In a typical school building in Lisbon it is expected that the main comfort problems occur when high direct radiation levels and the maximum outdoor temperatures are combined with high internal gains, easily leading to cooling loads of up to 100W/m^2.

Figure 71: Inside, exterior and courtyard views of the CML Kindergarten.

Figure 72: Lateral, front and inside views of the German school.

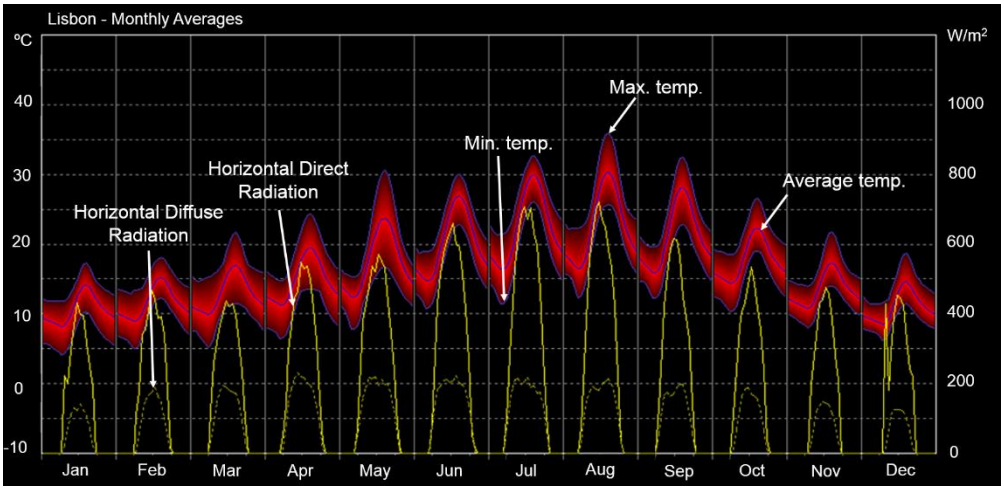

Figure 73: Typical year of Lisbon weather (outdoor temperature and radiation).

Both schools have no mechanical ventilation system installed, the fresh air is introduced into the spaces through low level grilles on the façade and will be exhausted in the back of the room, through a chimney. For the thermal conditioning of the spaces, the buildings Portuguese national code (RECS) [147] only requires the installation of an active system for the heating period. For this purpose, a hydraulic radiator is installed in each classroom. For optimal performance of the ventilative cooling systems designed two operation modes were considered (winter and summer), as shown in Figure 74.

During heating period (winter mode), due to the buildings regulation impositions the airflow grilles should be opened to provide the required minimum airflow (fresh air) in order to not exceed CO_2 concentration limit (average below 1625ppm over an 8h period). In this mode, the air that enters though the grilles and was pre-heated directly in front of the passive heating convector that maintain the interior air temperature always above 19ºC.

In summer mode (during the cooling period), all the openings on the façade (low level grilles and openable windows) will be available to be opened, in order to enable larger flow rates to remove the higher heat gains. Taking advantage of the exposed concrete

structure and building thermal inertia, passive night cooling used to pre-cool the building during non-occupied periods. In both modes, blinds are user-controlled and can be used to minimize solar gains.

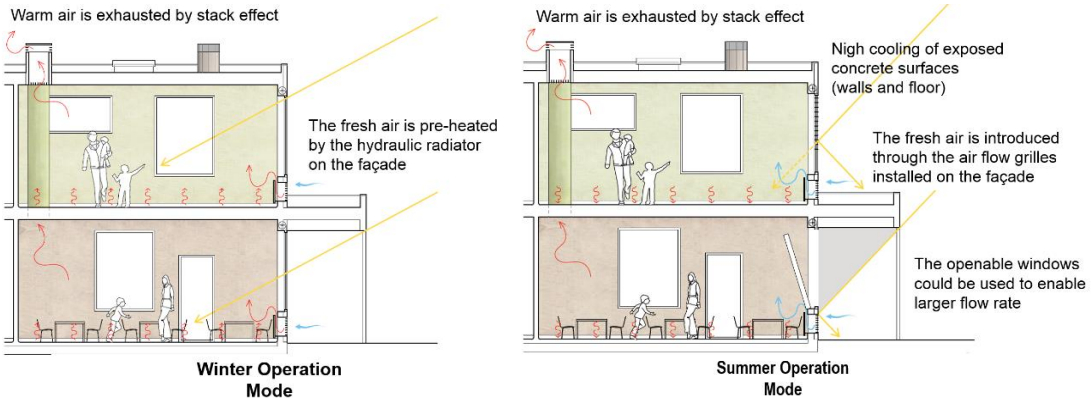

Figure 74: Kindergartens ventilative cooling systems operation modes (winter and summer).

6.2.2 Thermal simulation - methodology

The dynamic thermal simulations were performed using the open source thermal building simulation software EnergyPlus. To simulate natural ventilation the airflow network approach was used [148], modelling infiltration and openings in detail.

Both kindergartens are shielded by surrounding buildings and for that reason wind effects were neglected and only buoyancy was considered in simulations (a conservative approach). In both cases, to analyze the performance of the natural ventilation systems only a representative classroom of each building was considered. These spaces including the principal features of natural ventilation systems: airflow grilles, thermal chimney and openable windows. Figure 75 shows the EnergyPlus model used to simulate CML Kindergarten and German School.

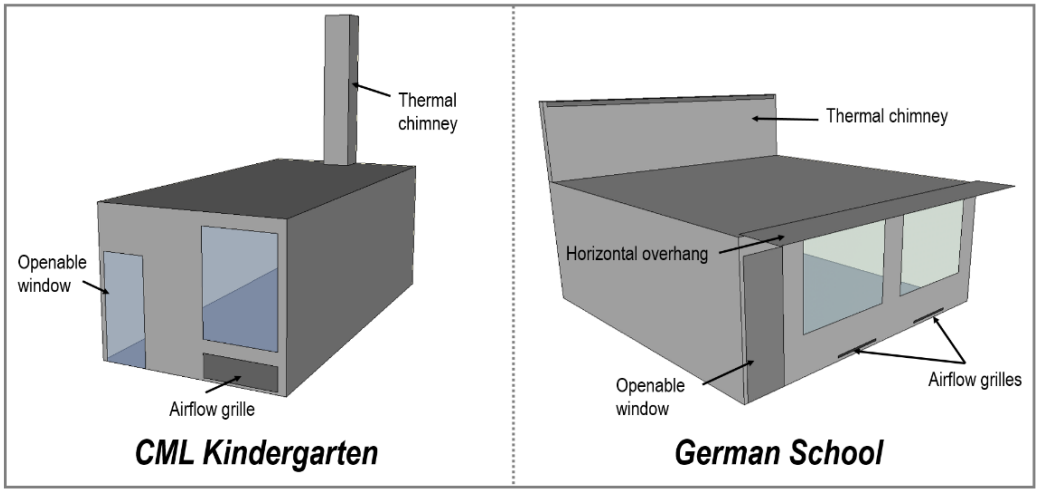

Figure 75: CML Kindergarten and German School EnergyPlus model.

In order to consider the thermal stratification effects, both models are composed by two thermal zones (connected by a virtual horizontal window that is always open): room and thermal chimney. The simulations were performed for a whole year, using the TMY weather file for Lisbon (EnergyPlus weather file), the rooms IAQ level promoted by the natural ventilation systems should be in agreement with buildings Portuguese code [147] and the users thermal comfort was analyzed considering two international standards (CEN, 2007; ASHRAE, 2010):

- The rolling average of CO_2 concentration in 8 consecutive hours should not exceed 1625 ppm (RECS, [147]).
- Operative temperature range between 19-26ºC, (kindergartens limits, EN 15251 [149]).
- Adaptive comfort model (80% acceptability limits for naturally conditioned spaces, ASHRAE 55-2010 [150]).

In the simulation, the airflow grilles were open when the outdoor temperature is below the interior temperature. The hydraulic radiator is used during the heating months (from October to April) to ensure an interior air temperature above 19ºC. The openable windows will be used to increase the air change rates during the warmer months (from May to September) when additional heat removal will be needed. The Table 32 presents the internal heat loads considered for each case. Table 33 shows the size of opening areas considered for the winter and summer operation modes.

The smaller opening configuration is sized for the heating and mild seasons, corresponding to 1-3% of room floor area, while in the cooling season the total opening area should meet the minimum code requirement of 5% of floor area, that in the case of CML kindergarten reach the 8%.

Table 32- CML Kindergarten and German School heat loads scenarios used in simulation.

School	**Occupancy**	***Internal Gains***		
		Occupants (W/occupant)	**Lighting (W/m²)**	**Total (W/m²)**
CML Kindergarten	19 children + 1 adult	70 + 100	8	53
German School			7	33

Table 33 - Opening areas summary.

Floor Area (m^2)		***German School***	***CML Kindergarten***
		55	32
Opening Area (m^2)	*Winter mode*	0.8	1.0
	Summer Mode	2.7	2.6
Max. Opening Area/Floor Area (%)	*Winter mode*	**1.5**	**3.1**
	Summer Mode	**5.0**	**8.1**

6.2.3 Results: natural ventilation systems performance

This subsection presents the simulation results for the two kindergartens (CML and German School). Figures 76-77 and 80-81 present the predicted performance for a typical day, in both operation modes (winter and summer). Finally, figures 78-79 and 82-83 show the predicted yearly operative temperature and indoor air quality (CO_2 concentration), evaluated according to the EN 15251 and ASHRAE 55-2010 criteria.

6.2.3.1 CML Kindergarten

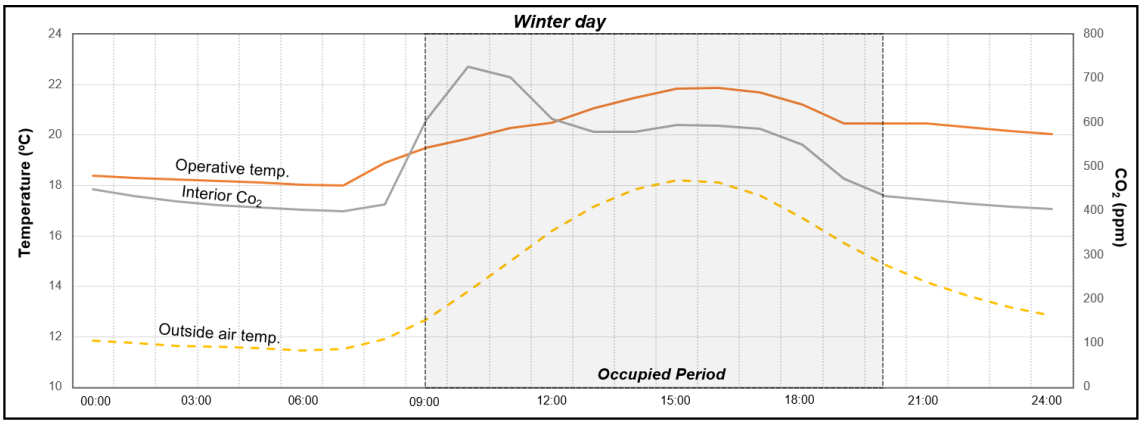

Figure 76: CML Kindergarten results: Operative temperature and CO_2 level (winter operation day).

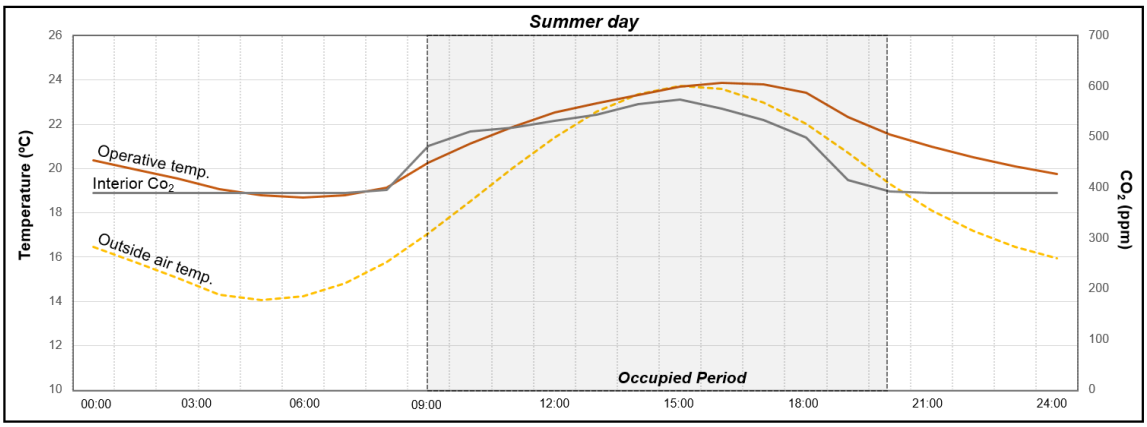

Figure 77: CML Kindergarten results: Operative temperature and CO_2 level (summer operation day).

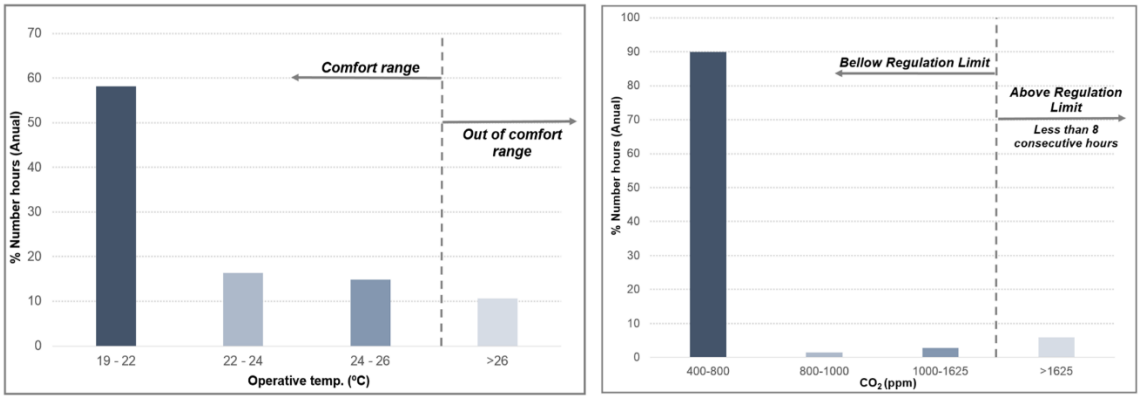

Figure 78: CML Kindergarten statistical analysis: operative temperature (EN 15251) and indoor air quality (RECS).

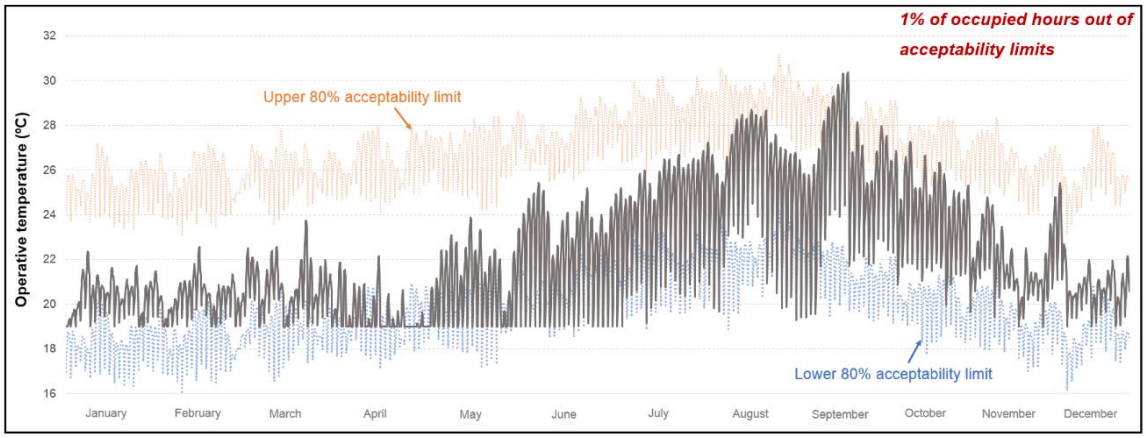

Figure 79: CML Kindergarten operative temperature adaptive comfort analysis (ASHRAE 55-2010).

6.2.3.2 German School

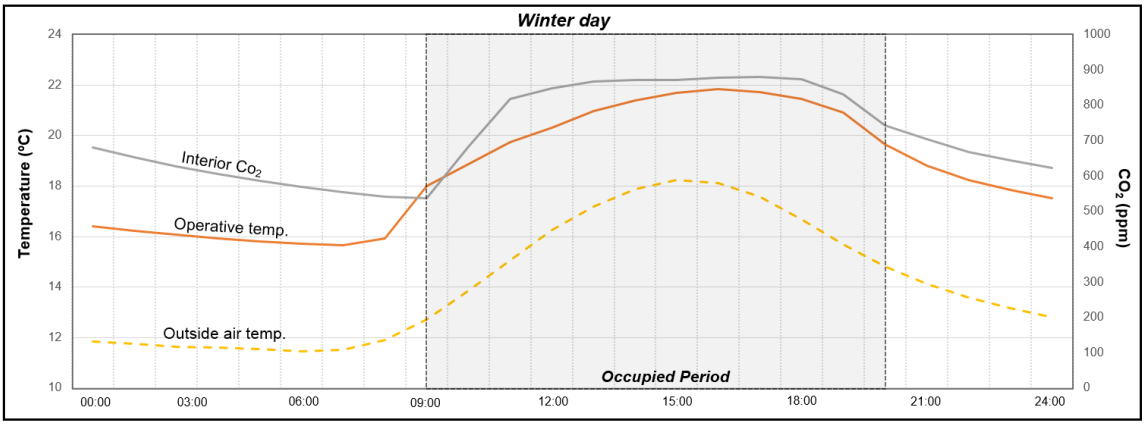

Figure 80: German School results: Operative temperature and CO_2 level (winter operation day).

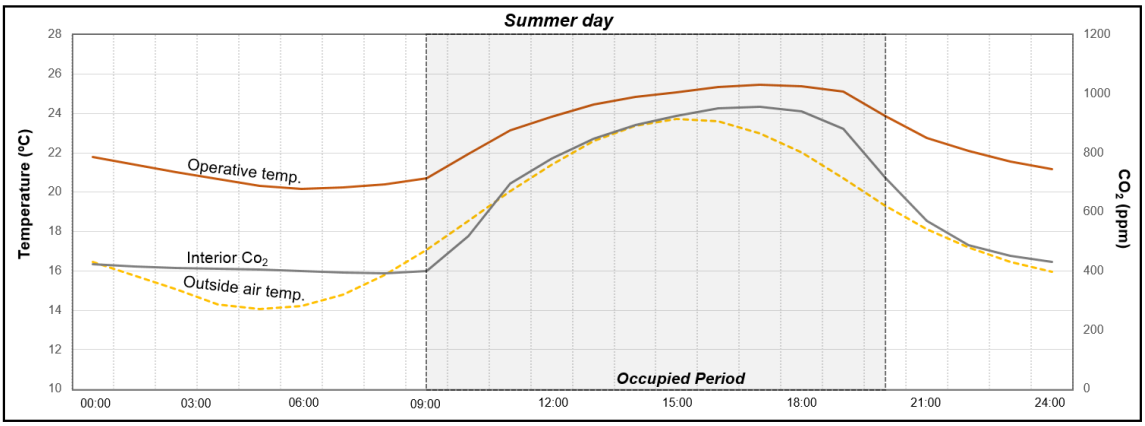

Figure 81: German School results: Operative temperature and CO_2 level (summer operation day).

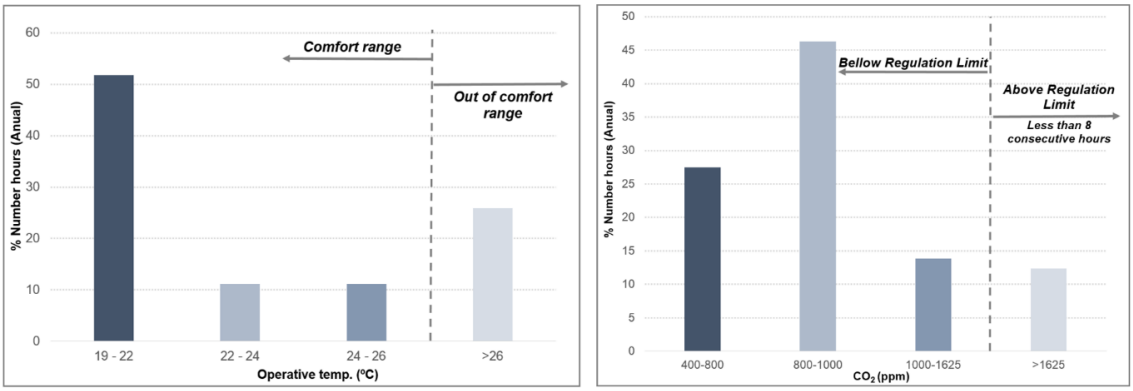

Figure 82: German School statistical analysis: operative temperature (EN 15251) and indoor air quality (RECS).

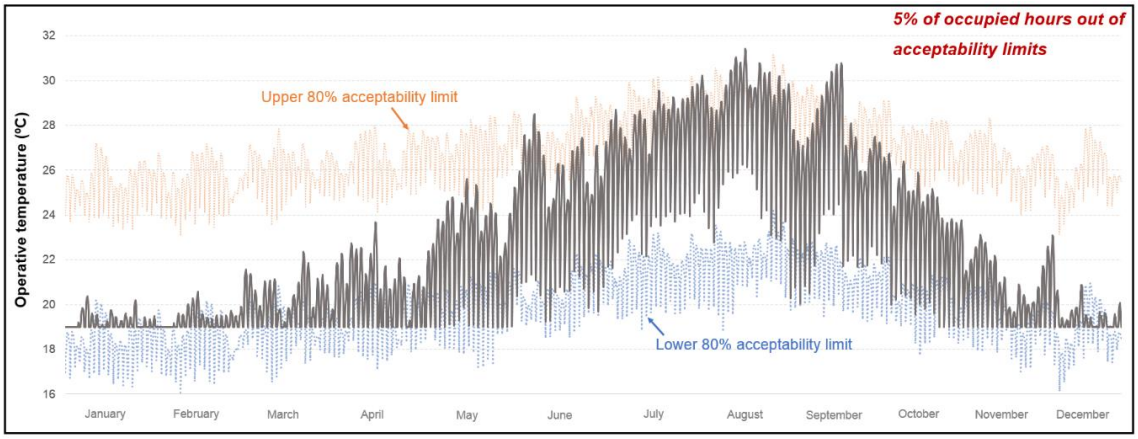

Figure 83: German School operative temperature adaptive comfort analysis (ASHRAE 55-2010).

The typical summer and winter operation days results (figures 76-77 and 80-81) reveal that the system is capable to provide a natural ventilation airflow that is sufficient to ensure the thermal comfort and IAQ level in the majority of occupied periods. As expected, in both schools, when the occupants get into the space CO_2 concentration and operative temperature begin to increase until in the end of the working day. The night cooling approach effectively pre-cools the spaces until the beginning of the next occupied period. The proposed ventilative cooling designs meet the IAQ requisites defined by buildings Portuguese national code: the rolling average of CO_2 concentration in the 8 consecutive hours does not exceed 1625ppm.

The main problems occur in the summer, when it is necessary to promote the interior air renewal (to maintain acceptable CO_2 concentration) but the outside air is warmer. Ideally, in these moments all the openings should be closed to achieve comfortable interior air temperature but open to do not exceed 1625ppm (CO_2 concentration). In these cases, the users will determine what comfort parameter is more relevant to his comfort and to define if the openings should be maintained closed or be opened.

Analyzing the annual operative temperature results using the adaptive comfort model shows that the occupants comfort is obtained in 99% of the occupied hours in CML and 95% in German school. However, when these results are compared with those obtained when using the limits proposed by EN 15251 (19-26ºC) the CML kindergarten obtain similar performance results (10% hours in discomfort), but the German school occupants are expected to be out of comfort during 28% of occupied periods. This poor performance is probably due to the lower opening area per floor area ratio that is used in this design. In light of these results, the designers recommended the installation of an active cooling system in German School to be used in conjunction of natural ventilation system. This

recommendation was not followed by the building manager. As a result, there have been systematic user discomfort complaints in the warmer weeks of the year. These results indicate that the adaptive thermal comfort model may be “optimistic” in the proposed limits. To obtain a high performance ventilative cooling system (like in the CML kindergarten case), i recommend the use of EN 15251 instead of to ASHRAE 55-2010 standard to analyze the occupant’s thermal comfort, due to the more restricted temperature limits.

6.2.4 Conclusions

In the two case studies presented in this section, EnergyPlus simulations were used to fine-tune the designs and diagnose possible thermal comfort and IAQ problems. The opening sizes used in both designs depend on system operation mode: 1-3% of room floor for winter mode and 5-8% for summer mode. Both projects meet the requirements imposed by Portuguese buildings code CO_2 concentration bellow 1625ppm (during 8 consecutive hours).

The capability to meet thermal comfort goals depends on the criteria used: both designs perform well when assessed using the adaptive thermal comfort standard. However, only the CML kindergarten meets the thermal comfort standards proposed by ASHRAE 55-2010 and EN 15251 (1% and 10% of occupied hours out of limits, respectively). Limited user feedback indicates that the stricter assessment is more accurate. The German school, deemed adequate by the adaptive thermal comfort analysis, has had excessive air temperature related user complaints since its inauguration (in 2008).

Sizing and controlling ventilative cooling systems is a complex task that is affected by many uncertainties that impact system performance. In this context, the use of a simulation tool such as EnergyPlus can be beneficial.

7. General conclusions

Modelling DV systems is a complex task because the stratified room air environment cannot be adequately described using the a single room air node. Additional temperature nodes are needed to correctly simulate the vertical temperature gradient that depends on the convective heat gain sources, room surface heat transfer and inflow rate.

This thesis developed and validated a simplified three-node model for prediction of temperature gradient and neutral level location in DV. The model was tested in several buildings including different configurations of DV systems, comprising the following cases: DV and CC/DV nearly adiabatic test cells, naturally ventilated DV schools and two large rooms. Model inputs are limited to the height, number and magnitude of the heat sources in the occupied region. The proposed model is easy to use when implemented in a whole year building thermal simulation tool.

In total the model was compared with 30 measured temperature profiles (21 from existing independent studies and 9 measured in this thesis). The average prediction error for the three room node temperatures was 5% corresponding to an average deviation of 0.4ºC. The largest errors were obtained in natural DV cases, possibly due the errors in the prediction of bulk airflow rate (an essential input to the DV model). Still, even in these cases, the proposed model provides significantly improved precision when compared to existing DV nodal models. In particular, in the most relevant variables used to assess the occupants thermal comfort in DV system design: floor level temperature (6.2 instead of 31%error) and occupied zone temperature (3.7 instead of 28%error).

In addition, the capability of the model to predict the effect of inflow rate on the location of the neutral height allows for straightforward fine-tuning of DV designs. A methodology for locating the neutral height in temperature profiles was developed and a verification of the applicability of Taylor's plume flow equation to predict the neutral level in DV rooms was performed. Tests of the Taylor point plume flow equation using a database composed by 25 cases showed that, when applying the total plume flow to inflow matching approach, using Taylor's expression to model plumes generated by real heat sources, the average error in neutral level prediction is 12%, corresponding to an under prediction of 14cm and results in a correlation factor of 0.80 (r^2).

In light of the complexity and diversity of the cases tested, the results of the comparisons performed between measurements and simulations should contribute to increase confidence in the use of the proposed three-node model to simulate any configuration of DV systems. Future model development work will include the incorporation of CO_2 concentration balance in the model structure and will further investigate the energy balance and air mixing that occur in T_{af} node that results in the highest node error (≈7%).

The implementation of the proposed three-node DV model in the release source code of EnergyPlus thermal simulation software will be also considered.

Bibliography

[1] Hai-xiang Zhao, Frédéric Magoulès, A review on the prediction of building energy consumption, Renewable and Sustainable Energy Reviews, Volume 16, Issue 6, August 2012, Pages 3586-3592, ISSN 1364-0321, http://dx.doi.org/10.1016/j.rser.2012.02.049.

[2] Novoselac A, Srebric J. Comparison of air exchange efficiency and contaminant removal effectiveness as IAQ indices. Transactions-American Society of Heating Refrigerating and Air Conditioning Engineers. 2003;109(2):339-49.

[3] Ahmed Qasim Ahmed, Shian Gao, Ali Khaleel Kareem, A numerical study on the effects of exhaust locations on energy consumption and thermal environment in an office room served by displacement ventilation, Energy Conversion and Management, Volume 117, 1 June 2016, Pages 74-85, ISSN 0196-8904, http://dx.doi.org/10.1016/j.enconman.2016.03.004.

[4] Q.Y. Chen, L. Glicksman, System Performance Evaluation and Design Guideline for Displacement Ventilation, American Society of Heating, Refrigerating and Air-Conditioning Engineers Inc., Atlanta, USA (2003).

[5] Svensson, A. G. L. "Nordic experience of displacement ventilation systems." ASHRAE Transactions 89.1 (1989): 1013-1017.

[6] Sandberg, M., Sjoberg, M. 1984. A comparative study of the performance of general ventilation systems in evacuating contaminants. Proceedings of indoor Air, Vol. 5, pp. 59-64.

[7] Skaret, E. 1987. Displacement ventilation. Proceedings of Roomvent-87, Session 5, Stockholm.

[8] Yuan X, Chen Q, Glicksman LR. Performance evaluation and design guidelines for displacement ventilation. ASHRAE Transactions 1999;105 (1):298–309.

[9] Elisabeth Mundt, Contamination distribution in displacement ventilation—influence of disturbances, Building and Environment, Volume 29, Issue 3, July 1994, Pages 311-317, ISSN 0360-1323, http://dx.doi.org/10.1016/0360-1323(94)90028-0.

[10] Sandberg H, Lindstrom S. 1987. A model for ventilation by displacement, Proceedings of International Conference on Air Distribution in Rooms, Stockholm, Sweden.

[11] Linden, P.F., Lane-Serff G.F., Smeed D.A. Emptying filling spaces: the fluid mechanics of natural ventilation. Journal of Fluid Mechanics, Volume 212, February 1990, Pages 309-335, http://dx.doi.org/10.1017/S0022112090001987.

[12] P. Cooper and P. F. Linden. Natural ventilation of an enclosure containing two buoyancy sources. Journal of Fluid Mechanics, Volume 311, March 1996, Pages 153-176, http://dx.doi.org/10.1017/S0022112096002546.

[13] Q.Y. Chen, L. Glicksman, System Performance Evaluation and Design Guideline for Displacement Ventilation, American Society of Heating, Refrigerating and Air-Conditioning Engineers Inc., Atlanta, USA (2003).

[14] Elisabeth Mundt, Displacement ventilation systems—Convection flows and temperature gradients, Building and Environment, Volume 30, Issue 1, January 1995, Pages 129-133, ISSN 0360-1323, http://dx.doi.org/10.1016/0360-1323(94)E0002-9.

[15] G.C. da Graça, P.F. Linden. 2004. A simple model for heat transfer in displacement-ventilation. Proceedings of 9th International Conference on Air Distribution in Rooms, Coimbra, Portugal.

[16] Drury B. Crawley, Jon W. Hand, Michaël Kummert, Brent T. Griffith, Contrasting the capabilities of building energy performance simulation programs, Building and Environment, Volume 43, Issue 4, April 2008, Pages 661-673, ISSN 0360-1323, http://dx.doi.org/10.1016/j.buildenv.2006.10.027.

[17] Qingyan Chen, Jan Van Der Kooi, A methodology for indoor airflow computations and energy analysis for a displacement ventilation system, Energy and Buildings, Volume 14, Issue 4, 1990, Pages 259-271, ISSN 0378-7788, http://dx.doi.org/10.1016/0378-7788(90)90089-2.

[18] Yuanda Cheng, Jianlei Niu, Naiping Gao, Stratified air distribution systems in a large lecture theatre: A numerical method to optimize thermal comfort and maximize energy saving, Energy and Buildings, Volume 55, December 2012, Pages 515-525, ISSN 0378-7788, http://dx.doi.org/10.1016/j.enbuild.2012.09.021.

[19] Yi Wang, Xiaojing Meng, Xiaoni Yang, Jiaping Liu, Influence of convection and radiation on the thermal environment in an industrial building with buoyancy-driven natural ventilation, Energy and Buildings, Volume 75, June 2014, Pages 394-401, ISSN 0378-7788, http://dx.doi.org/10.1016/j.enbuild.2014.02.031.

[20] H. Brohus, P.V. Nielsen. 1994. Contaminant distribution around person in rooms ventilated by displacement ventilation. Proceedings of 4th International Conference on Air Distribution in Rooms, Krakow, Poland.

[21] Yuan, X., Measurements and computations of room airflow with displacement ventilation. ASHRAE Transactions105.1 (1999): 340-352.

[22] Mundt E., Non-buoyant pollutant sources and particles in displacement ventilation, Building and Environment, Volume 36, Issue 7, August 2001, Pages 829-836, ISSN 0360-1323, http://dx.doi.org/10.1016/S0360-1323(01)00008-7.

[23] Xu, M. , Yamanaka, T., Kotani, H., Vertical profiles of temperature and contaminant concentration in rooms ventilated by displacement with heat loss through room envelopes, Indoor Air 2001, volume 11, Pages 111-119, ISSN 0905 – 6947.

[24] He, G., Yang, X., Sebric, J., Removal of contaminants released from room surfaces by displacement and mixing ventilation: modeling and validation, Indoor Air 2005, volume 15, Pages 367-380, doi:10.1111/j.1600-0668.2005.00383.x.

[25] Olmedo, I., Nielsen, P., V., Ruiz de Adana, M., Jensen, R. L., Grzelecki, P., Distribution of exhaled contaminants and personal exposure in a room using three different air distribution strategies, Indoor Air 2012, volume 22, Pages 64-76, doi:10.1111/j.1600-0668.2011.00736.x.

[26] Simon J. Rees, Philip Haves, An experimental study of air flow and temperature distribution in a room with displacement ventilation and a chilled ceiling, Building and Environment, Volume 59, January 2013, Pages 358-368, ISSN 0360-1323, http://dx.doi.org/10.1016/j.buildenv.2012.09.001.

[27] Xiufeng Yang, Ke Zhong, Hui Zhu, Yanming Kang, Experimental investigation on transient natural ventilation driven by thermal buoyancy, Building and Environment, Volume 77, July 2014, Pages 29-39, ISSN 0360-1323, http://dx.doi.org/10.1016/j.buildenv.2014.03.013.

[28] Josephine Lau, Qingyan Chen, Floor-supply displacement ventilation for workshops, Building and Environment, Volume 42, Issue 4, April 2007, Pages 1718-1730, ISSN 0360-1323, http://dx.doi.org/10.1016/j.buildenv.2006.01.016.

[29] Lin Tian, Zhang Lin, Qiuwang Wang, Comparison of gaseous contaminant diffusion under stratum ventilation and under displacement ventilation, Building and Environment, Volume 45, Issue 9, September 2010, Pages 2035-2046, ISSN 0360-1323, http://dx.doi.org/10.1016/j.buildenv.2010.01.002.

[30] Mundt E. The performance of displacement ventilation systems experimental and theoretical studies. PhD thesis, Royal Institute of Technology, Stockholm, 1996.

[31] Li YG, Sandberg M, Laszlo F. Vertical temperature profiles in rooms ventilated by displacement: full-scale measurement and nodal modelling. Indoor Air, Volume 2, Issue 4, December 1992, Pages 225–243. ISSN 1600-0668, http://dx.doi.org/10.1111/j.1600-0668.1992.00005.x.

[32] G.C. da Graça, P.F. Linden. 2004. A simple model for heat transfer in displacement-ventilation. Proceedings of 9th International Conference on Air Distribution in Rooms, Coimbra, Portugal.

[33] Carrilho da Graça G. Simplified models for heat transfer in rooms. Ph.D. Dissertation. San Diego: Department of Engineering Physics, University of California; 2003.

[34] Huijuan Xing, Hazim B Awbi, Measurement and calculation of the neutral height in a room with displacement ventilation, Building and Environment, Volume 37, Issue 10, October 2002, Pages 961-967, ISSN 0360-1323, http://dx.doi.org/10.1016/S0360-1323(01)00079-8.

[35] Morton, B.R., Taylor, G.I. & Turner, J.S., Turbulent gravitational convection from maintained and instantaneous sources. Proceedings of the Royal Society of London. 1956 A 234 (1196), Pages 1-23.

[36] Elterman, V.M., 1980. Ventilation of Chemical Plants. Moscow. KHIMIA.

[37] E. Mundt. 1992. Convection Flows in Rooms with Temperature Gradients - Theory and Measurements. Proceedings of 3th International Conference on Air Distribution in Rooms, Aalborg, Denmark.

[38] Skistad, H., 1994. Displacement Ventilation. Research Studies Press, Jonh Wiley & Sons, Ltd., West Sussex. Uk.

[39] Skistad, H., Mundt, E., Nielsen, P., Hagstrom, K. & Railio, J., Displacement ventilation in non-industrial premises. REHVA Guidebook N1, 2002, Brussels.

[40] A. Bouzinaoui, J.R. Fontaine, F. Lemoine, P. Vallette. 2002. Experimental characterization of thermal plumes in confined ventilated spaces. Proceedings of 8th International Conference on Air Distribution in Rooms, Copenhagen, Denmark.

[41] Trzeciakiewicz, Z. An Experimental Analysis of the Two-Zone Airflow Pattern Formed in a Room with Displacement Ventilation. The International Journal of Ventilation, Vol.7, N°3, December 2008, ISSN 1473-3315.

[42] M. Deevy, Y. Sinai, P. Everitt, L. Voigt, N. Gobeau, Modelling the effect of an occupant on displacement ventilation with computational fluid dynamics, Energy and Buildings, Volume 40, Issue 3, 2008, Pages 255-264, ISSN 0378-7788, http://dx.doi.org/10.1016/j.enbuild.2007.02.021.

[43] Iman Fatemi, Bing-Chen Wang, Mike Koupriyanov, Brad Tully, Experimental study of a non-isothermal wall jet issued by a displacement ventilation system, Building and Environment, Volume 66, August 2013, Pages 131-140, ISSN 0360-1323, http://dx.doi.org/10.1016/j.buildenv.2013.04.019.

[44] Atila Novoselac, Brendon J. Burley, Jelena Srebric, Development of new and validation of existing convection correlations for rooms with displacement ventilation systems, Energy and Buildings, Volume 38, Issue 3, March 2006, Pages 163-173, ISSN 0378-7788, http://dx.doi.org/10.1016/j.enbuild.2005.04.005.

[45] Incropera, Frank P. Fundamentals of heat and mass transfer. John Wiley & Sons, 2011.
[46] N. Mateus, G. Carrilho da Graça. 2013. Thermal and Airflow Simulation of the Gulbenkian Great Hall. Proceedings of 13th International Conference on Building Simulation, Chambery, France.
[47] Appleby, P. (1989) Displacement ventilation: a design guide. Build. Serv., April, 63–6.

[48] Martin Behne, Indoor air quality in rooms with cooled ceilings.: Mixing ventilation or rather displacement ventilation?, Energy and Buildings, Volume 30, Issue 2, June 1999, Pages 155-166, ISSN 0378-7788, http://dx.doi.org/10.1016/S0378-7788(98)00083-8.

[49] Sandberg, M., Blomqvist, C. 1989. Displacement ventilation systems in office rooms. ASHRAE Transactions 95(2).

[50] Xing, H., Hatton, A. and Awbi, H. B. (2001) A study of the air quality in the breathing zone in a room with displacement ventilation, Building and Environment, 36, 809–20.

[51] Y.J.P. Lin, P.F. Linden, A model for an under floor air distribution system, Energy and Buildings, Volume 37, Issue 4, April 2005, Pages 399-409, ISSN 0378-7788, http://dx.doi.org/10.1016/j.enbuild.2004.07.011.

[52] F. Alamdari, D.J.G. Butler, P.F. Grigg, M.R. Shaw, Chilled ceilings and displacement ventilation, Renewable Energy, Volume 15, Issues 1–4, September–December 1998, Pages 300-305, ISSN 0960-1481, http://dx.doi.org/10.1016/S0960-1481(98)00177-3.

[53] Atila Novoselac, Jelena Srebric, A critical review on the performance and design of combined cooled ceiling and displacement ventilation systems, Energy and Buildings, Volume 34, Issue 5, June 2002, Pages 497-509, ISSN 0378-7788, http://dx.doi.org/10.1016/S0378-7788(01)00134-7.

[54] M. Behne, Is there a risk of draft in rooms with cooled ceilings? Measurement of velocities and turbulences, ASHRAE Transactions 2 (1995) 100.

[55] K. Fitzner. 1996. Displacement ventilation and cooled ceilings, results of laboratory tests and practical installations. Proceedings of Indoor Air'96 1 (1996) 41-50.

[56] Keblawi A, Ghaddar N, Ghali K, Jensen L. Chilled ceiling displacement ventilation design charts correlations to employ in optimized system operation for feasible load ranges. Energy and Buildings, 2009;41(11):1155e64. http://dx.doi.org/10.1016/j.enbuild.2009.05.009.

[57] S.J. Rees, J.J. McGuirk, P. Haves, Numerical investigation of transient buoyant flow in a room with a displacement ventilation and chilled ceiling system, International Journal

of Heat and Mass Transfer, Volume 44, Issue 16, August 2001, Pages 3067-3080, ISSN 0017-9310, http://dx.doi.org/10.1016/S0017-9310(00)00348-3.

[58] Pedro Nunes, Maria M. Lerer, Guilherme Carrilho da Graça, Energy certification of existing office buildings: Analysis of two case studies and qualitative reflection, Sustainable Cities and Society, Volume 9, December 2013, Pages 81-95, ISSN 2210-6707, http://dx.doi.org/10.1016/j.scs.2013.03.003.

[59] Zhiqiang Zhai, Qingyan (Yan) Chen, Numerical determination and treatment of convective heat transfer coefficient in the coupled building energy and CFD simulation, Building and Environment, Volume 39, Issue 8, August 2004, Pages 1001-1009, ISSN 0360-1323, http://dx.doi.org/10.1016/j.buildenv.2004.01.023.

[60] Thijs Defraeye, Bert Blocken, Jan Carmeliet, CFD simulation of heat transfer at surfaces of bluff bodies in turbulent boundary layers: Evaluation of a forced-convective temperature wall function for mixed convection, Journal of Wind Engineering and Industrial Aerodynamics, Volumes 104–106, May–July 2012, Pages 439-446, ISSN 0167-6105, http://dx.doi.org/10.1016/j.jweia.2012.02.001.

[61] Tengfei (Tim) Zhang, Hongbiao Zhou, Shugang Wang, An adjustment to the standard temperature wall function for CFD modeling of indoor convective heat transfer, Building and Environment, Volume 68, October 2013, Pages 159-169, ISSN 0360-1323, http://dx.doi.org/10.1016/j.buildenv.2013.06.009.

[62] S.J Rees, P Haves, A nodal model for displacement ventilation and chilled ceiling systems in office spaces, Building and Environment, Volume 36, Issue 6, July 2001, Pages 753-762, ISSN 0360-1323, http://dx.doi.org/10.1016/S0360-1323(00)00067-6.

[63] Simon J. Rees, Philip Haves, An experimental study of air flow and temperature distribution in a room with displacement ventilation and a chilled ceiling, Building and Environment, Volume 59, January 2013, Pages 358-368, ISSN 0360-1323, http://dx.doi.org/10.1016/j.buildenv.2012.09.001.

[64] A.H. Taki, D.L. Loveday, K.C. Parsons, The effect of chilled ceiling temperatures on displacement flow and thermal comfort-experimental and simulation studies, in: The Fifth International Conference on Air Distribution in Rooms-RoomVent, vol. 3, Yokohama, Japan, 1996, pp. 307–314, ISBN 492455701 3.

[65] W. Chakroun, K. Ghali, N. Ghaddar, Air quality in rooms conditioned by chilled ceiling and mixed displacement ventilation for energy saving, Energy and Buildings, Volume 43, Issue 10, October 2011, Pages 2684-2695, ISSN 0378-7788, http://dx.doi.org/10.1016/j.enbuild.2011.06.019.

[66] Mohamad Kanaan, Nesreen Ghaddar, Kamel Ghali, Georges Araj, New airborne pathogen transport model for upper-room UVGI spaces conditioned by chilled ceiling and mixed displacement ventilation: Enhancing air quality and energy performance, Energy Conversion and Management, Volume 85, September 2014, Pages 50-61, ISSN 0196-8904, http://dx.doi.org/10.1016/j.enconman.2014.05.073.

[67] Stefano Schiavon , Fred Bauman , Brad Tully & Julian Rimmer (2012) Room air stratification in combined chilled ceiling and displacement ventilation systems, HVAC&R Research, 18:1-2, 147-159, http://dx.doi.org/10.1080/10789669.2011.592105.

[68] S.G. Hodder, D.L. Loveday, K.C. Parsons, A.H. Taki, Thermal comfort in chilled ceiling and displacement ventilation environments: vertical radiant temperature asymmetry effects, Energy and Buildings, Volume 27, Issue 2, April 1998, Pages 167-173, ISSN 0378-7788, http://dx.doi.org/10.1016/S0378-7788(97)00038-8.

[69] Mohamad Ayoub , Nesreen Ghaddar, Kamel Ghali, Simplified Thermal Model of Spaces Cooled with Combined Positive Displacement Ventilation and Chilled Ceiling System, HVAC&R Research, Volume 12, Issue 4, October 2006, Pages 1005-1030, http://doi: 10.1080/10789669.2006.10391448.

[70] Mohamad Kanaan, Nesreen Ghaddar, Kamel Ghali, Simplified Model of Contaminant Dispersion in Rooms Conditioned by Chilled-Ceiling Displacement Ventilation System, HVAC&R Research, Volume 16, Issue 6, November 2010 , Pages 765-783, http://doi:10.1080/10789669.2010.10390933

[71] Nuno M. Mateus, Guilherme Carrilho da Graça, A validated three-node model for displacement ventilation, Building and Environment, Volume 84, January 2015, Pages 50-59, ISSN 0360-1323, http://dx.doi.org/10.1016/j.buildenv.2014.10.029.

[72] http://www.trox.de/en (accessed 04/03/2015).

[73] Air Conditioning Engineering, W.P. Jones. Fifth Edition. Butterworth-Heinemann, 2001.

[74] ASHRAE, ANSI/ASHRAE standard 55-1992, Thermal environmental conditions for human occupancy, American Society of Heating, Refrigerating and Air-Conditioning Engineers, Inc., Atlanta, 1992.

[75] D. Grimsrud, B. Bridges, R. Schulte, Continuous measurements of air quality parameters in schools, Building Research and Information 34 (5) (2006) 447–458.

[76] M. Mendell, G.A. Heath, Do indoor pollutants and thermal conditions in schools influence student performance? A critical review of the literature, Indoor Air – International Journal of Indoor Air Quality and Climate 15 (1) (2005) 27–52.

[77] Norbäck D, Nordström K. An experimental study on effects of increased ventilation flow on students' perception of indoor environment in computer classrooms. Indoor Air 2008;18(4):293-300.

[78] Salleh NM, Kamaruzzaman SN, Sulaiman R, Mahbob NS. Indoor air quality at school: ventilation rates and it impacts towards children-a review. In: 2nd International conference on environmental science and technology, vol. 6; 2011. pp. 418-22.

[79] Zs. Bakó-Biró, D.J. Clements-Croome, N. Kochhar, H.B. Awbi, M.J. Williams, Ventilation rates in schools and pupils' performance, Building and Environment, Volume 48, February 2012, Pages 215-223, ISSN 0360-1323, http://dx.doi.org/10.1016/j.buildenv.2011.08.018.

[80] Wargocki P, Wyon DP. Providing better thermal and air quality conditions in school classrooms would be cost-effective. Build Environ 2013;59:581-9.

[81] Mendell MJ, Eliseeva EA, Davies MM, Spears M, Lobscheid A, Fisk WJ, et al. Association of classroom ventilation with reduced illness absence: a prospective study in California elementary schools. Indoor Air 2013;1:14.

[82] CEN. 2007d. Indoor environmental input parameters for design and assessment of energy performance of buildings addressing indoor air quality, thermal environment, lighting and acoustics. EN15251 Standard. Brussels: European Committee for Standardization.

[83] ASHRAE, (2009) Indoor Air Quality Guide (ISBN 978-1-933742-59-5).

[84] American Society of Heating, Refrigeration and Air-Conditioning Engineers (ASHRAE). (2007): ''ANSI/ASHRAE standard 62.1-2007, Ventilation for acceptable indoor air quality.'': American Society of Heating Refrigerating and Air Conditioning Engineers, Atlanta, USA.

[85] Chris J. Koinakis, Combined thermal and natural ventilation modeling for long-term energy assessment: validation with experimental measurements, Energy and Buildings, Volume 37, Issue 4, April 2005, Pages 311-323, ISSN 0378-7788, http://dx.doi.org/10.1016/j.enbuild.2004.06.022.

[86] G. Carrilho da Graça, N.C. Daish, P.F. Linden, A two-zone model for natural cross-ventilation, Building and Environment, Volume 89, July 2015, Pages 72-85, ISSN 0360-1323, http://dx.doi.org/10.1016/j.buildenv.2015.02.014.

[87] Luísa Dias Pereira, Daniela Raimondo, Stefano Paolo Corgnati, Manuel Gameiro da Silva, Assessment of indoor air quality and thermal comfort in Portuguese secondary classrooms: Methodology and results, Building and Environment, Volume 81, November 2014, Pages 69-80, ISSN 0360-1323, http://dx.doi.org/10.1016/j.buildenv.2014.06.008.

[88] Asit Kumar Mishra, Maddali Ramgopal, A comparison of student performance between conditioned and naturally ventilated classrooms, Building and Environment, Volume 84, January 2015, Pages 181-188, ISSN 0360-1323, http://dx.doi.org/10.1016/j.buildenv.2014.11.008.

[89] P.A. Scheff, V.K. Paulius, S.W. Huang, L.M. Conroy, Indoor air quality in a middle school. Part I: Use of CO2 as a tracer for effective ventilation, Applied Occupational and Environmental Hygiene 15 (11) (2000) 824–834.

[90] M. Santamouris, A. Synnefa, M. Asssimakopoulos, I. Livada, K. Pavlou, M. Papaglastra, N. Gaitani, D. Kolokotsa, V. Assimakopoulos, Experimental investigation of the air flow and indoor carbon dioxide concentration in classrooms with intermittent natural ventilation, Energy and Buildings, Volume 40, Issue 10, 2008, Pages 1833-1843, ISSN 0378-7788, http://dx.doi.org/10.1016/j.enbuild.2008.04.002.

[91] Eusébio Z.E. Conceição, João M.M. Gomes, Nuno H. Antão, M Manuela J.R. Lúcio, Application of a developed adaptive model in the evaluation of thermal comfort in ventilated kindergarten occupied spaces, Building and Environment, Volume 50, April 2012, Pages 190-201, ISSN 0360-1323, http://dx.doi.org/10.1016/j.buildenv.2011.10.013.

[92] Ricardo Forgiarini Rupp, Natalia Giraldo Vásquez, Roberto Lamberts, A review of human thermal comfort in the built environment, Energy and Buildings, Volume 105, 15 October 2015, Pages 178-205, ISSN 0378-7788, http://dx.doi.org/10.1016/j.enbuild.2015.07.047.

[93] Ricardo M.S.F. Almeida, Vasco Peixoto de Freitas, Indoor environmental quality of classrooms in Southern European climate, Energy and Buildings, Volume 81, October 2014, Pages 127-140, ISSN 0378-7788, http://dx.doi.org/10.1016/j.enbuild.2014.06.020.

[94] Guilherme Carrilho da Graça, Paul Linden. Ten questions about natural ventilation of non-domestic buildings. Submitted to Building and Environment.

[95] Linden, P. F. (1999). The Fluid Mechanics of Natural Ventilation. Annual Review of Fluid Mechanics. Volume 31, 1999, Pages 201–238. http://dx.doi:10.1146/annurev.fluid.31.1.201.

[96] Alex Yong Kwang Tan, Nyuk Hien Wong, Natural ventilation performance of classroom with solar chimney system, Energy and Buildings, Volume 53, October 2012, Pages 19-27, ISSN 0378-7788, http://dx.doi.org/10.1016/j.enbuild.2012.06.010.

[97] Rakesh Khanal, Chengwang Lei, A numerical investigation of buoyancy induced turbulent air flow in an inclined passive wall solar chimney for natural ventilation, Energy and Buildings, Volume 93, 15 April 2015, Pages 217-226, ISSN 0378-7788, http://dx.doi.org/10.1016/j.enbuild.2015.02.019.

[98] Qingyan Chen, Ventilation performance prediction for buildings: A method overview and recent applications, Building and Environment, Volume 44, Issue 4, April 2009, Pages 848-858, ISSN 0360-1323, http://dx.doi.org/10.1016/j.buildenv.2008.05.025.

[99] Drury B. Crawley, Linda K. Lawrie, Frederick C. Winkelmann, W.F. Buhl, Y.Joe Huang, Curtis O. Pedersen, Richard K. Strand, Richard J. Liesen, Daniel E. Fisher, Michael J. Witte, Jason Glazer, EnergyPlus: creating a new-generation building energy simulation program, Energy and Buildings, Volume 33, Issue 4, April 2001, Pages 319-331 , ISSN 0378-7788, http://dx.doi.org/10.1016/S0378-7788(00)00114-6.

[100] DOE, US. "EnergyPlus Engineering Reference." The Reference to EnergyPlus Calculations (2015).

[101] Sara Gilani, Hamid Montazeri, Bert Blocken, CFD simulation of stratified indoor environment in displacement ventilation: Validation and sensitivity analysis, Building and Environment, Volume 95, January 2016, Pages 299-313, ISSN 0360-1323, http://dx.doi.org/10.1016/j.buildenv.2015.09.010.

[102] Zhen Zeng, Xiaofeng Li, Cheng Li, Yingxin Zhu, Modeling ventilation in naturally ventilated double-skin façade with a venetian blind, Building and Environment, Volume 57, November 2012, Pages 1-6, ISSN 0360-1323, http://dx.doi.org/10.1016/j.buildenv.2012.04.007.

[103] Yang Wang, Fu-Yun Zhao, Jens Kuckelkorn, Di Liu, Jun Liu, Jun-Liang Zhang, Classroom energy efficiency and air environment with displacement natural ventilation in a passive public school building, Energy and Buildings, Volume 70, February 2014, Pages 258-270, ISSN 0378-7788, http://dx.doi.org/10.1016/j.enbuild.2013.11.071.

[104] Ines Khalifa and Leila Gharbi Ernez and Essia Znouda and Chiheb Bouden, Coupling TRNSYS 17 and CONTAM: simulation of a naturally ventilated double-skin façade, Advances in Building Energy Research, Volume 9, Issue 2, 2015, Pages 293-304, http://dx.doi.org/10.1080/17512549.2015.1050694.

[105] F.R. Mazarrón, J. Cid-Falceto, I. Cañas, An assessment of using groundthermal inertia as passive thermal technique in the wine industry around the world, Applied Thermal Engineering 33–34 (2012) 54–61,http://dx.doi.org/10.1016/j.applthermaleng.2011.09.010.

[106] Z. Zhai, M. Johnson, M. Krarti, Assessment of natural and hybrid ventilation models in whole-building energy simulations, Energy and Buildings 43 (9)(2011) 2251–2261, http://dx.doi.org/10.1016/j.enbuild.2011.06.026.

[107] Taleghani, M., Tenpierik, M., & van den Dobbelsteen, A. (2014). Indoor thermal comfort in urban courtyard block dwellings in the Netherlands. Building and Environment, 82, 566–579. doi:10.1016/j.buildenv.2014.09.028.

[108] Nuno M. Mateus, Armando Pinto, Guilherme Carrilho da Graça, Validation of EnergyPlus thermal simulation of a double skin naturally and mechanically ventilated test cell, Energy and Buildings, Volume 75, June 2014, Pages 511-522, ISSN 0378-7788, http://dx.doi.org/10.1016/j.enbuild.2014.02.043.

[109] D. Kim, C. Park, Difficulties and limitations in performance simulation of a double skin façade with EnergyPlus, Energy and Buildings 43 (12) (2011)3635–3645, http://dx.doi.org/10.1016/j.enbuild.2011.09.038.

[110] E.H. Mathews, D.C. Arndt, Validation of models to predict the thermal and ventilation performance of horse stables, Building and Environment, Volume 38, Issue 2, February 2003, Pages 237-246, ISSN 0360-1323, http://dx.doi.org/10.1016/S0360-1323(02)00036-7.

[111] Nuno M. Mateus, Guilherme Carrilho da Graça, Simplified modeling of displacement ventilation systems with chilled ceilings, Energy and Buildings, Volume 108, 1 December 2015, Pages 44-54, ISSN 0378-7788, http://dx.doi.org/10.1016/j.enbuild.2015.08.054.

[112] N. B. Kaye, M. Flynn, M. J. Cook, Y Ji, The role of diffusion on the interface thickness in a ventilated filing box, Journal of Fluid Mechanics, 2010, Volume 652, Pages195-205. http:// dx.doi.org/ 10.1017/S0022112010000881.

[113] Santos, C. A. P.; Matias, L., 2006. Coeficientes de transmissão térmica de elementos da envolvente dos edifícios, 1ª edição. ICT informação técnica, edifícios- ITE 50.Laboratório Nacional de Engenharia Civil, Lisboa, Portugal.

[114] A. Persily, Evaluating building IAQ and ventilation with indoor carbon dioxide, ASHRAE Transactions 103 (1997) 1–12.

[115] R. Wallider, D. Norback, G. Wieslander, G. Smedje, C. Erwall, Nasal mucosal swelling in relation to low air exchange rate in schools, Indoor Air 7 (1997) 198–205.

[116] Birgit Krausse, Malcolm Cook, Kevin Lomas, Environmental performance of a naturally ventilated city centre library, Energy and Buildings, Volume 39, Issue 7, July 2007, Pages 792-801, ISSN 0378-7788, http://dx.doi.org/10.1016/j.enbuild.2007.02.010.

[117] F. Flourentzou, J. Van der Maas, C.-A. Roulet, Natural ventilation for passive cooling: measurement of discharge coefficients, Energy and Buildings, Volume 27, Issue 3, June 1998, Pages 283-292, ISSN 0378-7788, http://dx.doi.org/10.1016/S0378-7788(97)00043-1.

[118] Walton, G. N., Thermal Analysis Research Program Reference Manual. NBSSIR 83-2655. National Bureau of Standards, 1983.

[119] CHAM, PHOENICS VR. http://www.cham.co.uk. (2015).

[120] CIBSE Guide B (2005) Heating, Ventilation, Air Conditioning and Refrigeration, Chartered Institution of Building Services Engineers, http://www.cibse.org/

[121] J. van der Maas, Air Flow Through Large Openings in Buildings. Ecole Polytechnique Federale de Lausanne, LESO-PB (1992). Switzerland, Lausanne.

[122] J. Arce, M.J. Jiménez, J.D. Guzmán, M.R. Heras, G. Alvarez, J. Xamán, Experimental study for natural ventilation on a solar chimney, Renewable Energy, Volume 34, Issue 12, December 2009, Pages 2928-2934, ISSN 0960-1481, http://dx.doi.org/10.1016/j.renene.2009.04.026.

[123] Z. Yang, M. Peng, L. Wang, Characteristic analyse of air-condition's load in large space building, Refrig. Air Condition. 1 (2006) 53–56.

[124] Mathisen, H. M. 1989. Cases studies of displacement ventilation in public halls. ASHRAE Transactions 95(2).

[125] P. Ricciardi, A. Ziletti, C. Buratti, Evaluation of thermal comfort in an historical Italian pera theatre by the calculation of the neutral comfort temperature, Building and

Environment, Volume 102, June 2016, Pages 116-127, ISSN 0360-1323, http://dx.doi.org/10.1016/j.buildenv.2016.03.011.

[126] M. Kavgic, D. Mumovic, Z. Stevanovic, A. Young, Analysis of thermal comfort and indoor air quality in a mechanically ventilated theatre, Energy and Buildings, Volume 40, Issue 7, 2008, Pages 1334-1343, ISSN 0378-7788, http://dx.doi.org/10.1016/j.enbuild.2007.12.002.

[127] A. Scanlon, A. Calderone.2011. CFD benchmarking: Hammer hall auditorium case study. Proceedings of 12th International Conference on Building Simulation, Sydney, Australia.

[128] K.W.D. Cheong, E. Djunaedy, Y.L. Chua, K.W. Tham, S.C. Sekhar, N.H. Wong, M.B. Ullah, Thermal comfort study of an air-conditioned lecture theatre in the tropics, Building and Environment, Volume 38, Issue 1, January 2003, Pages 63-73, ISSN 0360-1323, http://dx.doi.org/10.1016/S0360-1323(02)00020-3.

[129] H Hangan, F McKenty, L Gravel, R Camarero, Case study: Numerical simulations for comfort assessment and optimization of the ventilation design for complex atriums, Journal of Wind Engineering and Industrial Aerodynamics, Volume 89, Issues 11–12, September 2001, Pages 1031-1045, ISSN 0167-6105, http://dx.doi.org/10.1016/S0167-6105(01)00097-6.

[130] M.W. Muhieldeen, N.M. Adam, B.H. Salman, Experimental and numerical studies of reducing cooling load of lecture hall, Energy and Buildings, Volume 89, 15 February 2015, Pages 163-169, ISSN 0378-7788, http://dx.doi.org/10.1016/j.enbuild.2014.12.026.

[131] Mohammad Hassan Fathollahzadeh, Ghassem Heidarinejad, Hadi Pasdarshahri, Producing a better performance for the under floor air distribution system in a dense occupancy space, Energy and Buildings, Volume 126, 15 August 2016, Pages 230-238, ISSN 0378-7788, http://dx.doi.org/10.1016/j.enbuild.2016.05.008.

[132] Yuanda Cheng, Jianlei Niu, Naiping Gao, Stratified air distribution systems in a large lecture theatre: A numerical method to optimize thermal comfort and maximize energy saving, Energy and Buildings, Volume 55, December 2012, Pages 515-525, ISSN 0378-7788, http://dx.doi.org/10.1016/j.enbuild.2012.09.021.

[133] Gon Kim, Laura Schaefer, Tae Sub Lim, Jeong Tai Kim, Thermal comfort prediction of an underfloor air distribution system in a large indoor environment, Energy and Buildings, Volume 64, September 2013, Pages 323-331, ISSN 0378-7788, http://dx.doi.org/10.1016/j.enbuild.2013.05.003.

[134] REHVA.2002. Displacement Ventilation in Non-Industrial Premises,ed. Skistad, H. et al.

[135] Wyon, D. and Sandberg, M. (1996) Discomfort due to vertical thermal gradients, Indoor Air, 6, 48–54.

[136] S.A. Howell, I. Potts, On the natural displacement flow through a full-scale enclosure, and the importance of the radiative participation of the water vapour content of the ambient air, Building and Environment, Volume 37, Issues 8–9, August–September 2002, Pages 817-823, ISSN 0360-1323, http://dx.doi.org/10.1016/S0360-1323(02)00048-3.

[137] Etheridge DW, Sandberg M. Building ventilation: theory and measurement. Chichester, UK: John Wiley & Sons; 1996.

[138] H. Manz, P. Loutzenhiser, T. Frank, P.A. Strachan, R. Bundi, G. Maxwell, Series of experiments for empirical validation of solar gain modeling in building energy simulation codes—Experimental setup, test cell characterization, specifications and uncertainty analysis, Building and Environment, Volume 41, Issue 12, December 2006, Pages 1784-1797 , ISSN 0360-1323, http://dx.doi.org/10.1016/j.buildenv.2005.07.020.

[139] C. Buratti, E. Moretti, E. Belloni, F. Cotana, Unsteady simulation of energy performance and thermal comfort in non-residential buildings, Building and Environment, Volume 59, January 2013, Pages 482-491 , ISSN 0360-1323, http://dx.doi.org/10.1016/j.buildenv.2012.09.015.

[140] Gates, A., Liley, B., Donn, M.. 2011. New Zealand's new weather data – How different? Proceedings of 12th International Conference on Building Simulation (Building Simulation 2011), Sydney, Australia.

[141]http://apps1.eere.energy.gov/buildings/energyplus/weatherdata/6_europe_wmo_region_6/PRT_Lisboa.085360_INETI.zip (accessed in 02/2012).

[142] ASHRAE Handbook – Fundamentals. American Society of Heating, Refrigerating and Air-Conditioning Engineers, Atlanta, 2009.

[143] H Hangan, F McKenty, L Gravel, R Camarero, Case study: Numerical simulations for comfort assessment and optimization of the ventilation design for complex atriums, Journal of Wind Engineering and Industrial Aerodynamics, Volume 89, Issues 11–12, September 2001, Pages 1031-1045.

[144] A. Scanlon, A. Calderone, CFD BENCHMARKING: HAMER HALL AUDITORIUM CASE STUDY, Proceedings of Building Simulation 2011, 12th Conference of International Building Performance Simulation Association, Sydney, 14-16 November.

[145] Andreopoulos, J., Rodi, W., 1984, Experimental investigation of jets in a crossflow, Journal of Fluid Mechanics, 138, pp 93-127.

[146] Chan, C., and Lam, K., 1998, Centerline velocity decay of a circular jet in a counterflowing stream, PHYSICS OF FLUIDS, volume 10, number 3.

[147] RECS, Regulamento de Desempenho Energético dos Edificios de Comércio e Serviços, Decreto-Lei nº 118/2013 de 20 de Agosto. Diário da República nº159 - Ministério da Economia e do Emprego, Lisboa, 2013.

[148] EnergyPlus (2013). Energy Plus Documentation: Getting Started with EnergyPlus, EnergyPlus Engineering Reference, Input and Output Reference.

[149] CEN, CEedN., CEN Standard EN 15251. In: Indoor environmental input parameters for design and assessment of energy performance of buildings addressing indoor air quality, thermal environment, lighting and acoustics. CEN: Brussels; 2007.

[150] ASHRAE, ASHRAE standard 55-2010. In: Thermal environmental conditions for human occupancy. ASHRAE Atlanta, GA; 2010.